DOCTOR OF PHILOSOPHY

Development of an Autonomous Parallel Action Tissue Grasper to Minimise Tissue Trauma.

Brown, Andrew

Award date:
2014

Awarding institution:
University of Dundee

DOCTOR OF PHILOSOPHY

Development of an Autonomous Parallel Action Tissue Grasper to Minimise Tissue Trauma.

Andrew Brown

2014

University of Dundee

Development of an Autonomous Parallel Action Tissue Grasper to Minimise Tissue Trauma.

By

Andrew William Brown

Submitted for the degree of

Doctor of Philosophy

on the completion of research

in the

School of Engineering, Physics and Mathematics

of the

University of Dundee

April 2014

Declaration

I, Andrew William Brown, hereby declare that the work presented in this thesis was carried out by myself at the Institute of Medical Science and Technology of the University of Dundee, except where due acknowledgement is made, and has not been submitted for any other degree.

Andrew William Brown

April 2014

I state that the conditions of the relevant Ordinance and Regulation have been fulfilled.

Prof. Sir Alfred Cuschieri

Supervisor

April 2014

Acknowledgements

Throughout the tenure of this research there are many people whom the Author would like to thank for their contributions and assistance. First and foremost the Author would like to express his most sincere of thanks, gratitude and appreciation to his PhD supervisors; Prof. Sir Alfred Cuschieri, Dr. Stuart Brown and Dr. Zhigang Wang, all of the Institute for Medical Science and Technology (IMSaT). Prof. Cuschieri and Drs. Brown and Wang have always made time in their schedules to give the most impeccable and honest advice and guidance on the research subject and the direction of study. This guidance has not only been restricted to research studies but also into other academic areas. The continual support of the supervisors along with their guidance, enthusiasm for research and their personalities has made this research thoroughly enjoyable and rewarding. For all of these reasons and many more, the Author will be forever grateful to, and have great admiration for, his PhD supervisors. Thanks are also due to fellow Biomag group members Dr. Pascal and Dr. Florence of the University of St. Andrews for their advice and contributions to this research. Special thanks must also go to Mr. Donald Maclean for his fantastic technical support throughout the project.

Thanks are due to many members of the surgical technology and robotics group, in particular Mr. Duncan Martin and Mr. James Gove who provided fantastic design and manufacturing advice and support, both of whom have a wealth of knowledge in the field which was imperative to the success of this research. Thanks must also be given to Mr. Stuart

Coleman for the many discussions about research and his advice in the area of mechanical engineering.

Thanks are due to anyone from the surgical technology and robotics group that has contributed in any way towards this research and that thanks extends to IMSat and the University of Dundee.

Most of all the Author would like to express his gratitude and thanks to his parents (William and Christine) for their continued support, guidance, enthusiasm and sacrifice over the years. Also to his big sister Dr. Elaine Brown who has provided the Author with great support, advice, friendship and beer throughout the years and has certainly expanded his repertoire of scientific theory and debate.

Abstract

Trauma caused by grasping during laparoscopic surgery is something which will never be fully eradicated however efforts should be taken to reduce the potential to cause trauma by grasping. Tissue is often grasped with excessive forces for long periods of time during surgeries such as cholecystectomies and colectomies. This along with failed grasping actions and the occurrence of slip has been shown to damage the tissue.

Design features often employed within graspers such as profiling and the occlusion mechanism of the instrument cause areas of high, uneven distribution of pressures on the tissue which can result in perforation or tissue tearing. By investigating these contributing factors, development of graspers with a low risk to cause damage this combined with actuating the grasping force should reduce the incidence of grasping trauma, currently at estimated at one incidence per procedure. These trauma events can lead to conversion to open surgery, peritonitis and even death.

Development of an autonomous grasping instrument to detect and prevent slip by actuating the grasping force is reported. Piezoelectric sensors are used to detect incipient slip and slip events. A closed loop control system then reacts to these perceived slip events to prevent slip occurring by actuating the applied force by small increments to increase or decrease grasping force. This leads to a system in which only the required amount of force necessary to overcome pull force is applied to the tissue.

Other areas of investigation to reduce tissue trauma are presented. In chapter 3 design features such as surface profiling and fenestrations are evaluated to determine the potential to

cause damage. A variety of profiles and fenestrations are studied and each is reported by representing the applied force to retention force ratio which indicates how good the profile is at retaining tissue against a pull force. The aim of this study was to develop surface profiling which had a high retention force but a reduced number of high stress areas which can lead to tissue damage.

Three new parallel action grasping designs are presented and evaluated using finite element analysis. Parallel action grasping is important in reducing tissue trauma as it distributes pressure evenly across the active grasping area as opposed to more conventional pivot style graspers which have high stress concentration areas in the proximal opening.

Each area of study within the thesis addresses areas of concern which have been shown to cause tissue trauma and postulates viable solutions to reduce the incidences of tissue trauma during laparoscopic surgery with the ultimate aim of developing a deployable and autonomous grasping device which will detect and prevent slip.

Table of Contents

List of figures

List of Graphs

List of Tables

List of equations

List of Abbreviations

ANN	Artificial neural network
ANOVA	Analysis of variance
ASIC	Application specific integrated circuit
CNT	Carbon nanotubes
DC	Direct current
DOF	Degrees of freedom
EMG	Electromyogram
FEA	Finite element analysis
FEM	Finite element modelling
FFT	Fast fourier transform
FIR	Finite impulse response
IIR	Infinite impulse response
MAS	Minimal access surgery
NI	National instruments
NOTES	Natural orifice transluminal endoscopic surgery
PCB	Printed circuit board
PDMS	Polydimethylsiloxan
PID	Proportional integral derivative
POEM	Peroral endoscopic myotomy
PVDF	Polyvinylidine fluoride
PWM	Pulse width modulation
PZT	Lead zirconate titanate
SMA	Shape memory alloy

SME	Shape memory effect
SoC	System on a chip
SPLS	Single port laparoscopic surgery
SPRINT	Single port laparoscopy bi-manual robot
VCSEL	Vertical cavity surface emitting laser
VECTOR	Versatile Endoscopic Capsule for gastrointestinal tumour recognition and therapy

1. Introduction

Since the inception of modern laparoscopic surgery in the mid 1980's[1] there has been continual development of the surgical procedure to produce improved outcomes for the patients [2-4]. This has led to a reduction in the number of ports which in turn presents complications in respect to instrument design. Instrument clashing and triangulation[5] have both been reported to be by products of single port surgery or natural orifice surgery whilst the long standing concern of lack of haptic feedback through the instruments is still a concern.

Through this progression of laparoscopic surgery the instruments themselves have not changed all that much; long, rigid bodies with manipulators, dissectors and graspers attached which the surgeon and the assistants are expected to control in difficult and stressful positions for long periods of time[6]. Within the past decade, with the dramatic increase in computing power more and more surgical robots are being developed in order to address some of the concerns of traditional laparoscopic surgery. The Da Vinci telepresence surgical robot provides motion scaling and inversion however it comes at high costs and is only found to be beneficial for certain surgeries[7]. More recently deployable robotic devices have been developed [8, 9] for a number of applications with the drive towards therapeutic and deployable devices which provide their own locomotion with all electronics on board. It is clear that the appropriate use of robotics within laparoscopic surgery could provide a number of benefits. One method of this integration would be to develop more traditional instruments to have a basis in robotics and to use robotics to carry out some of the minor tasks during surgery.

During a laparoscopic cholecystectomy or colectomy the tissue is grasped multiple times throughout and on occasion for long periods of time[10]. Tissue is often retracted out of

the field of view or to gain access to a particular surgical site. This is done by grasping and retracting the tissue. Excessive forces are often applied to the tissue from this action which has been shown to lead to bowel damage at a frequency of 1 per procedure[10]. Grasping tissue for extended periods of time with high forces will also reduce blood flow and encourage local necrosis of the tissue. This action of retracting and holding of tissue during surgery, performed by a surgeon or surgical assistant has a number of detriments to the overall surgery, including; high risk of causing tissue trauma, fatigue and stress to the surgeon and a laparoscopic port being used which could be put to better use with other assisting instruments which further aid the surgeon.

The design of surgical graspers along with excessive applied forces, long holding periods, failed grasping attempts and tissue slipping from the graspers contribute to tissue damage during surgery. The surface profiling of tissue graspers has been investigated showing the impact on which surface profiling can have of the damage to tissue with explicit recommendation to not use toothed designs. Another concern is the grasping mechanism which works in a pivotal manner. This design creates an uneven pressure distribution on the tissue when it is grasped [11].

The aim of this thesis is to reduce the potential to cause trauma to tissue by investigating the design features of surgical graspers. Concurrently a device is developed to autonomously grasp tissue by detecting and reacting to slip events by incrementally increasing and decreasing the applied grasping force. This will produce a system which has the design features enabling it to maximise the instruments ability to successfully retain tissue within the jaws of the grasper while preventing excessive applied forces and reducing the potential to cause tissue damage.

Chapter 3 investigates the surface profiling and fenestrations design features which are commonly found in laparoscopic graspers. Varying surface profiling has been shown to

have a large impact on tissue damage by investigating a number of profiles which have been described previously along with novel surface profile designs. The aim is to develop a profile which will replicate retention forces of more aggressive surface profiles such as large toothed designs which cause high stress areas and tearing frequently at high pull forces with a design which is less likely to present these issues

Fenestrations are also frequently found in the jaws of laparoscopic instruments even though they have been reported to increase the damage to tissue while having no effect on the retention ability. Therefore fenestrations will also be investigated. The impact of the size and shape of the fenestrations will be evaluated.

Chapter 4 will introduce the development of piezoelectric sensors as a way of determining incipient and slip events. The sensors are encased in a silicone body, the surface of which is adorned with compliant features. These act to transmit vibrations and deformation on the surface caused by the tissue in the jaws of the instrument. These vibrations and surface deformations in turn create an output signal which is proportional to the magnitude of the deformation.

This output voltage is then investigated to determine Boolean conditions for incipient slip and slip events in chapter 5. These Boolean conditions are implemented into a closed loop control system which is run on a state machine architecture. Piezoelectric sensors are mounted on the distal tip of a tissue grasper which is actuated by a DC motor to control the grasping force. The grasping instrument acts in a parallel fashion to negate the uneven pressure distribution of the scissor action graspers[11].

The closed loop control system acts upon triggers which could be user inputs or as described, sensory inputs. When a trigger occurs a reactive action will be performed. Increase in grasping force, decrease in grasping force, excessive grasping force warning and user controlled grasping are all integrated into the system.

The autonomous system was tested to determine how well it reacted and detected slip events which were induced by a tensiometer. The grasping force and pull force were also investigated to determine the efficacy of the force control system.

Chapter 6 will present a new parallel grasping instrument design to address some of the concerns of current parallel grasping mechanisms. A strict design specification is presented along with 3 mechanism designs. Finite element analysis of each of the design is performed to determine stress distributions. Prototypes of each of the designs are also presented.

Each of the chapters reports on a method which is aimed at reducing the potential to cause trauma to tissue. Investigations of design features such as parallel action grasping, surface profiling and fenestrations helped to develop an instrument which reduce high stress being concentrated on the tissue while also providing the necessary grip to retain tissue within the jaws.

Autonomous grasping will mean that excessive grasping forces are not used to secure tissue and that only the necessary grasping force to overcome the pull force will be used. This integration of robotics into a standard laparoscopic grasper will reduce the incidence of slip and failed grasping attempts. All of which contribute to tissue damage.

2. Prior Literature

The broad range of topics covered within the scope of this thesis necessitates an expansive review of the literature within the following chapter. An overview of each of the topics which will be investigated in following chapters is provided.

Firstly an overview of the current state of laparoscopic surgery is discussed which will provide a focus as to why this work has been undertaken. Section 2.1 will give a brief history of laparoscopic surgery along with the benefits which laparoscopic surgery provide when compared to more traditional open techniques. The engineering and ergonomic issues associated with laparoscopic surgery are presented with a view to frame some of the reasoning why it is important to develop autonomous devices to aid surgeons and operating theatre staff when performing surgeries.

Following directly on from this, tissue grasping is discussed in section 2.2. Incidence of trauma caused by tissue grasping is investigated within the published literature. A number of publications which have focused on the causes of tissue trauma caused by design features within the laparoscopic graspers are then reviewed in detail. These design features include fenestrations and surface profiling of the graspers, of which there is limited literature. Forces and pressures applied to tissue through the use of laparoscopic graspers is also discussed within this section. Due to the limited number of research papers discussing the effect of design features, a studies are presented in chapter 3 which will help to expand on the current published literature in this field.

The final two sections of the literature review are the largest and provide an overview of actuation and slip sensing technologies suitable for implementation into surgical graspers and devices. Due to research constraints, lab based investigation into various types of actuation

or slip sensing technologies was not possible and thus an in depth analysis of the literature to inform any decisions within the scope of the thesis was seen as the most prudent way to proceed with the research into the development of an autonomous actuated grasper with slip sensing abilities.

Four suitable actuation technologies were identified early; Direct current motors (DC), piezoelectric motors, shape memory alloy actuators and hydraulics and pneumatics. These actuation technologies have all been used within the field of laparoscopic or endoscopic surgeries. Particular areas of interest when analysing these topics were; accuracy, size, force or torque output, how they are controlled and power usage as well as any prohibitive features such as heat production.

Each technology is introduced with an overview of the theory of operation before continuing onto an analysis of published literature. Papers selected span a wide range of topics from colonoscopy to surgical grasping and present approaches used to actuate surgical devices which may be of interest in developing an actuated surgical grasper.

Slip sensing technologies were investigated on a similar basis. Piezoelectric and piezoresistive based tactile sensing is the main focus and this is briefly extended into alternate methods of slip sensing to include capacitive and optical sensing. Papers selected within this section may not be directly related to medical research but provide an insight into the various advantages and disadvantages of each sensing technology; circuitry, response, manufacture, cost and accuracy were the main factors in selection of research papers. Slip sensing technologies are covered in depth to provide the reading with a full understanding of the topic when slip sensing studies are carried out in chapter 4 and 5.

2.1 Current state of laparoscopic surgery

2.1.1 Grasper devices and design.

Since the first reported incidence of modern laparoscopic surgery in 1985 where a laparoscopic cholecystectomy was performed by Prof. Erich Mühe[1], a number of pioneers around the world (Mouret, Cuschieri, Reddick to name a few) begun to adopt the surgery and since, there has been a rapid uptake which has led to a revolution in regards to abdominal surgery. The new surgical approach desined to reduce the trauma of access had become so popular that by 1993 it had become gold standard operation for removal of the gallbladder[12]. By 2008 90% of the laparoscopic cholecystectomies performed in the United States were carried out laparoscopically[13], as were millions of other procedures in other specialties, i.e., gynaecology, thoracic, gastrointestinal and vascular.

Traditionally laparoscopic surgery is carried out using long rigid instruments placed through small incisions in the abdominal wall in order to gain access to the abdominal cavity which is insufflated with CO2. The diameters of the instruments when the approach was first introduced was 10mm, but over the past two decades the diameter has been gradually reduced such that most instruments are now 5.0mm and some indeed favour 3.0mm instruments (mini-laparoscopic surgery) or even less (2.0mm). The decrease in the size of the instrument leads to smaller incisions needed for insertion and they also lend themselves to further advances in laparoscopic techniques such as single incision or single port laparoscopic surgery[14].

2.1.2 Benefits and challenges of laparoscopic surgery.

The benefits associated with laparoscopic surgery are well documented in the literature and include perioperative benefits as well as longer term benefits of clinical and patient outcomes. Perioperative improvements over more conventional open surgery have shown to be; reduced mortality rates[2], fewer wound infections[15], reduced adhesion formation[16], earlier return of bowel function[17], reduced blood loss[18] and blood transfusions[19] as well as less post-operative pain and fatigue[20] which ultimately reduces the analgesic medication required by patients[21]. Patient benefits have also been well documented in the literature including both improved post-operative quality of life[4], improved cosmesis[3].

A number of these benefits could be interdependent, Cali *et al.* [22] have shown that a reduction in analgesic medicines, namely morphine, post-operatively will reduce the amount of time for normal bowel function to resume. Other studies [23, 24] have also shown a net benefit to the cell mediated immune response of laparoscopic patients when compared to open surgeries after bowel resection

With regard to post-operative mortality, some studies have shown either no difference as reported in a meta-analysis of laparoscopic versus open cholecystectomy, encompassing 38 studies from Keuss *et al.*[25] or reduced mortality and morbidity after laparoscopic surgery as reported by Arezzo *et al*[2] for colonic resections, with mortality rates of 1% (MAS) vs. 2.4% (open surgery) in a review of 23 clinical studies comprising 4,539 patients.

The reduced post-operative hospital stay time associated with laparoscopic surgery is widely accepted and has been shown true for a diverse range of procedures, including but not limited to; cholecystectomy [25], appendectomy [26], colonic resection [27], pancreatectomy [28] and gastric bypass in obese patients [29].

The advantages afforded by laparoscopic surgery over conventional surgery provide the patient with the best possible post-operative outcome and explains the rapid uptake of the procedure since its introduction. Laparoscopic surgery is not without its problems and limitations however. A number of engineering challenges are posed by the laparoscopic surgical approach, which are currently unmet and can be to the detriment of the surgeon and the patient.

The ergonomic and practical concerns of laparoscopic surgery are well documented. One of the major concerns is the minimal haptic feedback to the surgeon. Wagner *et al*[30] showed that with no force feedback, the magnitude of the applied force increases by at least 50% and the peak force increases by at least 100% and the number of errors resulting in tissue damage increased by a factor of three. A review of the literature by Van der Meijden *et al* [31] has shown that due to a lack of haptic feedback, operating time increases and there are more technical errors. It also shows that there are two possible approaches to tackling the problem of haptic feedback: increasing the mechanical efficiency of laparoscopic instruments or provision of sensory feedback. However, the author concludes that there is insufficient evidence to provide a definitive conclusion on the value of haptics as the literature, although it may be helpful in the early stage of training. This is contested by Westebring-Van Der Putten *et al.*[32] which conclude that regardless of experience, participants in a study of the efficacy of augmented feedback (visual, haptic or a combination) benefited when factors such as pinch force were investigated.

Laparoscopic surgery can also be counter-intuitive, particularly to surgeons in training. The fulcrum effect reduces the number of degrees of freedom to 4 and also causes an inversion of movement around the central point or trocar. More experienced surgeons can become 'automated' to the fulcrum effect[33]. Motion scaling can be seen as a by-product of the fulcrum effect, that is that small movements by the surgeon are translated into large movements at the tip of the instrument. This has been investigated by Prasad *et al* [34] in

relation to surgical robotics. The team investigated the effect of motion scaling and the tremor effect by performing accuracy tests using a 29 gauge needle to pierce a target using a robotic system with 3 different degrees of motion scaling, the latter two comparable to that of standard laparoscopy (1:1, 2.5:1 and 7:1). The results show that there was no difference between unassisted laparoscopy and robotic surgery with a motion scaling ratio of 1:1. Accuracy was significantly improved with both other motion scaling ratios ($p = < 0.001$). The study also confirmed that motion scaling by the surgical robot equalised the performance of both hands.

Throughout the execution of laparoscopic operations, the surgeon is in a stationary position, and this static position held for long periods, often leads to problems muscle with strain and fatigue. Neck and shoulder stiffness is associated along with fatigue. Studies by Berguer *et al.*[6] established that between 8% and 12% of surgeons frequently encounter pain in the neck and upper extremities as well as pain in other areas of the body as shown in figure 1. This conclusion was based on the results of a questionnaire which was held among a large cohort of surgeons, of which 149 questionnaire responses were received. The study also quantified the workload by the thumb and forearm when performing grasping actions using traditional laparoscopic techniques and haemostat. Volunteer surgeons (27 in total) carried out these exercises with collection of electromyogram (EMG) signals from the thumb and forearm muscles.

	Never (%)	Occasionally (%)	Frequent (%)
Neck pain	41	43	9
Neck stiffness	33	44	18
Shoulder/arm pain	39	43	12
Shoulder/arm stiffness	40	39	11
Hand and wrist pain	45	36	11
Hand and wrist stiffness	43	40	9
Hand and wrist numbness	59	26	8

Fig 2.1; SAGES ergonomic results questionnaire. [6]

The EMG results showed that for all muscle groups, the peak processed EMG signal was significantly higher ($p < 0.001$) when carrying out laparoscopic grasping in comparison to the haemostat confirming that laparoscopic instruments put far greater strain on a range of muscle groups [6].

In a subsequent publication Berguer *et al* discuss the problems concerning existing design issues of laparoscopic surgical instruments, particularly in regards to tissue grasping. In essence this report [2] identifies three problems: (i) the ringed pistol handle design as inadequate as it causes excessive flexion and ulnar deviation of the surgeons wrist when manipulating tissue; (ii) inefficient force transmission from handle to instrument tip such that the muscles have to work harder to accomplish the necessary forces; (iii) the handle which is not designed to accommodate the surgeons' fingers and is often too narrow leading to excessive pressures on the palm and fingers of the surgeons' hand. Laparoscopic surgery is also a more stressful task than performing the same surgery using the open surgical method. Berguer *et al* [35] showed that more concentration was needed and higher mental stress was recorded during laparoscopic surgery however the effect of this was not as varied with more experienced surgeons.

Another major concern of laparoscopic surgery is the trauma caused by grasping tissue which is related to the design of the instrument[36]. Laparoscopic surgery affords many benefits to the patient as discussed however it is not without its challenges which often come at the expense of surgeon comfort or ease of task performance due to the nature of laparoscopic surgery being restricted by small access ports to the surgical site. Progress has been made to reduce the number of access ports in order to maximise the benefits to the patient such as improved cosmesis but will often exacerbate the engineering and ergonomic issues (triangulation instrument clashing [5]) which are still true to the surgery and have not been sufficiently addressed 25 years after the first laparoscopic cholecystectomy[37].

2.1.3 Related minimal access approaches

Single incision laparoscopic surgery, also known by a variety of other names, single port laparoscopic surgery (SPLS), reduced port surgery etc. and natural orifice transluminal endoscopic surgery (NOTES) has garnered interest in the past ten years at the clinical level. The uptake of SPLS by surgeons has been substantial across the specialties, with a wide variety of procedures including cancer operations[38] Conversely NOTES has not been as widely accepted or applied to as many procedures but has led to the development and uptake in the more niche fields of endoluminal (as opposed to transluminal) surgery exemplified by per-oral endoscopic myotomy (POEM) for achalasia[39] which is likely to replace laparoscopic cardiomyotomy.

Specific ports have been designed to accommodate SPLS. The Dundee EndoCone [40], figure 1.2, provides access for instruments via 8 valved inlets of diameters between 5mm and 15mm, allowing for a range surgical instrumentation.

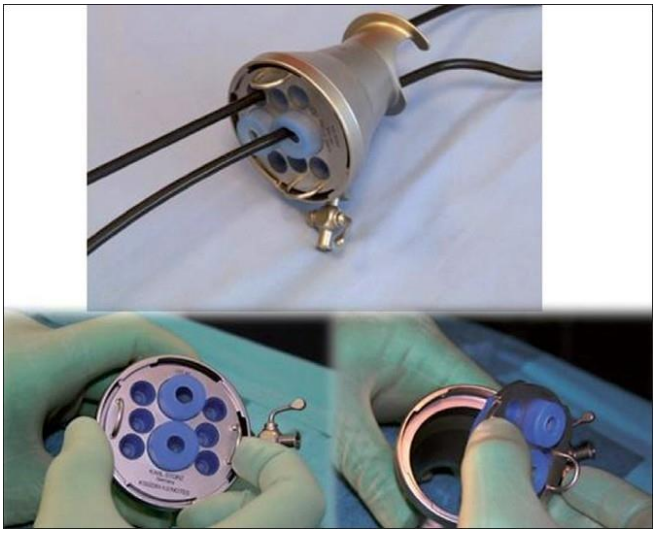

Fig 2.2; The Dundee EndoCone with detachable bulkhead [40] for extraction of specimen

Canes *et al*[41] discuss some of the major concerns associated with SPLS and NOTES in a review of the literature on the subject of single site surgery. It is stated that triangulation, retraction, instrument crowding and in-line vision are of the biggest concerns. Triangulation in SPLS is lost by the instruments being parallel to one another and often leads to the surgeon having to cross instruments and other counterintuitive movements. As many of the instruments used in SPLS are standard instruments which were designed for multi-port laparoscopic surgery, the rigid design does not provide the triangulation necessary and often surgeons must cross the instruments which is not ideal [41, 42].

In order to achieve optimal surgical manipulation during laparoscopic surgery, the instruments should subtend a manipulation angle of 60° with equal azimuth angles on either side of the optical axis (30°)[43]**.** Developments are being made to overcome the restrictions imposed by SPLS, e.g., curved laparoscopic instruments reduce the problem of triangulation, instrument crowding and clashing caused by straight instruments[44] Considerable work is still needed to fully optimise SPLS and the design of task-specific instruments is crucial to address many of the problems. These sentiments are echoed by Cuschieri[40] as well as other concerns he raises about the efficacy of this surgical approach, especially as currently there is insufficient evidence to suggest major benefits other than improved cosmesis over standard laparoscopy. It is suggested that in regard to instrumentation, robotics and master-slave devices may be a more effective way to fully realise the potential of single port surgery[37].

2.2. Trauma from grasping

2.2.1 Incidence of trauma and clinical consequences

A long standing issue of laparoscopic surgery is that of grasper-induced trauma and the possibility that graspers and grasping forces used in laparoscopy may have an adverse effect on patient health, with the potential of perforation, cell exfoliation and mucosal and serosal damage. A number of authors indicated the need for improved designs of laparoscopic graspers to reduce grasping-induced trauma on tissue. The design of the forceps grasper has not changed much since the introduction of laparoscopic surgery, often very slim with ridges or teeth to help grip tissue[45]. The size of contact area of the grasper determines the pressures exerted onto the tissue. If excessive, this pressure will damage the tissue unless a smart system is used which exerts sufficient force to hold the tissue without traumatizing it.

Heijnsdijk *et al.* performed a number of studies to investigate the effectiveness of laparoscopic graspers and their potential for tissue damage depending on the design[10] [45]. The first study was aimed at investigating the effectiveness of grasping and the duration of clamping using laparoscopic graspers. They found that the design of laparoscopic forceps does not provide the surgeon with any significant tactile feedback system and so the surgeon tends to exert excessive force on the target tissue, thereby causing tissue damage. It is also the case that positioning the long, rigid forceps may not be optimal because grasping has to be repeated often. Two operations: colectomies and cholecystectomies were studies to obtain insight into the mechanisms involved. During colectomies frequent short term grasping of the bowel occurs, the inverse is the case with cholecystectomies with a low number of grasping actions being performed however, for longer periods.

Twenty[36] five operations were analysed from video recordings of the procedures (ten colectomies and ten cholecystectomies, a further five cholecystectomies were performed by

resident surgeons with less than one year experience in order to evaluate the learning curve associated with this procedure). Each procedure was analysed with the clamped tissue, type of grasper and the outcome of grasping action being analysed. Each grasping action was labelled on the basis of; a) successful b) repeated clamping c) slip d) damage and e) undefined.

In the ten colectomies, the laparoscopic part of the duration of the procedure varied between 24 and 119min. The average success rate of the grasping action was 63% with the bowel being grasped an average of 117 times per procedure. During the cholecystectomies, which lasted between 14 and 62 minutes, a similar result on the percentage of successful grasping was recorded (61%) however the gallbladder was only grasped, on average, 26 times per operation. Grasping actions of the colon were more often than with the gallbladder (10% vs. 7%); however the gallbladder slipped significantly more often (17% vs. 7%). With damage occurring in 1% to 3% of all actions performed, this equates to around once every procedure. Gallbladder perforation occurred in five cases. Procedures carried out by resident surgeons lasted significantly longer but did not use many more actions; however fewer of the actions were successful.

High levels of repeated clamping indicates that positioning of the forceps was difficult to achieve in order to grasp the desired location and visible tissue damage indicates that excessive forces were used to grasp tissue, this may be due to the limited force feedback in the instruments. During procedures the surgeon was very careful not to perforate the colon because of the high morbidity and mortality risk. Greater force was needed when grasping the gallbladder than the colon probably to prevent slip. These greater forces caused perforation in five of the procedures studied. There is also an obvious learning curve as residents found it difficult to exert the correct amount of force (often too little) and this led to less successful actions and longer operating times. This study advocates that the design of graspers should be improved to provide more grip and less damage to tissue along with a force feedback system which would help to prevent tissue tearing and slipping.

Trauma caused by laparoscopic forceps has been the subject of a number of studies. Marucci *et al.*[46] in 2000 studied grasper-induced trauma during laparoscopic cholecystectomy. This prospective study had two main objective: to demonstrate the extent of the traumatic potential of laparoscopic instruments and to characterize by histology the nature of the tissue damage. In addition, the study produced a reproducible human model to allow future comparison of laparoscopic instruments with respect to their traumatic potential.

The gallbladders of 19 patients who had undergone a laparoscopic cholecystectomy were examined. A standard laparoscopic procedure was performed with four trocar access ports and Debakey pattern forceps were used in each case. The total time for which the forceps grasped the gallbladder was recorded. Once the gallbladder had been removed through the umbilicus, the site which had been grasped was identified and then excised and stored in 10% buffered formalin. A random second site was then excised and stored in the same way; this second piece would be the control specimen. The specimens were randomly labelled A and B. The specimens were then prepared and sectioned for histological evaluation and stained with haemotoxylin and eosin. A pathologist examined each specimen and rated the level of serosal change, interstitial haemorrhage, epithelial loss and focal thinning of the gallbladder wall [46].

From nineteen specimens, the pathologists was able to identify the gripped specimen in thirteen cases. In the remaining cases there was no damage found (4) or severe inflammation prevented assessment (2). The laparoscopic forceps grasped the gallbladder fundus for between 21 and 73 minutes (mean: 38min). Statistical analysis (Chi-squared tested) showed focal thinning and epithelial loss was present in significantly more sample specimens than control and that specimens which had been gripped for longer than 30 minutes showed greater focal thinning of the gallbladder wall than those that had been grasped for less than 30 minutes. Although no statistical difference was seen in interstitial haemorrhage there was more seen in the sample specimens.

Tissue trauma during laparoscopic surgery is largely avoidable by good surgical handling and technique (instrument and environmental awareness including grasping forces and depth perception) which is often gained with experience[47], it is however frequent as illustrated by the high established incidence of gallbladder perforation during laparoscopic cholecystectomy, with incidence rates of 13-40% of cases, and significantly higher than that of open surgery[46]. One of the main reasons for this is the limited tactile feedback to the surgeon through the instrument. It has been shown that tissue damage by graspers is directly related to the duration of grasping at any one time[46].

The same study [46] described how the angles at which laparoscopic forceps are deployed can cause problems for the surgeon. A study by Cartmill *et al*[11] investigated how pressures are generated at the tip of laparoscopic graspers and demonstrate increasing pressures with increasing angles. Furthermore, these pressures are not relayed to the surgeon when performing the procedure. In the study, 6 different laparoscopic graspers were taken from an operating suite stock, all of which were in good working order and a further two disposable instruments were used for testing. Tissue for grasping was simulated by a small strap of leather (1cm x 4cm) used as a resilient and reliable and reproducible model. A 250g (2.5N) load was applied to the end of the tip of the instrument, shown in figure 1.3.The force on the handle of the instrument was kept constant at all times throughout the experiment by using a rubber band. In order to record and evaluate the pressures exerted by the forceps a thin (0.1mm) pressure sensor was used in each experiment. Each sensor had 121 sensors in a 13mm square, giving a resolution of 1.4mm. The angle of the instrument was increased incrementally from 0° to 135° in stages of 22.5° perpendicularly to the simulated tissue, as shown in figure 1.4.

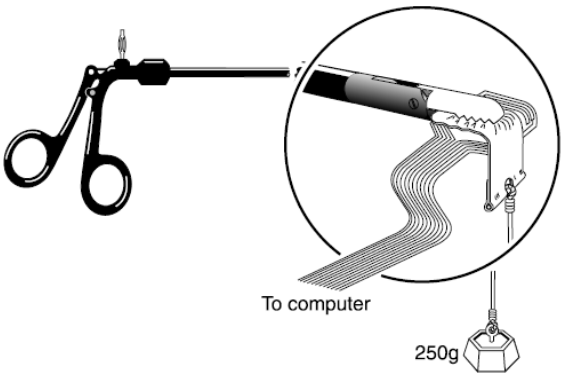

Fig 2.3; A schematic of the pressure sensor and load in relation to the forceps.[11]

The results show that as the angle of retraction increased, the pressures generated the tip of the graspers increased significantly. This was evident in all the instruments tested. There were considerable variations in the measurements for each instrument from each experiment shown by the magnitude of the standard deviation; thus pressures cannot be accurately gauged just by the angle of retraction. The mean of the maximum pressures of all the instruments increased from 216 to 643KPa as the angle of incidence increased from 0° to 135°. As a reference the maximal pressure which could be generated between the thumb and index finger were recorded to be in the order of 200kPa [11].

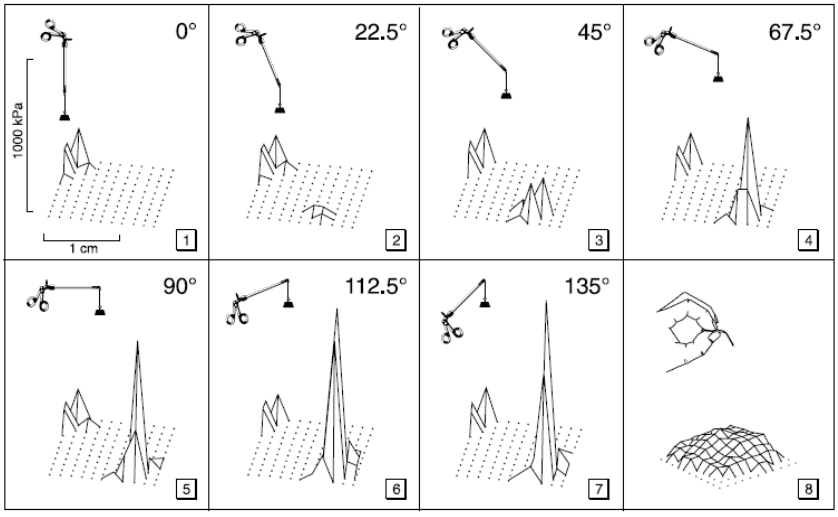

Fig 2.4; Typical example of the spatial distribution of pressure exerted by a laparoscopic grasper at various angles and the maximal pressure generated by thumb and index finger (bottom right).[11]

The operator of the instrument has no indication of the pressure generated at the end of the instrument as it occurs independently of the force applied to the handle. This means that even with careful handling by the surgeon, there will be potential to damage the tissue as the surgeon does not know how much pressure is being applied.

2.2.2 Measures to reduce trauma

2.2.2.1 Parallel occlusion and atraumatic grasping actions

The hinged mechanism of the vast majority of endoscopic surgical graspers creates a scissor like effect and causes unevenly distributed loads when force is applied to the tissue. This design causes high pressures in the proximal and distal areas of graspers during closure of the jaws. Alternative designs have been proposed to prevent or minimize the uneven distribution of these applied loads.

One such design is an atraumatic tissue grasper by Cuschieri and Frank[48] in which the grasper is designed to mimic how a hand would grasp an object as opposed to the pinching affect which most graspers exert. This grasper was evaluated on 32 patients over a year with the device being primarily used as a retractor and no trauma was recorded even in cases when retraction lasted up to an hour. Although these results are promising the device has not been widely accepted in laparoscopic surgery, probably due to the larger than usual diameter of 10mm for grasping instruments.

Parallel motion opening/occlusion mechanisms have also been shown to be advantageous over standard grasping mechanisms. The design of such devices provides an even load distribution across the surface of jaws when grasping tissue. Frank *et al* [49] developed a deployable parallel action clamp for the occlusion of the bowel when performing an anastomosis. The device comprised of a stationary lower jaw connected to the upper jaw by a shape memory

alloy (SMA) spring which applied the closing force necessary to successfully occlude the bowel.

More recently, Vakili *et al* [50] reported the development of a laparoscopic parallel action grasper which provides force feedback to the surgeon through a pressure sensor. The aim of the grasper was to minimise the amount of tissue damage, whilst providing the surgeon with haptic feedback. In addition the device had an ergonomically designed handle, with the opening and closing mechanism provided by a ten-bar linkage as shown in figure 1.5.

To provide feedback to the surgeon, three methods were considered; auditory, haptic and visual but the researchers[50] chose tactile feedback in the form of a vibrating trigger, as this was the most natural method. A piezo-resistive force sensor was used to detect the applied forces on the tissue, this was used in a closed loop system. At the pre-set force, the vibration motor vibrated to indicate excessive pressures were being applied to tissue.

Analysis of the mechanism design was performed to establish the opening width of the jaws in regards to the link lengths, the stresses on the links and pins when actuation was performed and the non-parallel ‘play’ in the jaws.

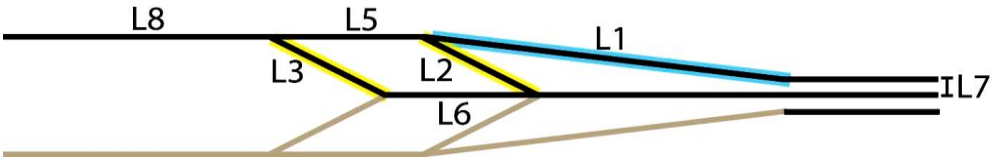

Fig 2.5; Schematic deign of the 10-bar linkage showing the relationship between link lengths. The length of the mechanism for actuating the jaws is greater than the whole length of the grasping area [50].

To provide the required distance of 25mm between the upper and lower jaw when fully opened the length of the L1 link was found to 40mm. The maximum stress on the linkages was found to be around 18Mpa assuming that there was a force of 0.5N acting on the tip of the upper jaw. This is lower than the fracture point of surgical stainless steel by a substantial margin; however

the assumed applied load would be small for this application. Under the same conditions the stress on the pins of the instrument was found to be 30Mpa. The amount of horizontal play found in the mechanism design was substantial when the mechanism was fully closed as shown in figure 1.6. This resulted in problems with grasping thin tissue.

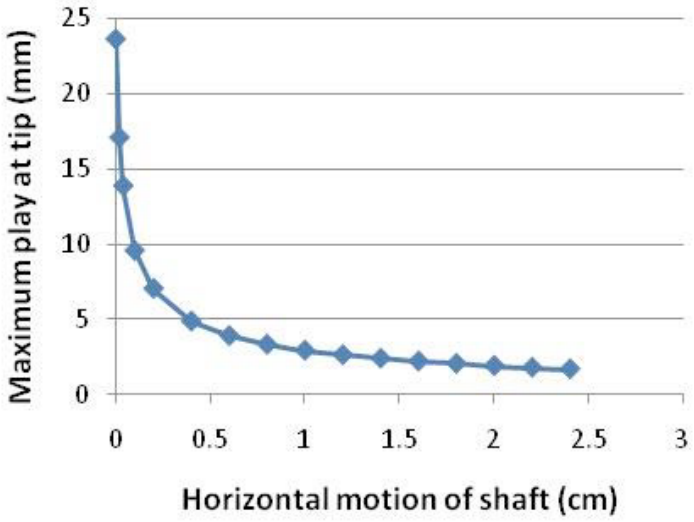

Fig 2.6; Tip deviation vs. Motion of the shaft [50].

Empirical verification of the data showed that, by in large, the theoretical predictions were correct or within the range of the observed region. The horizontal deviation at the tip of the instrument was found to be up to 10mm which is the same as the diameter of the instrument. This seems like an unacceptably large amount of horizontal movement for the application.

The device design provides an insight into the difficulties of developing an instrument which provides parallel action motion. The proposed 10-bar linker in this design would mean that to open the jaws of the instrument by 25mm the linkage would have to be in the region of 130% to 140% longer than the tissue contact area. The designed mechanism would also cause a translational movement due to the opening and closing of the parallelograms within the design. Although this would not be as great as that observed in the 4-bar linker design, it would still be of a concern when used in a two dimensional laparoscopic system. The 10 bar link design

differs from a standard 4 bar link as the linkages are mirrored around to central body (fig 1.5) this creates an outward motion meaning that both surgical instrument jaws are displaced in the opening and closing of the mechanism, a 4 bar design would mean that one jaw would remain stationary at the cost of a larger translational movement.

2.2.2.2 Fenestrations

Fenestrations are often found in the jaws of surgical (including laparoscopic) instruments as it is widely believed that the fenestrations prevent tissue slipping from the jaws due to tissue bulging through the aperture, thus preventing the tissue from being extruded through the small opening between the instrument jaws. However the benefits of fenestrations in the instrument jaws have been contested by at least one published study [51] which concluded that the bulging effect was not observed during experiments and that fenestrations have a negative effect on tissue grasping as they lead to more frequent tissue damage at lower applied loads. Such damage is due to the fenestrations reducing the surface contact area between instrument and tissue which inevitably means higher local pressures and potential to cause damage when large grasping forces are applied.

The study was performed by testing the position of fenestration on the jaws of the grasper. The fenestrations used were circular with diameters of 3mm and 6mm. A pair of equal but opposing jaws was used to clamp tissue and loads of between 1N and 10N were applied. Pull forces of 2.5N, 4N and 5N were used to pull the tissue from the jaws. The tissue was then investigated for macroscopic damage caused during the clamping and retraction. Tissue damage was defined as visible changes in colour or transparency, tears to the layers of the bowel or imprints on the tissue after clamping. The results were analysed by analysis of variance (ANOVA).

The results showed that with the larger fenestration caused tissue damage at around 1N. The graspers which caused least damage were non-fenestrated. The amount of pinch force necessary to cause damage was also found to be lower when the fenestration was closer to the

distal tip of the jaws. The difference in retention force or amount of force necessary to cause the tissue to slip from the graspers was not significantly different.

This is the only study found in a review of the literature on the impact of fenestrations in laparoscopic graspers [51]. The authors conclude that because fenestrations reduce the surface contact area, the pressures resulting on the tissues at various applied forces during closure of the instrument increase, in comparison to non-fenestrated designs. Although this conclusion appears logical, this study used circular fenestration designs which are not often employed in surgical instruments. Most fenestrated graspers and clamps used in laparoscopic graspers are rectangular in shape and of a larger area than those used in this reported study.

2.2.2.3 Surface profiling

Heijnsdijk *et al* performed a study[45] aimed at understanding the slip and damage properties of laparoscopic graspers in order to predict the optimum design features incorporated into laparoscopic graspers which would minimize both tissue damage and slip. When grasping tissue surgeons exert a combination of pinch and pull forces. The correct combination of these two forces is crucial for successful grasping without causing damage. If the pull is high compared to the pinch force the tissue will slip and if the pinch is high compared to pull forces then damage will occur. If both forces are too high then damage will occur with the possibility of tearing. This study examines the slip and damage properties of a number of standardized laparoscopic grasper designs.

The experimental setup which was used to test the various graspers consisted of a lever hung by three ropes. Two springs attached to the lever meant that pinch force could be changed by moving the springs. Pull force was applied by a spring scale at the end opposite the graspers. The grasper jaws were exchangeable and the tissue was clamped between the jaws. During the experiment the tissue was kept wet [45].

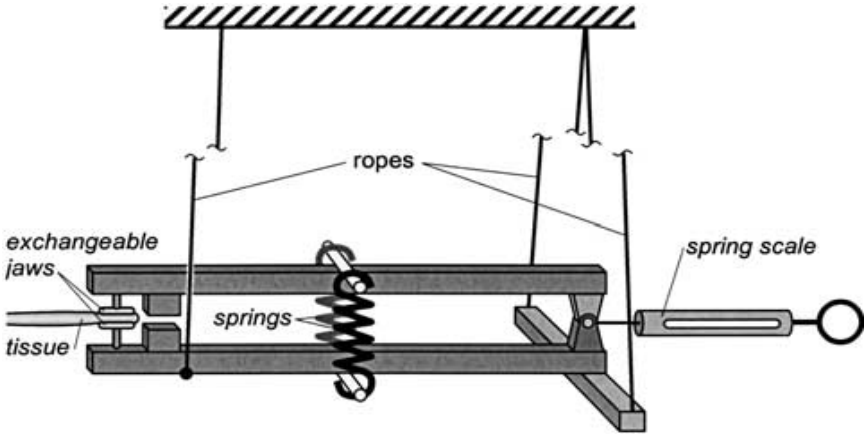

Figure 2.7; Experimental setup which shows the lever is suspended from three ropes which creates frictionless motion in the longitudinal direction. Tissue is clamped between the jaws with pinch force being provided by the lever mounted springs. Pull force is provided by the spring scale. [45]

Five different types of jaws were tested in this experiment; a) Flat, each 8mm wide and 4, 8 and 16mm long. B) 8x8mm rectangle with protruding hemispheres which were 2mm in diameter and protruded from the surface by 0.25, 0.5 and 1.0mm. There were two configurations of the hemispheres. C) Profiles used were the same as those in laparoscopic forceps with a diamond profile and a ribbed profile which protruded 0.3mm from the surface. D) Consisted of three rectangles of the same shape with a diamond profile, profiles protruded 0.15, 0.3 and 0.6mm from the surface.

The slip force F_s was defined as the minimal pinch force required to prevent slip while pulling with 5N; as the study found that the average pull force which surgeons apply to provide enough tension in the tissue is 2.5N with the maximal pull force being just below 5N. The pinch forces applied ranged between 2N-27N. The pull force was increased at a rate of 1N/s until the tissue slipped out of the forceps entirely. Damage was defined by a visual tear in one of the layers of the bowel wall; this was evaluated by two observers. The damage force F_d was defined as the maximal pinch force that could be applied without causing damage to the tissue when pulling at 5N. A slip-damage ratio was then calculated.

The results show that for the flat graspers, increasing size of jaws increased slip force significantly. The slip-damage ratio was just above one, i.e., a pinch force slightly higher than that needed to prevent slip would cause damage. The jaws with the hemisphere profiles showed that both F_{Damage} and F_{Slip} decreased with increasing protrusion. The slip-damage ratio for these jaws was between 2 and 4. In the final group with the diamond and ribbed profiles the slip force decreased significantly in comparison to the flat jaws from 22N to approximately 3N however the damage force remained approximately the same. The slip force was significantly higher with the protrusions of 0.15mm compared to those of 0.6mm.

These experiments give valuable information about the size of contact area, type of profile and depth of profile when it comes to designing laparoscopic graspers with regard to safety and usefulness. The diamond shaped profile provided a slip-damage ratio of 9 which implies that the surgeon can safely exert a pull force 9 times larger than that which is necessary to prevent slip. Even a small profile of 0.15mm was enough to provide a significant change in slip force without effects on damage force. The friction coefficient previously suggested to be best for bowel clamping was between 0.6 and 0.9 however in this study a higher coefficient of friction seemed to be best at 1.7. In conclusion the shape and profile influence to a large extent the slip and damage forces and ultimately tissue damage. A laparoscopic grasper with a large surface area and a slight profile would provide the best performance as it would both lower the slip force and enhance the damage force. Combined these could reduce the number of laparoscopic injuries caused by grasper trauma to tissue.

2.3 Actuation methods for minimal access surgical instruments.

2.3.1 Direct Current Motors (DC motors)

2.3.1.1 Theory of operation

Direct current motors or DC motors generate torque based on a coupling between electrical and mechanical devices by way of magnetic field. Lorrentz law states that when a current carrying wire is placed in a magnetic field, each of currents moving charges will experience the Lorentz force and this induces a macroscopic force on the wire. This theory is applied to DC motors by placing an iron core wrapped in a coil inside a magnetic field. When a current is applied to the coil the attraction and repulsive forces produced by the electromagnetic field will cause the core to rotate and produce torque.

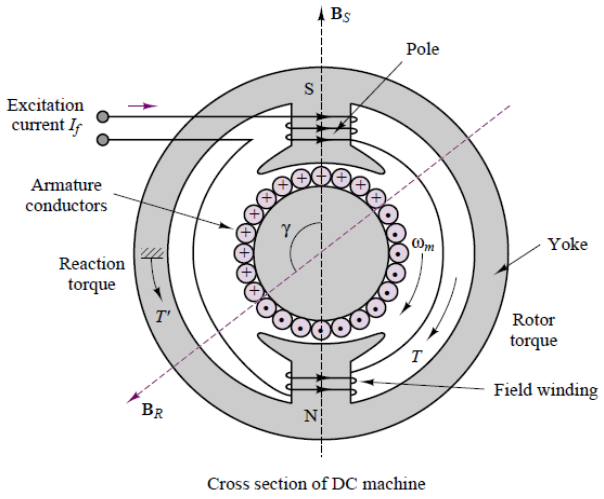

Figure 2.8; Two pole DC machine which shows the working principle of DC motors. Torque is produced due to the interaction between magnetic forces when an excitation current is applied [52].

A cross section of the DC motor is shown in figure 1.8 and is a basic two pole DC motor; however it is not representative of a practical motor. The two poles are clearly indicated in the diagram. Torque is produced by a consequence of the magnetic forces between the stator and

rotor. Maximum torque is produced when the angle, ϒ, between the stator and rotor poles is 90 degrees. In order to keep this torque angle constant and produce the maximum torque possible the current distribution in the rotor winding is kept constant by the commutator. The commutator is a mechanical switch and is shown in figure 1.9.

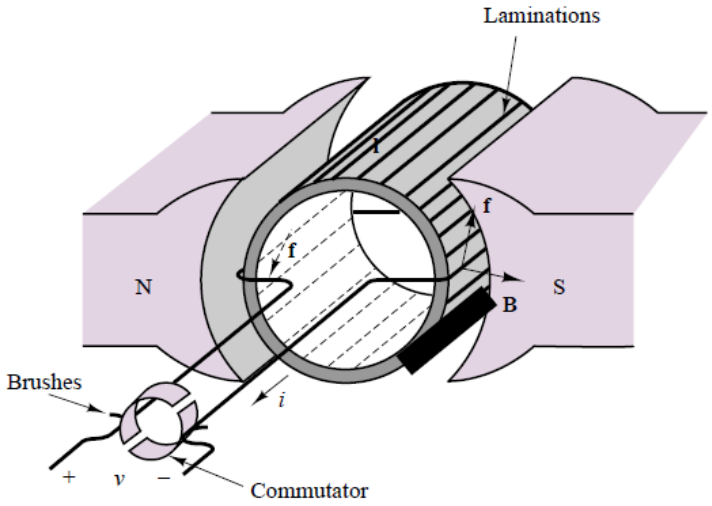

Figure 2.9; Simplified diagram of the stator, rotor and commutator of the DC machine in order to create an output torque. [52]

The instantaneous position of the rotor is given by the expression:

$$\emptyset = \omega_m t - \gamma \tag{2.1}$$

The commutator is fixed to the rotor and is made up of six segments. As the commutator rotates the rotor magnetic field rotates with it up to 30 degrees. At this point, the direction of the current reverses as the brushes make contact with the next segment. The direction of the magnetic field therefore becomes -30 degrees. This switch will continue again and again and will keep the rotor moving however in this example the torque angle is not always at is optimum of 90 degrees and so will not produce the maximum torque output continuously. This is addressed in real world situation by having many more segments on the commutator. This

will reduce the torque fluctuation greatly until almost constant torque output can be achieved [52].

The DC motor can be easily controlled over a wide range of speeds and to almost zero rotations. It also has the benefit of rapid acceleration and deceleration which can provide with relatively accurate positioning. The major drawback of the conventional DC motor is that it is prone to wear caused by the commutation through the brushes and can also produce a high amount of electrical noise which causes interference with neighbouring circuitry.

A variation of the DC motor which has a number of advantages is the brushless DC motor. The basic principle of operation is essentially the same however the brushless DC motor relies on the use of electrical switching to reverse the direction of the supply current as opposed to the mechanical switching via brushes in a conventional DC motor. The main advantage of this system over conventional DC motors is that it is less susceptible to wear (as it has no brushes) however the drive electronics needed to control the system are more complex. As the switching is performed by a transistor there are known to be voltage ripples and thus torque ripples in the output of the motor. Reducing these torque ripples by increasing the number of windings of coil on the stator is one option however this again leads to more complicated drive electronics[52].

Theoretically the power and torque output of a miniaturised electromagnetic motor should be similar to piezoelectric motors[53] however miniaturisation is an issue mainly because of manufacturing at such small scale. The DC motor is far more complex with coil windings and magnetic parts which are brittle and difficult to machine. To address these issues various manufacturing techniques have been proposed such as depositing magnets through sputtering[53]. These techniques have been applied to brushless DC motors however the power density of these motors are at least an order of magnitude lower than conventional DC motors[54].

2.3.1.2 Applications in surgery

DC motors have been integrated in numerous ways into minimally invasive instruments and therapeutic devices. One of the more advanced systems described which employs the use of DC motors is presented by Piccigallo *et al*[8]. The device is a highly dextrous miniature robot with 6 degrees of freedom (DOF) which is inserted through a 30mm diameter port and is teleoperated. It is intended for single port laparoscopic surgery (SPLS).

The single port laparoscopy bi-manual robot (SPRINT) developed by the ARAKNES IP Project funded by EU FP7 program and coordinated by P Dario and A Cuschieri is a master-slave device which will reproduce the movements of the surgeons hands. The device consists of up to four arms which are inserted sequentially through the Dundee EndoCone following insufflation of the abdomen, with full assembly of the robot inside the abdomen (figure 1.10 & 1.11).

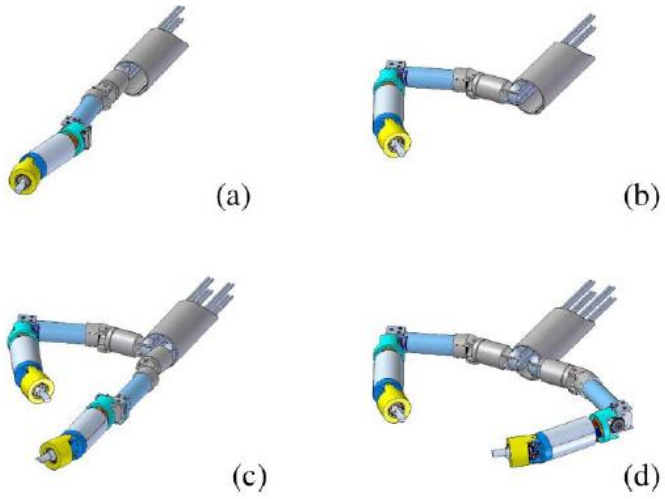

Figure 2.10; Sequential insertion of the SPRINT robotic arms. [46]

The SPRINT robot comprises two manipulator arms, each with 6 DOF and a stereoscopic camera. Extra instruments and assistive tools are inserted through the EndoCone. The wireless

computer interface with monitors is on a stand near the patient; as the surgeon operates in the sterile field close to the patient as distinct from the da Vinci robot (Intuitive Surgical, USA).

Each arm has 6 DOFs, shown in figure 1.12 comprising of a roll-pitch-pitch motion and a roll-pitch-roll motion which provides the dexterity necessary to replicate the movement of the surgeons' hand. Actuators for the robot where selected on merit of predefined requirements of gripping force and speed. The actuators were embedded into the device itself as opposed to using an external motor with flexible transmission rods with the exception of the motors for actuating the shoulder joint which were external due to size restrictions. In total 6 actuators were used to control the various joints.

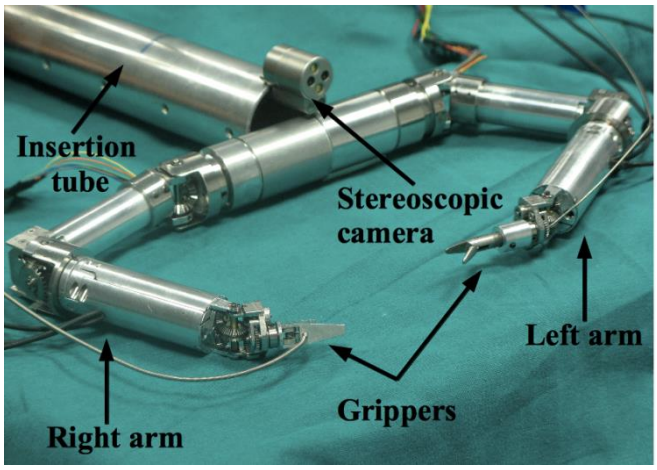

Figure 2.11; Assembled SPRINT robot with stereoscopic camera and two robotic arms. [8]

The shoulder mechanisms were actuated by two external DC motors which exerted a torque of 700Nmm at a speed of 500 degrees/second at a power of 18W. The elbow mechanisms employed brushless DC motors for actuation which could exert a torque of 360Nmm in a small space envelope of 12mm. This meant that the desired maximum force at the tip of 5N could be achieved. Finally the wrist mechanisms also contained brushless DC micro-motors (6mm diameter) which controlled the distal DOF (roll-pitch-roll) and provided a torque of up to 50Nmm.

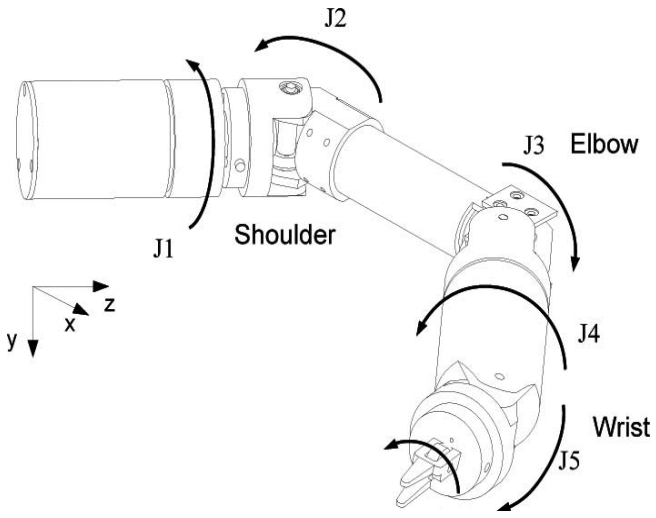

Figure 2.12; DOF at various joints of the SPRINT robotic arms. [46]

Preliminary test and evaluation of performance on a first prototype were carried out to validate the concept of the design. The group achieved the desired speed of motion and force with the first prototype, table 1.1, however the size of the instrument was larger than desirable. One issue which occurred when testing the first prototype was the occurrence of backlash at the joints; it is proposed that this will be resolved in subsequent designs with more accurate coupling and higher teeth numbers in the gears.

	Desired Performance	**First Prototype**
Speed	1 m/s	1 m/s
Force	5 N in every direction	5 N in every direction
Max. Diameter	18 mm	23 mm
Total Length	120 mm	142 mm

Table 2.1; Desired performance vs. prototype performance. Force and speed requirements were attained in the first prototype [46].

Pick and place tests were carried out with the first prototype where 5 engineers and one experienced surgeon were asked to pick rings up from one ring holder and place it on another which was 90 mm away in a horizontal direction and 60mm in the vertical. The subjects were

asked to view the scene on a monitor to mimic the surgical situation. Each subject carried out 10 replicates of the pick and place. Results from this small experiment showed that on average it took 25s for each action to be carried out.

The first prototype of the SPRINT robot consisting of 6 actuators and a number of geared joints to provide 6 DOF with the arm has shown that micro DC actuators can provide the necessary forces to manipulate tissue in relatively small areas. The drive in modern laparoscopy is towards instruments with a smaller diameter which is not met by this design but does show that DC micro motors can be integrated, not only externally, into laparoscopic device and achieve the desired effect.

There are a number of other multi-branched instruments which have been proposed in the literature or are currently on the market[32]. The SPRINT robot was selected for dexterity and the way in which a number of micromotors were used within a deployable device and configured in such a way to provide the necessary torque output.

In contrast to the SPRINT device Mirbagheri *et al*[55] proposed an instrument for the manipulation of large body organs during laparoscopic surgery which employed a linear actuator which would be external with a rigid transmission to open and close the instrument jaws. The instrument comprised three elongated fingers for the grasping and manipulation of organs attached to a rigid shaft similar to a standard laparoscopic instrument. It fits through a 10mm trocar and opens to an 80mm diameter in order to grasp organs. Figure 1.13 shows the parallel motion mechanism and the instrument for grasping organs. Detailed force analysis was carried out to determine the forces necessary to open and close the graspers as well as to exert the necessary forces to the tissue.

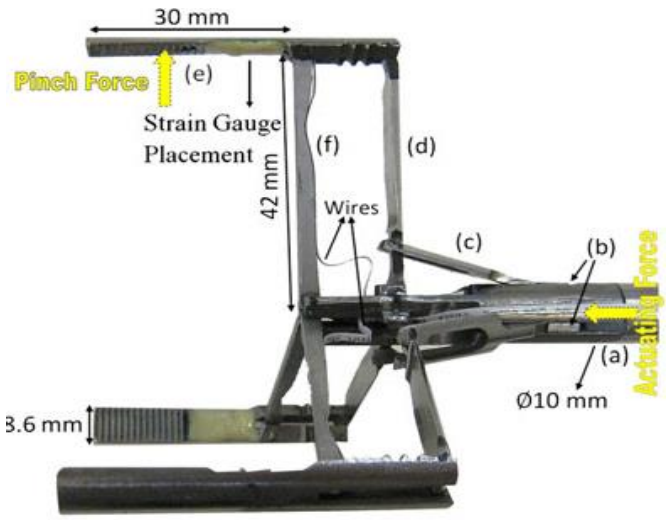

Figure 2.13; Parallel action grasper for large organ manipulation. Showing an opening diameter of 80mm and strain gauges mounted on the active grasping area. [47]

The group then optimized the design and actuation force by using MATLAB and reduced the required actuating force by 40%. After this optimisation the actuation force was still considerable and so the group selected a linear actuator that would be able to exert a maximum pressure under each finger of 50kPa and a maximum desired pinch force of 10N. The final actuator was a combination of two Maxon motors (Maxon motor, GmbH, Germany). The overall length of the actuator was 74mm which would be too large to fit into the distal tip of the instrument. The overall diameter of the actuator was not given.

Simulation of the actuator and design was carried out in order to investigate the efficacy of the device. The results of the force analysis indicate superior performance over previous designs as higher pinch forces are achieved with lower applied forces when dealing with large organs.

Therapeutic devices have also been integrated in devices with DC motors. The Versatile Endoscopic Capsule for gastrointestinal tumour recognition and therapy (VECTOR)[9] was developed as the first endoscopic capsule to have on-board locomotion. Wireless capsule cameras which are swallowed by the patient take thousands of images while

passing through the GI tract however as they are completely reliant on the peristaltic movement of the gastric wall to move there is no control over the position of the device which could lead to important anatomic structures being missed. Alonso *et al*. [9]describe the main problem of developing such a system was miniaturisation of the components, of which there are many for such a small device.

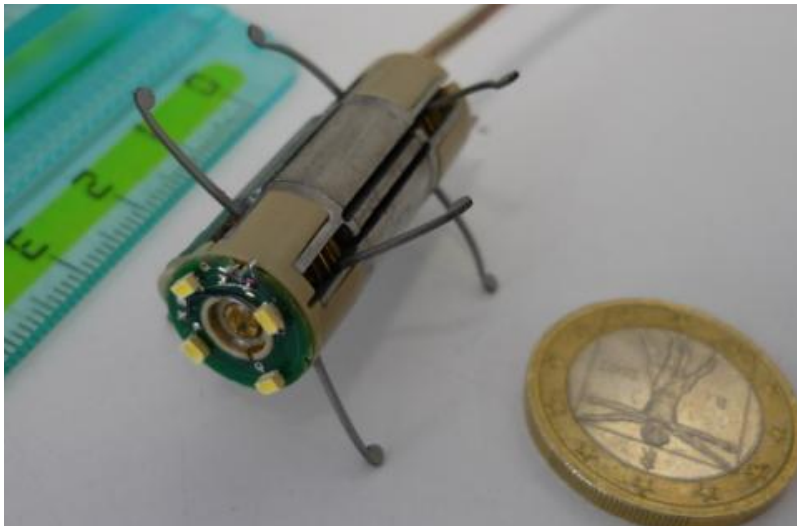

Figure 2.14; Overview of the VECTOR capsule endoscope. [9]

The VECTOR comprises of a central control unit, a CMOS camera, a bi-directional RF link and a group of peripherals, figure 1.14 shows an overview of these components. All of the electronics to control the motor, LED's and focus was also contained on-board. As the main purpose of the VECTOR is to obtain images of the GI tract the system integrated a CMOS camera along with a liquid lens which would allow for auto-focus and provide better images. These images were compressed and sent via the RF link.

The active locomotion of the VECTOR was performed by 4 legs connected to two brushless DC motors. Further advantages of the VECTOR include the ability to mount various actuators and sensors onto the device for measuring pH levels or tissue sampling. These peripherals would be interchangeable and patient specific due to the size of the device. The capsule is

33mm in length and 10mm in diameter. The group minimised the size needed for the electronics by developing a chip which would house all of the control and drive electronics for the capsule or an application specific integrated circuit (ASIC). The microcontroller was also implemented into the same chip.

The implementation of this ASIC and system on a chip (SoC) into the legged endoscopic capsule was initially tested on a wired prototype. The capsule was controlled via a USB cable to a computer. A JAVA based graphical user interface was developed to communicate with the capsule and control the locomotion. The capsule was only tested in a table top situation to investigate the power consumption. The authors had complete control of the system when using the SoC including the ability to drive motors one at a time or both at once. This method of assembling all of the control electronics onto one chip has meant the high voltages and currents needed for modern micro-robotic electronics can be achieved in a relatively small space. Furthermore the system described gives the surgeon control over the therapeutic capsule, which can be directed to areas of interest and the lens can be focused for a better image as well as reducing the time needed through active exploration and not relying on the natural movement of the GI walls.

These are just a few of the ways in which DC motors can be applied to a surgical environment. The benefits of the DC motors are; they can produce high torque, are reliable and easy to control with high accuracy. One of the drawbacks, as discussed, concerns limitations of the size reduction possible with DC motors however as stronger permanent magnets are being developed and become available, further size reduction will be available without such a drastic reduction in torque.

2.3.2 Piezoelectric motors

2.3.2.1 Theory of operation

The piezoelectric effect occurs when a crystalline structure exhibits an electrical charged when mechanically deformed. The inverse is also true, when exposed to an electric field the structure will mechanically deform. It is this inverse piezoelectric effect which is employed in the development of piezoelectric motors and actuators. There are a number of known piezoelectric materials including the ceramics lead zirconate titanate (PZT) and quartz amongst others and certain polymers like polyvinylidene fluoride (PVDF).

Piezoelectric materials produce acoustic or ultrasonic vibrations when subject to an electric field. These vibrations are in turn, through a wide variety of piezoelectric motor designs, translated into linear or rotational motion. This can be done in a number of ways, which are broadly divisible into two categories; standing and the propagating wave types.

Domain interactions and defects in the various piezoelectric materials have an effect on the piezoelectric properties and the hysteresis loop of the material[56]. This has led to these materials being defined as ‘hard’ and ‘soft’ piezoelectric materials. The soft materials are characterized by high hysteresis and piezoelectric constants and are preferred for bi-morph or multilayer actuators whereas hard materials exhibit the inverse effect.

Unlike standard electrostatic motors, the efficiency of piezoelectric motors is not influenced by the size of the motor. A basic piezoelectric motor is shown in figure 1.15; it consists of a high frequency power supply, a piezoelectric driver and a slider [57]

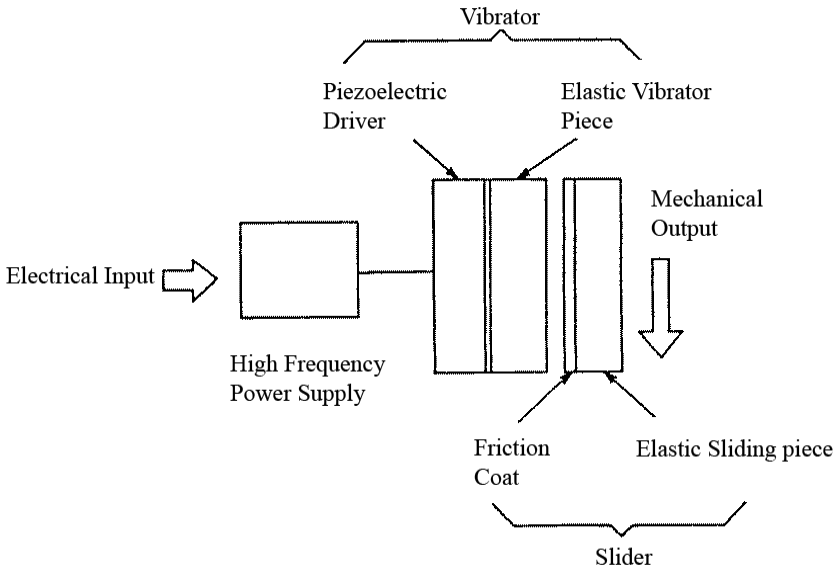

Figure 2.15; Basic piezoelectric motor. Mechanical movement is caused by vibrations due to the piezoelectric driver being driven by a high frequency power supply [57].

The standing wave piezo-motor consists of a vibrating tip which is connected to a piezoelectric driver. As the tip vibrates, it generates a flat elliptical movement. The rotor causes a restriction and thus the tip bends; between the vibration and the friction an elliptical movement is generated i.e. a torque. This is the basic principle of a standing wave piezoelectric motor. Theoretically the standing wave motor can be up to 98% efficient; however this type is difficult to control[57].

A propagating wave type motor consists of two standing waves at a 90 degree phase difference. The coupling of these waves creates an elliptical movement. This motor design requires two vibration sources and hence a low efficiency (50%) but it enables very good control of bi-directional movement. An illustration of the propagating wave piezoelectric motor is illustrated in figure 1.16.

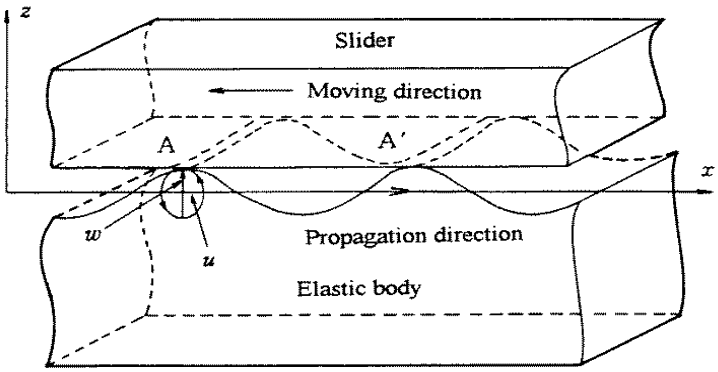

Figure 2.16; Propagating wave piezoelectric motor theory [50].

Both standing wave and propagating wave designs can be implemented to create linear or rotational motion.

2.3.2.2 Applications in surgery

Saedi *et al*[58] reported a conceptual design for an actuated endoscopic needle grasper. The group propose a hybrid design which contains both a DC motor and a small piezoelectric motor, each with a different objective. The team set out a number of design specifications which included; a diameter not exceeding 15mm, device grasping action with a pinch force between 16 - 40N, quick response time, operating room compatibility and stroke length and a maximum actuating force of 250N.

A hybrid actuator was also investigated and a combination of a PZT piezoelectric actuator (hollow stack type) and a DC micro-motor were selected. The design actuators were arranged in a two phase serial combination. The DC micro-motor would provide the large displacement necessary to open and close the jaws of the instrument whereas the PZT actuator provided the linear motion to grasp the needle with the necessary force, figure 1.17.

In the first phase, the DC motor rotated to close the jaws. After closure of the jaws, a voltage is applied to the PZT actuator which induced instant expansion (second phase), pushing all

components forward by a few microns sufficient it is enough to transmit the necessary force to the already closed jaws to secure a good grasp on the needle. To open the jaws the phase sequence is reversed and because of the high response time of the PZT the jaws can open very quickly. As the proposed design is conceptual simulation was performed by finite element analysis to determine if a prototype could achieve the displacement and force necessary to secure a needle in the jaws.

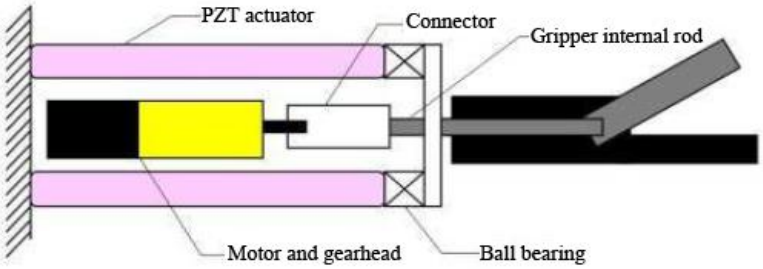

Figure 2.17; Schematic of the hybrid DC and PZT actuated needle grasper. [58]

Simulations were performed referencing commercially available PZT actuators. An actuator with a nominal displacement of 30 µm was selected. Geometrical considerations for the needle holder were also based on a commercially available product. The results of the FEM analysis showed that the needle rod moved by about 50µm under 250N of force. This results in a 22N gripping force which is within the range of the specification including a needle driver with a 10mm outer diameter.

Although, the results indicate superior functionality what would be achievable with a DC motor, there are a number of design considerations which would be difficult to simulate, e.g., backlash and a completely non-back driveable DC motor which would impair the gripping force. Along with these design constraints, there are engineering tolerances needed to prevent any parts moving a few micro meters when under the large forces exerted. The development

of hybrid style actuated surgical instruments could in the future address some of the problems when developing an actuated instrument with multiple degrees of freedom.

As described previously, work is being done to develop actuated capsule endoscopes in order to have more control. This would make procedures with the capsules quicker and give the surgeon more control to direct it to areas of interest. The capsule described in the previous section was based on 8 legs being driven by a DC motor. Kim *et al*[59] report on the development of a piezoelectrically driven capsule endoscope. As piezoelectric actuators have a relatively small displacement, the design of the actuator described was developed to provide a larger displacement through mechanical amplification. This was done by employing an impact based piezoelectric actuator which comprised of a piezoelectric actuator, a copper base plate, a printed circuit board (PCB), a mobile element and a shaft to guide the element as shown in figure 1.18.

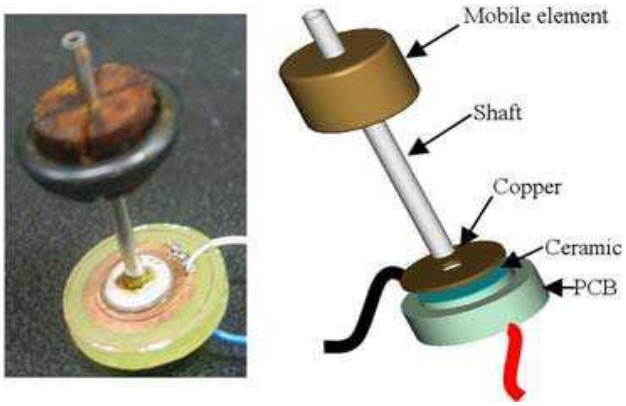

Figure 2.18; Left: Fabricated piezo actuator. Right: 3D model of the piezo actuator. [59]

The maximum diameter of the actuator is 11mm and it weighs only 0.6g. The actuator works by applying a high voltage saw-tooth wave to the ceramic part. By reversing the direction of the saw-tooth wave, the mobile part will start to retract and thus continuous motion is achieved along the 17mm in length shaft, figure 1.19.

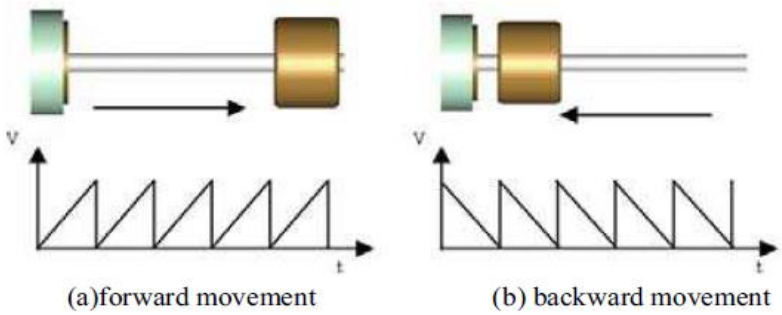

Figure 2.19; Working principle of the piezo actuator according to the direction of the applied pulse wave [59].

The proposed capsule had two separate bodies conjoined by a shaft. In order to address the problem of the device moving forward and then moving back to its original position, the outer bodies of the capsule have ridges (inspired by insect claws) described as clampers, figure 1.20. As the actuator reaches maximum stroke, these clampers will hold onto tissue and pull the rear part of the body towards it. This process is repeated to achieve a forward motion.

The prototype is made to a diameter of 14mm and the outer body is made from acetylene.. The total length of the body in retraction is 29.5mm and in elongation it is 41mm. The theoretical speed of the robot is 3.92mm/sec.

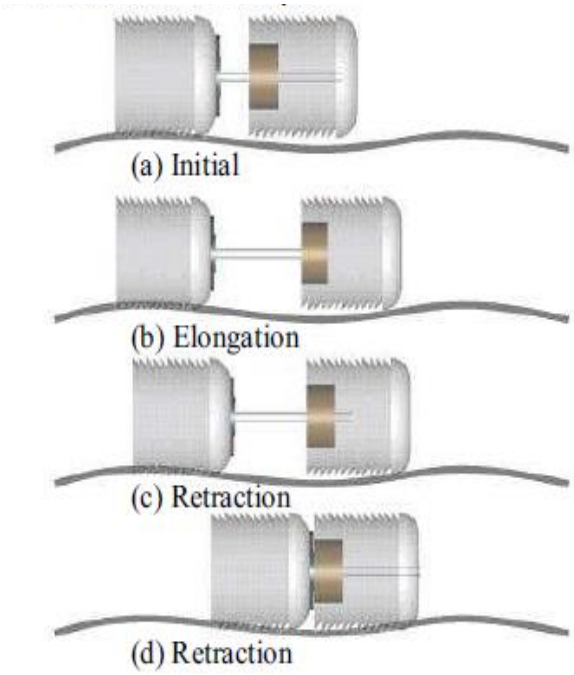

Figure 2.20; Proposed design with insect inspired clampers and the theory of locomotion for the capsule [59].

The wired prototype was tested under a number of different conditions including: on different surfaces, different clamping designs and different stroke lengths. The control and data acquisition was performed by Labview (National Instruments, Austin, Texas, USA). For the different surfaces, silicon coated with oil and ex vivo porcine small intestine was chosen and results were compared to theoretical results. The stroke lengths investigated were 5mm, 6.5mm and 11mm and the different clamping designs varied by changing the depth of pitch as well as having a stripe design.

The results from the varying surfaces experiment showed that when moving along silicon and small intestine, the speed was 3.34mm/s and 2.23mm/s respectively. This is 15% and 43% less than the theoretical speed..

The results from the clamper design showed that the higher depth of pitch performed most successfully as it caused the most amount of friction between the small intestine and the robot

although this is not significant and is only marginally better than other designs. A combination of longer stroke length and optimisation of clamper design could increase the speed and overcome the negative effect that the deformation of the intestine has. The drawbacks of such a design are that it has to maximise its stroke length which could be an issue when navigating through an internal organ. Also, piezoelectric actuators require a large voltage (100V) therefore a voltage amplifier and a large battery are necessary which makes it extremely difficult to develop a deployable, wireless endocapsule with this technology. Further improvements to these fields are needed before this concept can be realised.

Piezoelectric motors have also been integrated into a laparoscopic instrument by Schlaak *et al* [60]The INKOMAN (intracorporeal manipulator) device looks to overcome the issue of workspace and triangulation restrictions associated with laparoscopic surgery. It does this by providing the surgeon with an intuitively controlled instrument which has 4 DOF at the distal end. The instrument is driven by piezoelectric actuators and controlled with one hand using a 3-DOF joystick. There is also the possibility to accomplish pre-programmed cutting movements.

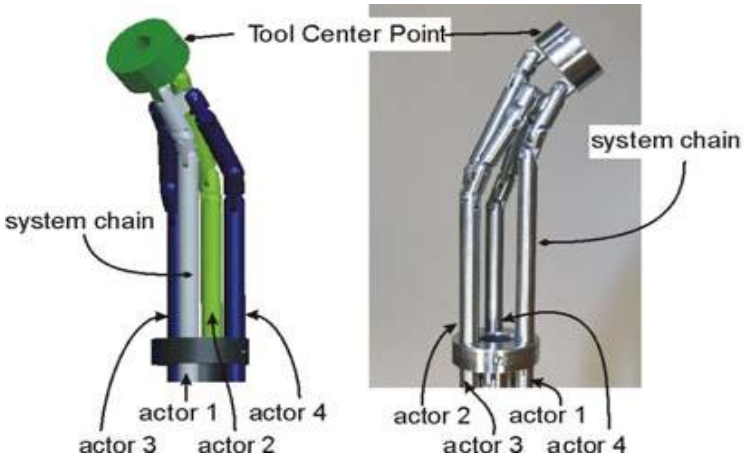

Figure 2.21; Parallel kinematic mechanism comprising of 4 actors driven by piezoelectric motors [60].

Piezoelectric motors are coupled with driving rods through a parallel kinematic mechanism, shown in figure 1.21. The mechanism is passive and thus the centre point of the mechanism must be calculated numerically on the fly. The selected piezoelectric motor is commercially available and is a travelling wave ultrasonic motor, the propagating wave in the stator drives the rotor. The motor can develop higher forces than a stepper motor and has a high dynamic response however suffers as the torque produced is non-linear and varies with speed, load and temperature. The velocity and position feedback of the motor is provided by a magnetic encoder integrated to the rear of the rotor. The group used proportional integral derivative (PID) control of the motor to minimize errors with tracking.

Figure 2.22; The INKOMAN user interface. A joystick is used by the thumb to direct the parallel kinematic mechanism [60].

The instrument – surgeon interfaced design proposed employs a 3-DOF joystick to control the movement of the tip of the instrument and a scroll wheel which can be used to determine the orientation of the instrument, figure 1.22.

The instrument has been constructed but as yet the authors have not reported any from animal experiments. The proposed design would provide intuitive control and provide more degrees of freedom than a standard laparoscopic dissector through the parallel kinematic mechanism. The selection of the piezoelectric motor is of upmost importance. The group selected a motor

which provided high output forces however the non-linear torque performance associated with this motor could pose some concern when used as an instrument for modulating grasping forces.

2.3.3 Shape memory alloy actuators (SMA)

2.3.3.1 Theory of operation

The shape memory effect (SME) occurs when the atomic bonding of the alloy changes as a function of heat. The two phases of shape memory alloys (SMA) are martensitic and austenitic and phase change between these two crystal structures occurs at the transitional temperature. These alloys also exhibit a super-elastic effect in which the material can be strained by up to 18% non-linearly and will recover[61].

The martensite phase of SMA is stable at low temperatures and the austenite phase is stable at temperatures above the transitional temperature. By way of adding a current to the SMA the phase change will occur and the SMA will revert to its predetermined austenitic shape. As the heat is removed and it is left to cool, the material will revert to its martensitic shape. This is exploited in SMA actuators as the deformation at the austenitic phase can lead to deformations of an SMA wire by a few percent of overall length which can be mechanically amplified.

2.3.3.2 Applications in surgery

Kim *et al* [62] developed an earthworm design which incorporates features from other reports[60]; however this design employs SMA actuators to provide locomotion for a micro-robot as an alternative to piezoelectric actuators which have to be wired as current batteries.

The Kim *et al* micro-robot comprised of one SMA spring actuator and a bellow, such that the repeated contraction and retraction result in forward motion. The SMA spring actuator was developed by winding SMA wire around a bolt and annealing it by heat treatment. The bio-

mimetic design resembles the movement of an earthworm.. The SMA wire acts as a contraction force with the silicon bellows providing the elongation when the SMA spring cools. As the bellows extend the setae-like needles clamp to provide a contact force with the surface. This process is shown in figure 1.23 and is repeated to provide a forward motion.

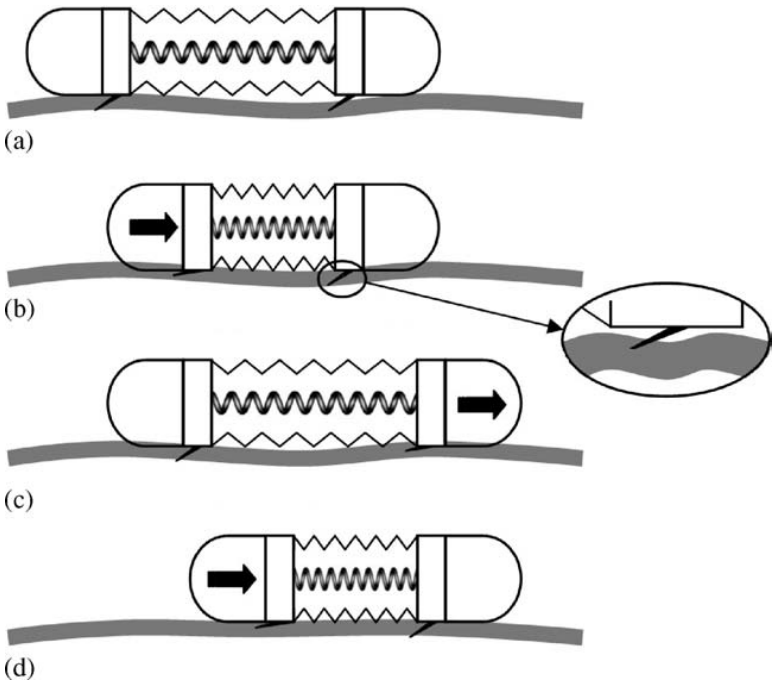

Figure 2.23; Contraction and extension of the earthworm like robot using the contraction of an SMA spring. The setae inspired micro-gripper is highlighted in section b. [55]

The two-way linear actuator was developed by coupling a silicon bellow with an SMA spring. These two materials have different spring rates at low temperature. The heating and cooling of the SMA will provide a two way actuation for the device[62].

As the micro robot was developed as a wireless device, a control system for activating the on/off states of the SMA actuator was needed. This was achieved by an on-board radio frequency receiver, microcontroller and power, all designed to fit on a small circular PCB with a diameter of 4.8mm. Initial experiments were carried out with a wired power supply to determine the optimum actuation time to maximise the stroke length. This was done by

applying a current for 1 and 2 seconds and testing cooling times. An ON time of 2s and off time of 6s was selected as the optimum to create displacement of 0.375mm/s.

Experiments were carried out on lubricated and flexible silicon rubber padding, acryl and paper pipes. Displacement was measured by a laser sensor and recorded to a PC using a data acquisition board. The stroke cycle was a total of 8 seconds, allowing for the heating and cooling for the SMA spring. The theoretical speed of the robot was 3.44mm/cycle however when using batteries only 2mm/cycle was achieved. Figure 1.24 shows the displacement of the robot on different surfaces.

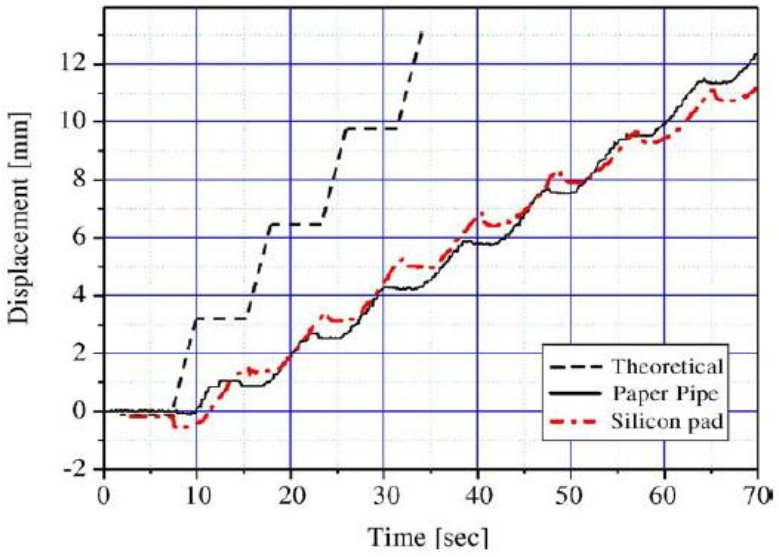

Figure 2.24; The displacement of the robot on three different surfaces with a total cycle time of 8 seconds. A displacement of about 2mm/s is shown, far lower than the theoretical 3.4mm/s [62].

A backward movement can be observed due to the clamping mechanism of the setae not engaging with the surface until a few hundredths of a millisecond after the elongation and retraction. The battery life only lasts for 8 minutes when with continuous ON/OFF cycles and the speed of this robot is considerably less than its piezoelectric counterpart[59].The proposed

use of the device is to travel along the human digestive tract wirelessly however the speed and battery life seriously limit the potential for this application.

SMA actuators have also been proposed by Gorini *et al* [63] as a driving mechanism for a capsule endoscope.. The specifications for the proposed legged capsule were:(i) no increase in the size, (ii) number of actuators must equal the number of legs, (iii) need low power as power must be stored on-board, (iv) must be biocompatible. For these specifications, SMA actuators were selected as they could provide a high force and high displacements without the need for complex mechanical amplification which is necessary with piezoelectric actuators. SMA has a relatively high power density at 30 W/cm^2 and but requires a low driving voltage. The author appears to have overlooked the negative aspects of heating, bad controllability and high power consumption associated with SMA actuators.

The proposed design would incorporate 6 legs and thus 6 SMA actuators. Each leg would consist of a body, pulley system, leg and two antagonistic SMA wires. By alternating the activation of each of the wires the pulley will rotate clockwise or anticlockwise. The leg is bonded to the pulley and will rotate at the same time. The body of an individual actuator is shown in figure 1.25 with the dimensions being 25mm x 3.4mm x 3.2mm.

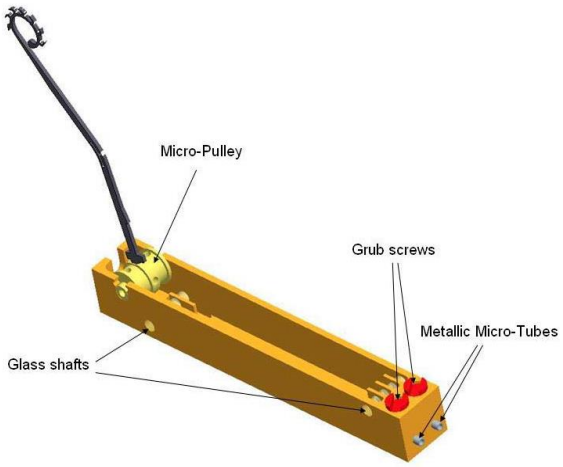

Figure 2.25; Prototype design for the leg actuator with 2 SMA wires fixed at the micro-pulley. A total of 6 of these legs would be used within the capsule endoscope [63].

In order to control the contraction and relaxation of the opposing SMA wires a microcontroller was used to generate pulse width modulation signals which will ensure a homogenous heating of the SMA actuator.

A MATLAB mathematical model was developed using a SMA wire of 100um in diameter. This was necessary to define which parameters would affect the actuators performance. It was concluded from the mathematical model that (i) for a fixed length of SMA wire, the rotation angle decreases as the force on the tip of the leg increases; (ii) for a fixed resistance the rotation angle of the pulley increases with the addition of more SMA windings; and (iii) the minimum number of windings to achieve the desired rotation was 6.

In the next stage of the development, the number of windings was increased to 6 in accordance with the theoretical model. For the initial experiments a wired power supply was used. The actuator was placed on a platform which could rotate in relation to the relative angle of the leg actuator. The experimental set-up is shown in figure 1.26. A 100um diameter SMA actuator was selected and 10V with a current of 360mA was applied to contract the wire.

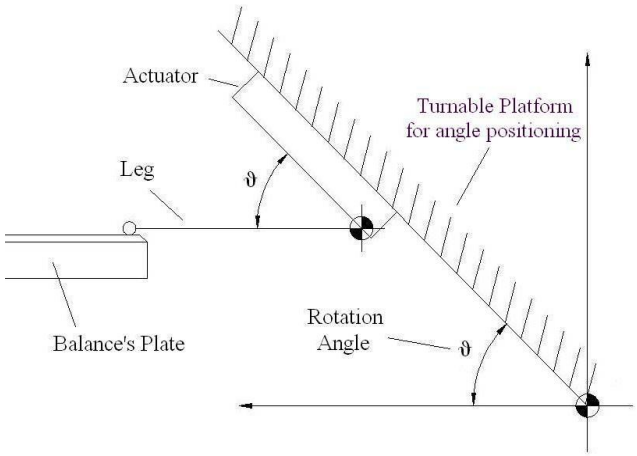

Figure 2.26; Experimental schematic. The actuator is placed on a turning platform to be able to adjust the relative angle between the base plate and leg actuator. This was to be able to measure the pulley rotation angle versus the force generated by the leg actuator [63].

The results show that the observed results differed from the theoretical results, figure 2.27. The author proposes the reasons for this being factors including friction, increased working cycles and micro slippages accounted for this difference.

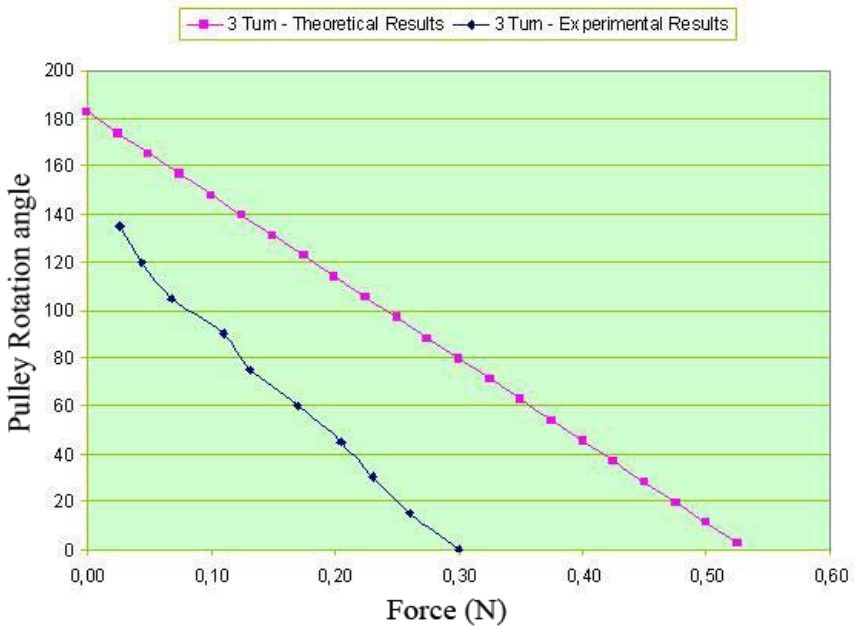

Figure 2.27; Comparison between theoretical (purple) and experimental (blue) curve. [63]

The proposed design employs antagonistic SMA wires to provide locomotion to a capsule endoscope. From the results it is shown that there are relatively low forces achieved by the SMA actuated legs and the forces generated make it difficult to conclude that a capsule endoscope could be driven in such a way, because the legs would have to transmit sufficient force to move the weight of the capsule as well as overcome any addition forces applied to the capsule from a collapsed bowels. This device would also suffer from the high power consumption of the SMA wires which could not be provided by current battery technology.

As previously mentioned there are a number of difficulties in controlling SMA actuators as they work in binary conditions however Yan *et al* [64] present a device which incorporates

tactile feedback control to relay force feedback to a gripper which is driven by SMA wires. The tactile sensor is a PVDF sensor which can detect applied loads and slip and the actuator is comprised of differential SMA wires with a stroke length of 150mm and a maximum output force of 1.5N.The two fingers of the gripper are driven by the actuator through a six bar linkage which provides the opening and closing. SMA wire of 1mm diameter is used with 5 windings and a coil diameter of 10. The design of the gripper is shown in figure 2.28.

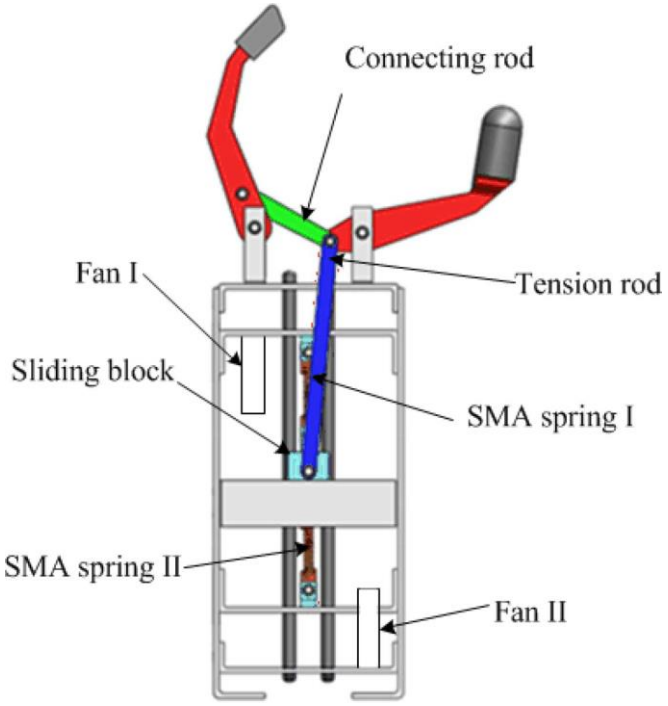

Figure 2.28; Mechanical structure of the intelligent gripper system driven by SMA springs [64].

The two SMA springs are triggered alternately and cooled by the respective fans. This should improve the reaction time of the actuation system. As spring 1 deforms it pulls the sliding block and connecting rod to drive the fingers open, spring 2 is used to open close the fingers by pulling in the opposite direction. A small double layered PVDF film with a rubber coating is used to provide tactile feedback. The surface of the rubber is patterned to act as a mechanical amplifier for the slip and tactile signals. The current supplied to the SMA actuators is

controlled by pulse width modulation (PWM) and a MOSFET is used to control the current of the PWM signal. The signal from the PVDF film is processed through charge amplification and filtering. The control diagram for the system can be seen in figure 2.29.

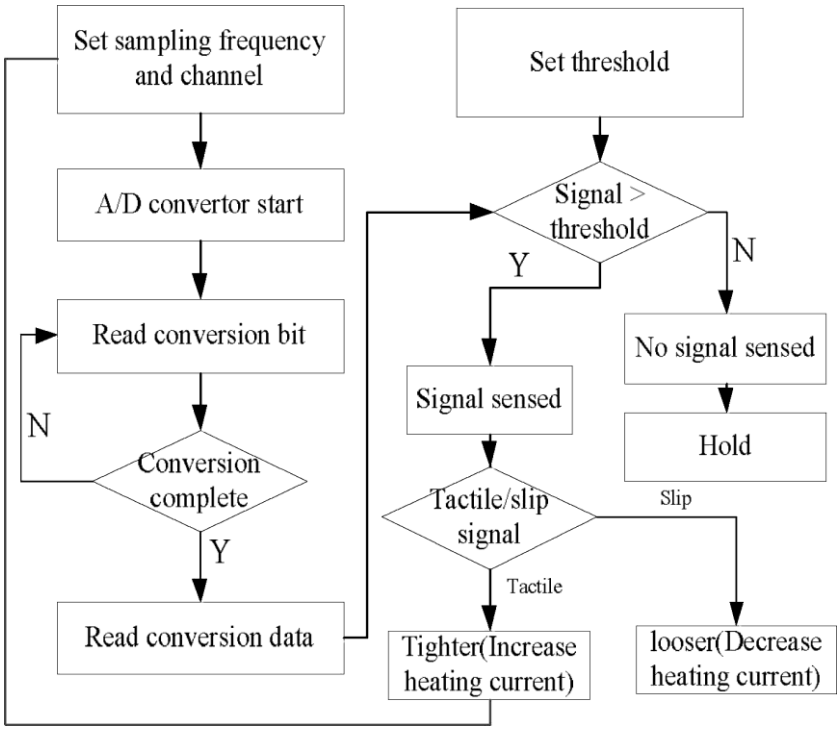

Figure 2.29; Control diagram of the actuated gripper system. [64]

The gripper will increase or decrease the grip depending on if the threshold for the signal has been met or not. The slip and tactile signals must be differentiated from one which is done by calculating the mean value of the voltage signal when considering the two voltage conditions and the system making an informed decision.

Experiments were carried out to test the gentle and hard grasping effect when the tactile feedback system is used. This data is then compared to the same gripper with no tactile feedback. Gripping experiments were performed on a soft paper cylinder and a hard cylinder

made of plastic as a comparison. A maximum of 2.8A of current was applied to the actuator for grasping both objects. Figure 2.30 shows the results comparing grasping a soft object with no tactile feedback to the same material with tactile feedback.

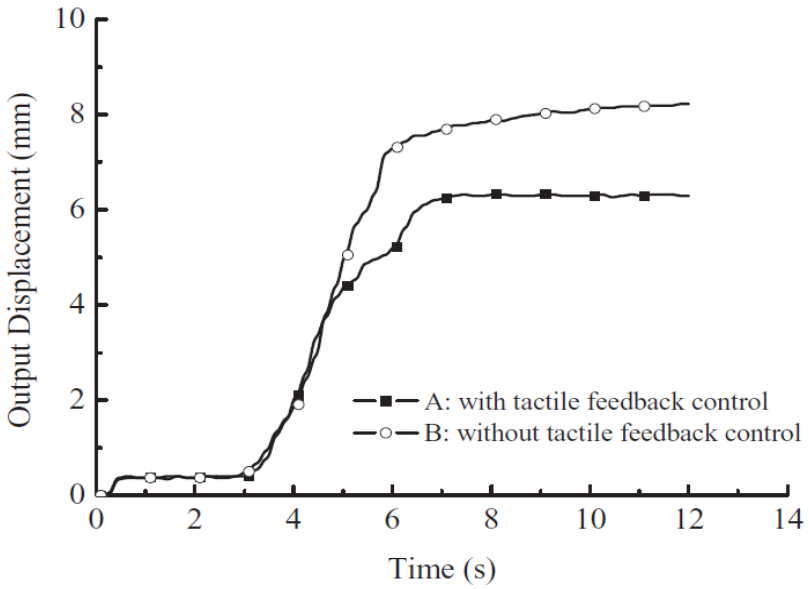

Figure 2.30; Grasping soft material with and without tactile feedback. [64]

The graph shows that the displacement of the gripper hands is significantly less when the system employs tactile feedback. As the threshold condition is met the applied heating current is reduced which regulates the applied force which would lead to more delicate handling of fragile objects. Although the presented data is limited with no statistical evaluation it has shown that SMA actuators could be more accurately controlled with a similar system architectures. Further study into the field would need to be carried out to discover how accurate this output force control of SMA actuators could be.

2.3.4 Hydraulic and Pneumatic actuators.

2.3.4.1 Application in surgery

The use of hydraulics and pneumatics for actuation prosthetics and surgical instruments has been proposed in the literature. Thomann *et al* [65] developed a colonoscope which employed a bellowed style pneumatic actuation system for the bending of the tip of a colonoscope to address the incidence of damage to tissue caused during the procedure. The device would limit the contact between intestine and colonoscope to prevent perforation or haemorrhage. A flexible micro-actuator approach was used in designing the actuator which is made from metal. The actuator design consists of three pressure chambers which would reproduce the movements of a colonoscope which would give the instrument two degrees of freedom and control the stiffness. An initial prototype was developed which was 26mm in diameter and 94mm in length, which is about twice the diameter of the standard colonoscope. Pressure in the chambers was controlled by a pressure sensor for each bellow. An image of the prototype bendable tip is shown in figure 2.31.

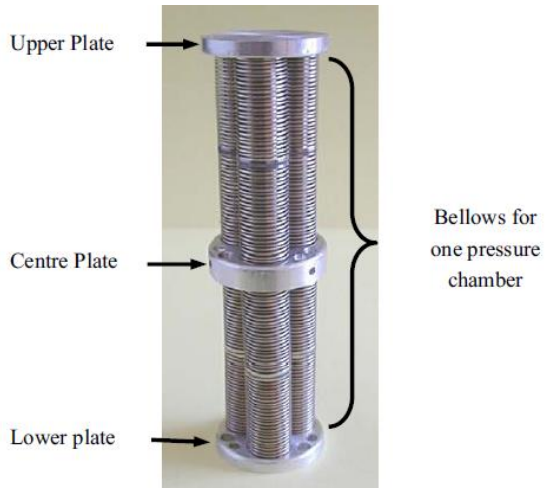

Figure 2.31; Prototype of a colonoscopic tip with bellows connected by three plates [65]

Autonomy of the tip of the instrument was a major aim of the project and so optical fibres which could detect the distance of the tip of the instrument from the intestinal wall were employed. Light was emitted from the device and the amount of light reflected to the receptive optical fibres would determine the distance, the output of the sensor used is shown in figure 2.32. The curve shows that the sensor is able to detect the intestinal wall from 8mm.

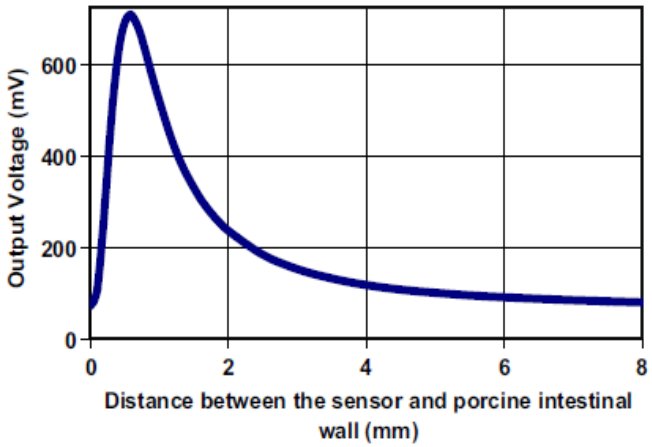

Figure 2.32; Output voltage of the light sensor versus the distance between the sensor and intestinal wall [65].

Experiments were carried out by advancing the colonoscope along a transparent, curved tube at a rate of 4cm/s. The experiments were only carried out using one deformable chamber and one optical fibre and thus could only move in one direction.

Results from the open loop experiments showed that the system had a slight delay due to the air velocity, causing the distal end of the bellows deform at a different rate from the proximal end. To address this issue the team applied a mathematical algorithm which made the delay negligible compared with the overall dynamics of the system. The results from the closed loop experiments show that the tip of the instrument was never closer than 1.7mm (fig 2.33) to the wall of the tube thus confirming the efficacy of the control by optical fibres of each independent axis.

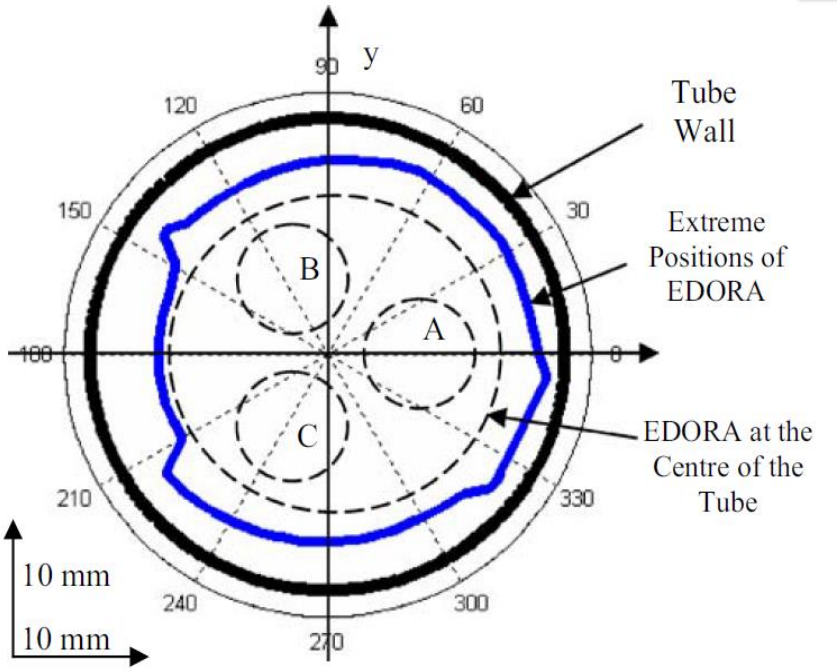

Figure 2.33; Position of the colonoscope during experiments. The colonoscope never gets closer than 1.7mm to the tube wall while they are controlled by the closed loop feedback system. [65]

This study shows that the autonomous control of the tip of the colonoscope by using pneumatic actuators and optical sensors is possible. The current dimensions of this prototype would be unacceptable for use and so the dimensions must be further scaled down to meet the standards of current colonoscopies. Further development of the system is reported in the study with a second prototype made from silicon which can deform up to 160 degrees.

Micro-hydraulic actuators have been developed and integrated into a surgical instrument by Moers *et al.*[66]. The purpose was to develop a laparoscopic surgical instrument which would provide up to 6 DOF, have an output force of up to 2N and fit through a 10mm access port (although the initial prototype has a diameter of 15mm). Modular, flexible, braided hydraulic muscle type actuators were selected as the actuation system and hydraulic valves were developed to control the fluid pressure to the actuators.

The instrument consists of a series of active segments; a single segment is shown in figure 2.34. When assembled the deformation of individual segments determines the relative position of the instrument. Three actuators are placed in parallel, concentrically around a hollow central channel which used to guide surgical tools such as a gripper, scissor or biopsy tool. This central channel also acts as a leaf spring which provides the neutral position of the device.

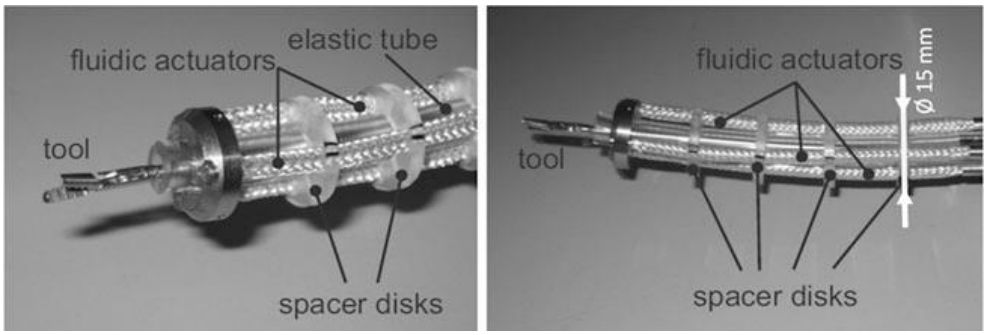

Figure 2.34; One active segment of the instrument consisting of 3 fluidic actuators and spacers [66].

Micro-fluidic actuators were selected for their relative high power densities and force output as well as the good positional accuracy without concerns of backlash or slip-stick associated with other methods of actuation. The working principles of the braided hydraulic actuators are shown in figure 2.35, consisting of a braded mesh surrounding an elastic tube as the pressure increases the diameter of this tube increases. This expansion is restricted by the braided mesh and as the angle of the braided mesh couples with the length contraction, as both ends of the actuator are fixed, it will generate a counteracting force.

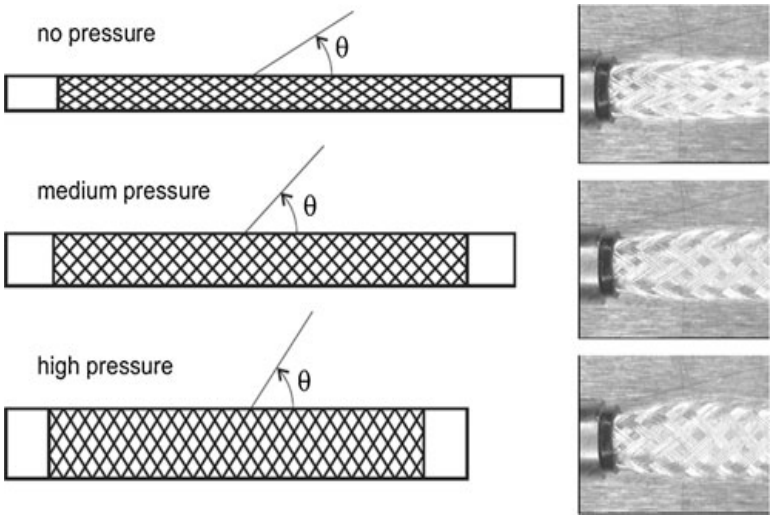

Figure 2.35; Working principle of the braided pneumatic actuator. As the pressure increases so does the angle, inversely the length decreases.[66]

Each section of the instrument has a hydraulic contains a hydraulic control unit which regulates pressure to each of the three actuators. The control unit consists of three channels for the actuators and individual valves, a tool channel and channel for electrical and hydraulic supply. The team also developed miniaturised hydraulic valves based on a plunger valve design specifically for the application.

The performance of the valves was verified by supplying water at 8 bar of pressure to the inlet valve. The input voltage was determined by measuring the output voltage of the valve. It was shown for an input pressure of 8 bar the output pressure could be controlled between 1.5 and 6.8 bar which were in good agreement with simulated results of between 1 and 7 bar carried out by the authors. Figure 2.36 shows the pressure at set values, it can be seen that there is an error in target values which decreases with increasing pressures which warrants more investigation into the performance of the valves.

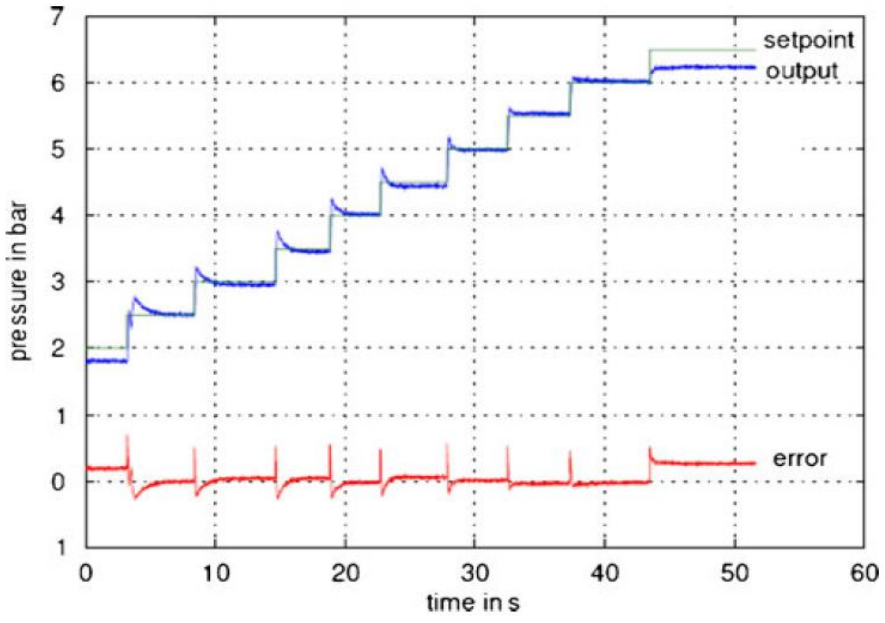

Figure 2.36; Pressure control experiments of the valve using a PI controller. Desired output pressure is changed over time and plotted with the error in the output pressure. [66]

The actuators of 1.5mm diameter were shown to achieve a contraction force of 6N at a supply pressure of 10 bar with sub-micron positioning accuracy. The stroke length was about 15% of the actuator at speeds of 350mm/s. There is no testing of an overall instrument presented in the paper, validation of the actuation system and custom valve are. It is estimated that the final device may be able to achieve 150 degree bending angles by redesigning the spacer disks and pre-stretching the actuators.

The proposed device, although in early stages, would provide a platform for carrying out complex surgical tasks laparoscopically with more ease and higher accuracy. This high accuracy should translate into lower surgical errors and reducing potential risk to tissue. The idea of having a channel which will provide a large number of DOF is a good one. However no thought has been given to the instruments which would be used with such a system. Instruments such as graspers and scissors are often rigid and efforts to create flexible

instruments, particularly with a bending angle of 150 degrees would present challenges in itself.

2.3.5 Conclusions

Precision control of any actuator implemented into a surgical instrument is of utmost importance, this high degree of control can only be found when using piezoelectric or electromagnetic motors, though control of miniaturised pneumatic and hydraulic systems are greatly improving [25].

SMA actuators exhibit a large amount of stress and can move relatively large forces over small distances but they generate a large amount of heat which would be difficult to dissipate in small enclosed spaces. They are also difficult to control with high precision and suffer from creep over the lifetime of the actuator which makes them an unsuitable candidate for minimally invasive applications.

Electromagnet and piezoelectric motors also present concerns. Miniaturisation of DC motors is limited to the strength of the magnet and thus as size decreases there is a loss in power density. Piezoelectric motors currently cannot exhibit the necessary output forces to actuate instruments. Both of these topics are large areas of research and piezoelectric and DC motors have drastically improved in recent years.

Hybrid style actuators have shown to be successful in achieving high output forces while minimising any negative characteristics of the individual actuators which provides a promising route for research for actuating surgical instruments.

2.4 Tactile and Slip detection suitable for biomedical application.

2.4.1 Piezoelectric slip detection

A number of piezoelectric elements have been investigated for their potential to provide tactile feedback. The two most common piezoelectric materials are Polyvinylidene fluoride (PVDF) and lead zirconate titanate (PZT). Piezoelectric materials provide a directly proportional mechanical to electrical conversion of dynamic loads, making them particularly suited to the detection of vibrations. These materials are widely used in the medical field although much of the research is carried out in relation to developing tactile sensors for implementation into prosthetics.

PVDF has been the subject of a number of studies on provision of force feedback from laparoscopic grasping instruments; however it has not been investigated as a slip sensor in the field. Sasaki *et al* [67] proposed a slip detection system for a two fingered robotic hand which comprised two PVDF strips embedded in silicon structures akin to the human thumb. The device was designed to detect the vibrations caused by slip. Two PVDF strips (2mm x 25mm) were embedded 1mm from the surface of the silicon thumb structure. The silicon thumb was cast in a rubber thimble, giving the surface a coarse texture. A voltage to charge converter was used to convert the charge generated by induced stress on the PVDF to a voltage. The voltage output of this converter was considered to reflect the rate of stress as the charge developed in the film is proportional to the stress. A low pass filter with a cut-off frequency of 5 KHz was used to reduce high frequency noise, a schematic of the sensor and initial signal processing unit is shown in figure 2.37.

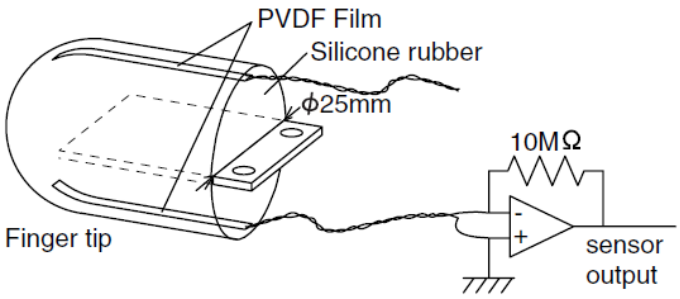

Figure 2.37; Schematic of the PVDF sensor and pre-amplifier circuitry.

Initial experiments were carried out to establish the stress rate of the sensor when the finger came into contact with an object. The sensor was pressed onto a flat surface for several seconds and then removed without sliding. This showed that a large amount of drift was occurring between the initial contact and the disengagement of the sensor. This was rectified by introducing a high pass filter with a low cut off frequency. A relationship could not be established between the applied force and the resultant voltage due to the large difference in the Young's modulus of the silicon and that of the PVDF.

The next stage investigated the waveform and power spectrum of the sensor in the event of slip, which occurred at a rate of 2.5cm/s and 7.5cm/s. The conclusion from the analysis of the results was that the frequency of the sensor output at 2.5cm/s was between 100Hz and 2 KHz; and at 7,5cm/s the frequency ranged between 100Hz to 4 KHz. The power spectrum was not stationary nor was there any discernible peak frequency. Both signals were noted as being similar to that found as random noise often found in small electrical signals.

Further signal processing was performed to differentiate between contact and slip. It was initially assumed that as the frequency of the slip signal would be higher than that of a contact signal, and thus a high pass filter would make it easy to distinguish between the two. However the introduction of the filter reduced the slip signal and made differentiation and implementation of a threshold too difficult. The waveform showed many jagged peaks during slip, as distinct from the larger, sharp peaks caused by contact. Using frequency domain

filtering, the number of peaks in a fixed time frame could be counted to determine a threshold for the occurrence of slip.

A 6.4ms time frame was set to count the number of peaks at a rate of 12.5 KHz. A peak was determined by the equation.

$$(y_{i-1} - y_i) - (y_i - y_{i+1}) > (threshold) \tag{2.2}$$

Where y_{i-1}, y_i and $yi+1$ are the three consecutive amplitudes and the threshold was set high enough to reject small peaks which occurred due to ambient noise. A further level of signal processing was added to reject small signals. This was done by using a moving average of squared amplitude.

Final experiments were performed using two of the sensor modules attached to robotic fingers which were suspended vertically from a frame. Both fingers had 3 DOF. A number of objects were experimented with for the detection of slip including tilting and pushing a wooden block, trying to lift a fixed wooden block and grasping a business card. The threshold for slip was set at 15 peaks in a 6.4ms interval. Waveforms of each of the grasping and moving of the wooden block are shown in figures 2.38.

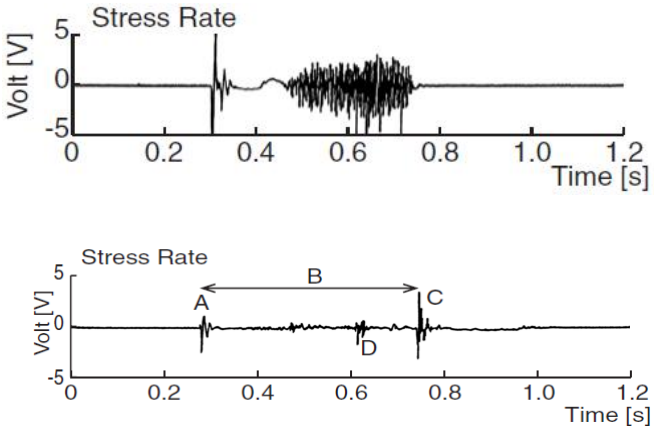

Figure 1.38; Top: Grasping a fixed wooden block. Bottom: Sliding a wooden block across a surface.

This study showed that the onset of slip or the occurrence of slip, the waveform between contact and slip were found to be distinct from each other. However the report does not provide any statistical validation and very limited data and so it is impossible to compare this method of signal processing to other, more common, methods of signal processing when PVDF is used as a slip sensor.

Goeger *et al* [68] approached the signal processing of a PVDF tactile sensor in a different manner. They developed a tactile sensor for integration into a robotic hand specifically to detect slip when an object is grasped. The sensor and algorithm were developed to distinguish between three states; no contact, slip occurring and contact. The sensor comprised of a snake like PVDF sensor attached by a conductive rubber to a PCB electrode. A rubber covering with conical protrusions was used to protect the sensor, which also aided in transmission of vibrations to the sensor surface.

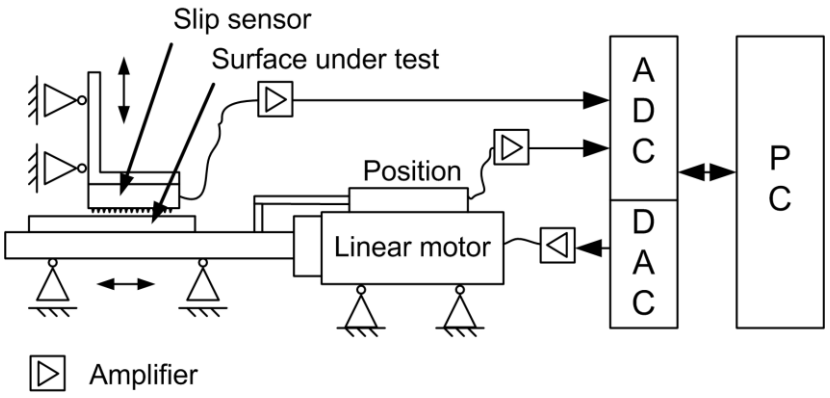

Figure 2.39; Experimental set up for testing various surfaces with PVDF sensor.

The initial signal processing used in this study differs in that this group did not integrate a charge amplifier to provide an absolute measure of charge build up on the surface of the PVDF. Instead a current to voltage conversion was used by an instrumentation amplifier. This provided the necessary signal and desired frequencies without the problem of drift which are

often a concern with charge amplifiers. The experimental set-up, as shown in figure 2.39, was used for testing of various surfaces. A linear motor controlled a sliders movement along the surface of the sensor which is held in a fixed position. The position of the slider was adjusted using a linear potentiometer. The slip sensor signal, position signal and motor were all controlled via Labview.

Post processing of the gathered signal was performed to characterise the three contact states. The signal was investigated in the frequency domain by a short-time Fourier transform method which entails a sampling interval of 17ms. As these sampling intervals overlap, no data loss occurs. Figure 2.40 shows a typical sensor output when movement occurs along with spectrogram of the same signal. The deep red colour shown in the frequency domain is indicative of the initial movement across various applied loads and several types of material. However, no comment was made by the authors on whether the sensor could determine between applied loads or different surfaces.

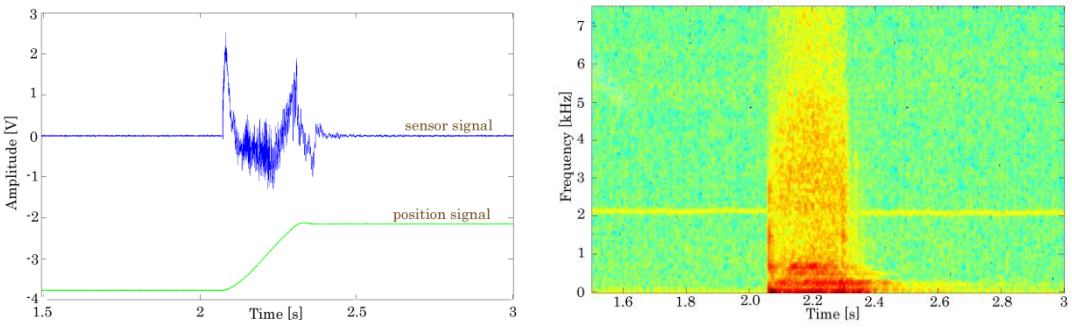

Figure 2.40; Left: Time domain output and position signal.

Right: Corresponding spectrogram signal [68].

Images, such as that shown in figure 2.40, were analysed by a learning matrix which determined which class the various signals would be appended to and which increased in

accuracy with time. Eigenvectors, a method commonly used in facial recognition software, were used to discriminate between the different features of the images and categorise them. Example classifications over 1.5 second time frames were used to train the algorithm between the different states.

The system was evaluated with various applied loads and surfaces and the classification of the signals were compared the known condition. Approximately 2600 data sets were evaluated. The results showed a high accuracy in determining when slip occurred (99.82%) but this was significantly less accurate in determining between the two other conditions; contact accuracy (53.33%) and no contact (78.23%). The accuracy in determining the class may improve with more training data.

A concern with this approach is that the signal processing is computational 'heavy', leading to higher power consumption and a slower response rate. It can also only accurately determine between slip and no slip conditions; whereas other investigations such as Fujimoto *et al*[69] have demonstrated the ability to detect incipient slip using PVDF as a sensor embedded in artificial fingers. In the study PVDF sensors were embedded in ridges of an artificial finger. In this study, incipient slip could be detected with minimal signal processing to reduce high frequency signals. Finite element modelling (FEM) studies were undertaken to optimise the design of the artificial finger. Experiments to characterise the frequency response and sensitivity of the system were then carried out.

The design of the artificial finger included nine ridges to replicate the epidermal ridges found on the human fingertip. FEM analysis showed that the selected nine ridges would be optimal as all would be in contact with the grasped object when a normal force of 4N was applied. The PVDF sensors were embedded into one of the ridges on the artificial finger. The PVDF sensors were connected to a pre-amplifier circuit, which consisted of a differential amplifier with a feedback resistor. This was used to reject common mode noise and convert the charge

generated on the sensor to a voltage. Frequency characterisation showed that the frequency range of interest was between 2Hz and 2 kHz, beyond which the gain of the system saturates. There was a linear relationship between gain and applied load, as expected and often referred to as the stress rate.

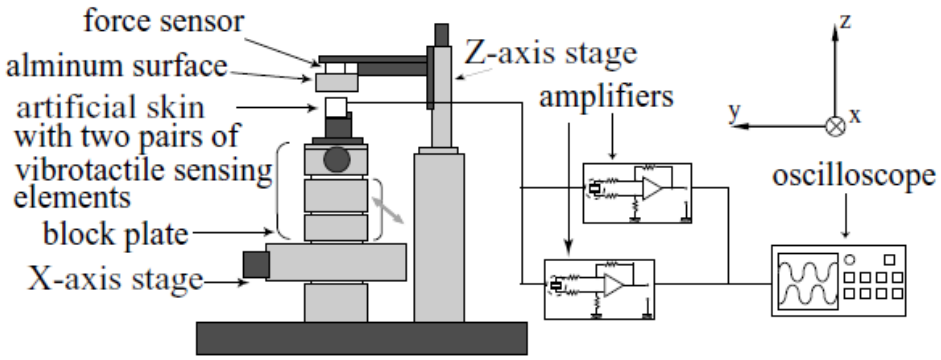

Figure 2.41: Experimental rig for testing incipient slip with PVDF. [69]

Incipient slip was investigated using the experimental rig shown in figure 2.41. The artificial skin was fixed to a block which was driven in the *x* and *z* directions by an *x*-*z* stage. The PVDF sensors are only sensitive to slip in the x direction. The output from the sensors were sampled at a rate of 1KHz. Initial results showed activity in the signal, figure 2.42, Pa is thought to be incipient slip on the ridge adjacent and Pb is incipient slip detection on the ridge with the embedded PVDF sensors. These results concur with simulated results. The signal from the PVDF signals when incipient slip occurred was of a low frequency with a large amount of noise imposed. The next stage was to use a low pass FIR filter to remove the high frequency noise.

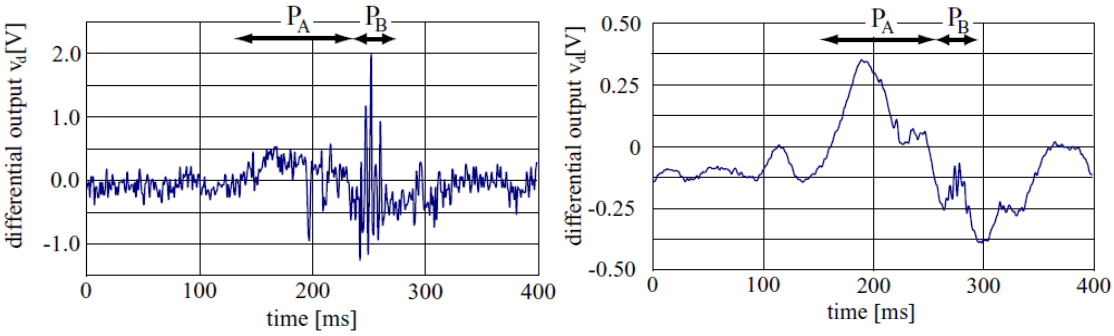

Figure 2.42: Slip and incipient slip shown on the left prior to filtration and after on the right.

A low phase finite impulse response filter (FIR) was employed with a cut off frequency of 28Hz. FIR filters require no feedback, are more stable and are more suitable for phase sensitive applications (such as this) over infinite impulse response filters (IIR) . This low phase filter reduced lag time and thus provided a faster response to slip. Incipient slip and slip could be detected by experiments; however the study also required the differentiation between incipient slip and other states of contact, namely rolling contact. This was achieved by a rotary stage which was brought in contact with the ridges of the artificial skin and rotating the semi-spherical head by 3.5 deg. This rolling contact was distinct from both incipient slip and slip signals. As rolling contact occurred the frequency of the change in signal was much higher than that for incipient slip.

Yamada *et al.* showed that PVDF sensors can be embedded into artificial skin. The signal of these various vibrations are distinct enough from one and other to be able to differentiate between 3 states of slip; incipient slip, slip and rolling contact. The circuitry and filtering used are very basic, leading to fast computation times which will ultimately makes the system more responsive. Simulation and experimental data provided matched well. However, no statistical analysis or large enough experimental data sets are provided to indicate the accuracy of the system can be in differentiating between contact states.

Goeger *et al*. suggested that patterning of the silicon coating of the PVDF sensor could help to transmit vibrations to the surface of the sensor. A similar approach was reported by Chuang

et al.[70]. In this study, a microstructure and microelectrodes were distributed on the surface of the PVDF film to help detect lateral motion with the ultimate aim of being able to detect slip and evaluate the coefficient of friction. The aim of this work was to develop a tactile system for a robotic hand for real-time feedback for control of grasping force.

An elastomeric column structure was added directly to the surface of the PVDF sensor. The PVDF was mounted on patterned electrodes which obtained the voltage output of the PVDF sensor, corresponding to the stress under the column structure when in contact with an object. The column transmitted the external contact force directly to the PVDF sensing area. This could be a compressive or shear force and would be differentiated between each other by the voltages obtained by the electrodes. When a compressive force is applied, a negative electric potential would be observed and for a shear force acting upon the sensor a positive voltage would occur. The stresses applied would only be detectable upon initial contact or when a change in force occurs due to the charge dissipating on the surface of the PVDF when in contact with static forces.

Finite element analysis simulations were performed and a real size 3D model was used with a 1N shear force set to uniformly load the top sensor of the surface. As a comparison a FEA was also performed under the same conditions without the microstructure. Results indicated that with loading both positive and negative voltages occurred on the sensor. The shear force induced a positive voltage at one edge of the column and negative at the other side, indicative of tensile stress at the proximal edge and compressive stress at the distal edge as shown in figure 1.47. Electrodes would be placed in the areas where the largest voltages occurred during simulation. FEA analysis of the same model without the microstructure showed very little out of plane stress and a very low voltage range. Comparisons between the two FEA models are shown in figure 2.43. This graph shows that the output voltage of the PVDF sensor is far greater with a microstructure due to the increase in stress.

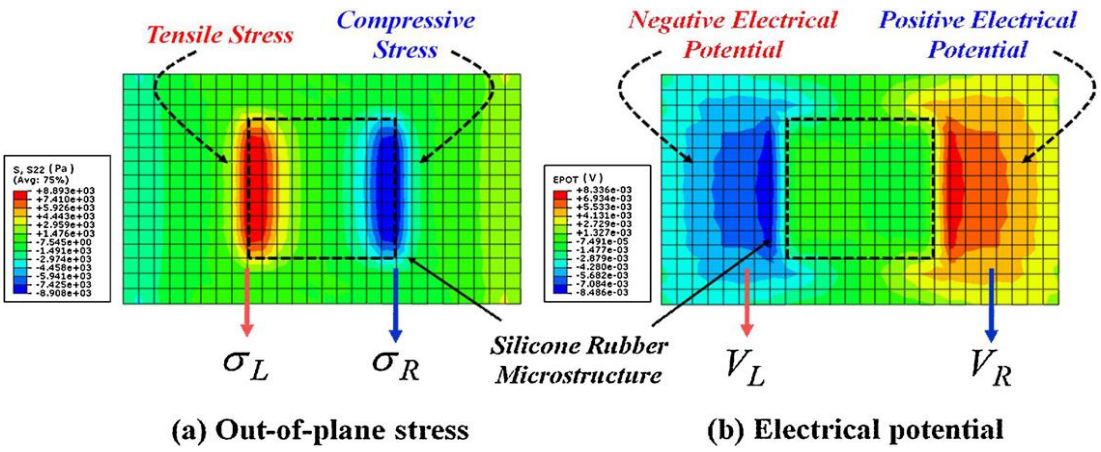

Figure 2.43; Left; Stresses induced by the column microstructure and Right; corresponding electric potential produced by these stresses acting upon the PVDF sensor [70].

Sensors were fabricated in house using flexible PCB electrodes which were etched using standard photoresist technology. A PVDF film was sandwiched between the two upper and lower PCB's electrodes. The silicon microstructure was attached, in alignment with the electrodes, to the surface of the upper PCB using adhesive. Experiments using the fabricated sensor comprised of clamping an object with a 100g fixed weight attached between two surfaces, one of which incorporated the PVDF sensor. A linear actuator and force sensor were used to control the load under a fix speed of 0.5mm/s. When the friction force between the sensor and object was smaller than the tangential force, the object would slip. The two signals from the sensor were passed through a charge amplifier with a gain of 1mV/pC. A low pass filter (100Hz) was also included in the signal conditioning circuit.

Two contrary peak voltages where apparent when slip occurred, in agreement with the FEA simulations. The direction of slip could also be determined by the polarity of the output signals. Slip signals were recorded for the different materials; wood, aluminium and silicon rubber. The counter weights were increased from 50g to 350g. The object would slip when the external tangential force overcame the maximum static friction force. With this information, the coefficient of friction for objects of different materials could be obtained; thereby

distinguishing between different materials. Results for this are plotted in figure 2.45. The friction coefficients are in respect to the surfaces between object and the tactile sensor. The peak voltages for each of the objects when slip occurred varied indicating that output voltages of the sensor were dependant on both the weight and rigidity of the object.

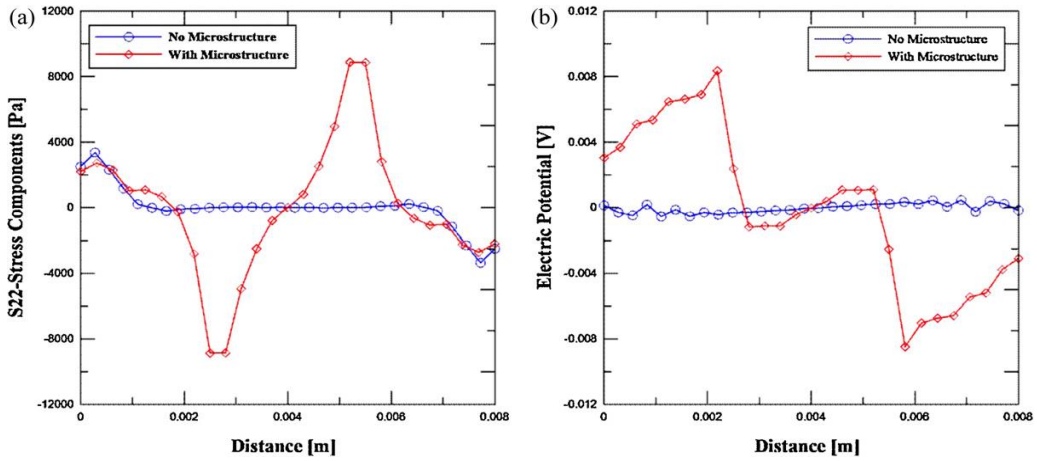

Figure 2.44: Comparisons of voltage outputs with and without column microstructures. [70]

From the data obtained, the group was able to develop a system capable of detecting slippage which would enable a grasping robot hand to react to slip events. The distribution of electrodes provided two separate signals, when slip occurred opposing signals were recorded, this enabled slip to be distinguished from other events. The electrodes were positioned under the high stress areas when slip occurs in a direction transverse to the alignment of the electrodes. If the slip occurred in a parallel plane to the alignment of the electrodes the areas of high stress would not be in the ideal position to detect slip and would thus not produce the contrary signals. As this sensor can only distinguish slip on one axis, it is unsuitable for a number of applications. The use of structural columns increased the output of the PVDF sensor due to increasing the stress on the PVDF.

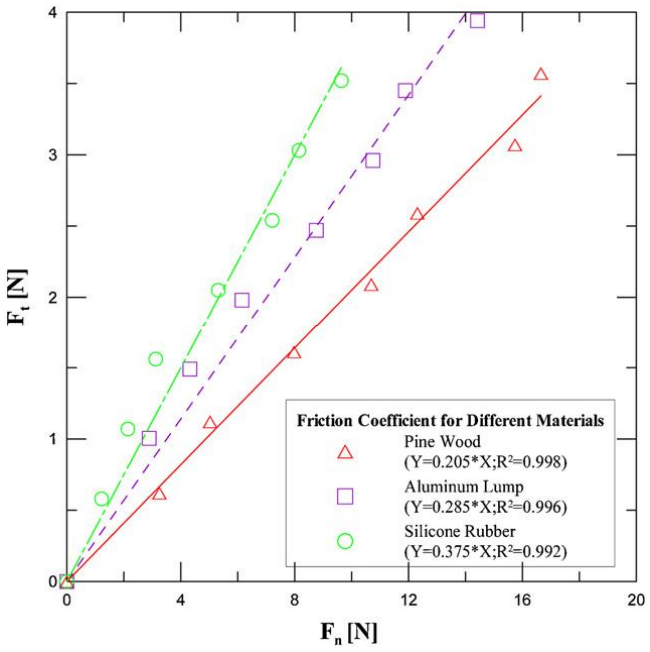

Figure 2.45: Results from the coefficient of friction results which showed the sensor ability to distinguish between different materials. [70]

Surface profiling and microstructures are not the only approach used to maximise the amount of stress on the PVDF. Yamada *et al* [71] developed a vibro-tactile sensor by placing three PVDF sensors transversely and at right angles to the direction of the slip. This group moulded silicon with small microgrooves either side of a small column like structure containing the PVDF sensors used to detect the occurrence of high frequency micro vibrations. The structure of the PVDF sensor is shown in figure 2.46.

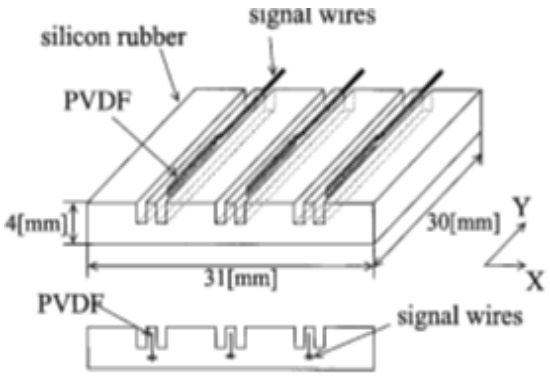

Figure 2.46; Sensor developed by Yamada *et al* [71].

PVDF signal wires are connected to a differential amplifier which rejects common mode noise. The sensors were initially investigated to determine if signals produced were distinct enough to allow for characterisation of a slip event. Various materials were tested by placing them atop of an XY-axis linear stage and bringing them into contact with the sensor. A 3-axis force sensor was placed below the object to determine the contact force. The objects investigated were aluminium sheet, plastic sheet and a paper sheet which were moved in the X axis at 16mm/s to stimulate a slip-stick conditions. This showed no significant signal output when the sensor was in a 'stick' phase, but when the material slipped a large impulsive signal was recorded. The magnitude of this signal was proportional to the length of time the sensor was under strain (stick condition). This was determined by the fitting a regression line however the R^2 values of the regression line. As these are never greater than 0.7, it is difficult to justify this conclusion based on the data set provided. There was also a distinct difference in magnitude of the impulsive signal between materials; aluminium (50mV), plastic (40mV) and paper (12mv). A Symlet wave function was performed on the slip signals to isolate the slip from the rest of the signal, this will exclude other conditions such as contact and rolling.

The processed signal was then used to control the grip of robotic fingers holding a notebook. The grasp force of the fingers was increased when a slip signal was recorded and reduced periodically until slip occurred again. Figure 2.471 shows the resultant graph of slip phases

and the reaction of increased torque to prevent further slip. Each time slip occurred, the notebook fell about 1mm before it was re-gripped.

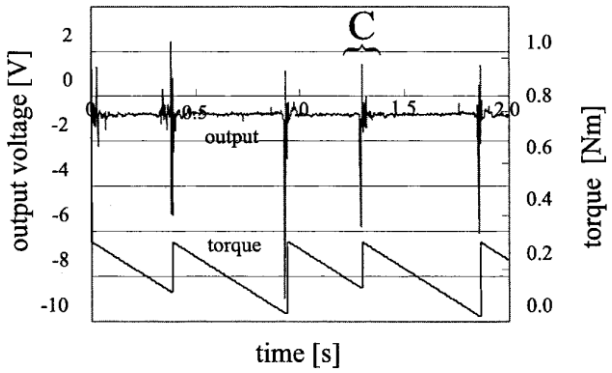

Figure 2.47; Slip signal and corresponding torque input during the objects release and grip.

A PVDF sensor with structured ridges has been proposed to detect and react to slip events and a signal processing method has been shown to be able to isolate the slip event from other conditions such as rolling contact. The flat PVDF sensor used in the study was not able to detect incipient slip as there was too little time between recorded slip instances for comparison of the three PVDF signals, which had been isolated by signal processing.

Shirafuji *et al* [72] developed a dextrous grasping hand which incorporated both PVDF sensors and strain gauges within an artificial neural network to control the grasping forces of the hand, PVDF being used to inform the system when slip had occurred, at which time, the system used the force data provided by the strain gauges to react to slip events.

PVDF sensors and strain gauges were embedded into artificial skin which transmitted vibrations indicative of slip and strain on the skin to determine static forces by the strain gauges. A total of 7 PVDF sensors were used within the fingertip. A threshold for slip detection was determined by averaging the absolute values of the sensor signals under stable conditions. The mean of this signal was then used as the threshold for slip detection. The artificial neural

network (ANN) determined the reaction to these slip events in real time through the information provided by 8 strain gauges, also embedded in the artificial skin of the robotic finger. The pattern of the strain gauge output with onset of slip was used to train the ANN by weighting the output of the strain gauges between -1 and 1. An output of 1 from the ANN indicated that a threshold to increase the force on the grasped object has been met and air was transmitted to the pneumatic muscles to increase the grasping force.

Cylindrical objects were grasped within the hand of the robot and slip was induced. Each time slip occurred, as determined by the output voltage of the PVDF, the strain gauge output was used to update and teach the ANN a new threshold for determining when slip was about to occur based on the strain detected by the strain gauges. After sufficient training, the grasping force of the hand could be sufficiently controlled based on the strain gauge outputs alone with no slip thresholds being met by the PVDF sensor output. This group has developed a viable method for determining the onset of slip by comparing the output voltages of PVDF sensors and strain gauges by an intelligent software system for discriminating between strain on the surface of a robotic finger and the onset of slip.

The system has no way of determining which type of object it grasps other than user input. This limits the practical usefulness of the system prohibitive as it would have to be trained for the dextrous grasping of all objects it would come into contact. If the system could be trained to discriminate between objects autonomously, possibly by investigating the percentage change from initial strain, then it would be a very attractive option for autonomous grasping systems.

Much of the research investigating PVDF as a slip sensor has been aimed at providing automated force control when slip is detected in the field of prosthetics. PVDF has previously been investigated for the integration in MIS instruments, grasping instruments in particular. The most recent publication in this field[73] is a review in which PVDF is integrated into the

jaws of a laparoscopic instrument to characterise tissue hardness, based on several publications by the same group.

PVDF has been shown to be able to distinguish between various conditions based on dynamic loadings. The difficulty in developing a viable PVDF sensor for the detection of slip and incipient slip lies in the signal processing and data analysis of the output signal of the PVDF sensor.

2.4.2 Resistive based slip detection

Resistive based sensors encompass a range of transducers including, but not limited to piezoresistive sensors and strain gauges. Okada *et al* [74] reported a silicon membrane tactile transducer capable of multi axis force sensing. The pneumatically distended transducer permitted deformation, caused by small protrusions on the surface on the sensor and is able to sense forces in the horizontal and vertical axis. Piezoresistive pixels are located below each of the nodules and are used to detect changes in forces. The working principle of the sensor array is shown in figure 2.48.

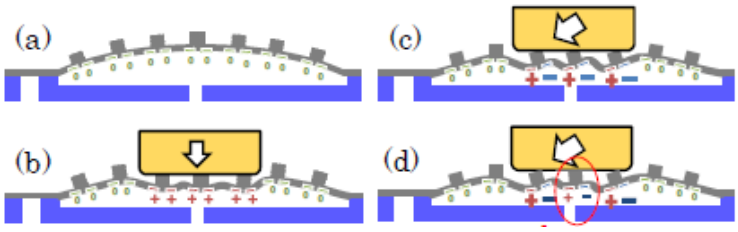

Figure 2.48; Working principle of Okada's piezoresistive tactile sensor. [74]

Finite element analysis (FEA) of the sensors was performed to investigate the theoretical output of the sensors under different loading conditions ranging from 0-40mN. It was estimated that an applied load of 40mN would cause a change in resistance of about 1.2%.

Sensors were fabricated by standard integrated circuit technology with CMOS post-processing. The initial signal processing circuitry was also integrated into the structure by way of MEMS technology. The overall size of the sensor and integrated circuit was 10mm x 10mm. The sensor was validated using experimentation involving applying a load to the surface of the sensor by way of ceramic probe. Loads were applied on each of the different axes.

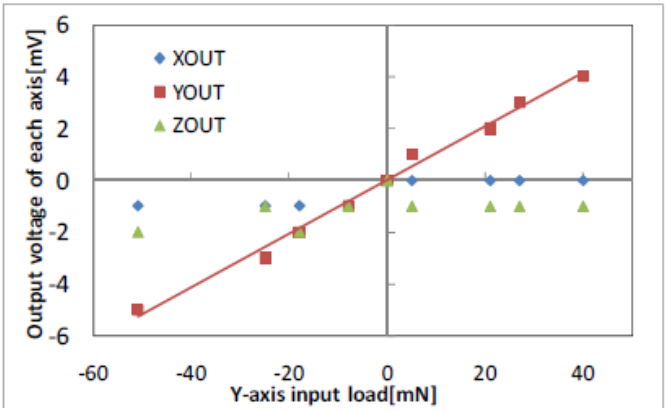

Figure 2.49: Output voltage on each axis when a normal force is applied. [74]

Figure 2.49 shows the measured output on the three different axes when the sensor was loaded on the *y* axis. It is obvious from the *y* axis outputs of the sensors that a direct vertical loading of the sensor provides a linear output. As no results are provided for either the *x* or *z* axis, it is impossible to determine the efficacy of such a sensor for determining slip, although the FEA of the sensor supports that this is a possibility. A point of interest is that, under loading on the *y* axis the output voltage for the other axis drifted considerably, this was ascribed by the author as essential error in the positional stage used for experimentation.

Artificial neural networks have also been used in the development of piezo-resistive tactile sensor by Schopfer *et al*[75] for incipient slip detection by a robotic hand. The authors

had previously developed the sensor for high speed data acquisition at low contact forces in a robotic hand. The sensor consists of a conductive elastomer, the resistance of which changes proportionally to the pressure applied; and is capable of detecting forces between 0.1g/mm^2 and 20g/mm^2. The sensors have a modular design and thus, a number of the sensors can be arranged in an array without difficulty. Each individual sensor is made of a matrix of 16 x 16 cells. The sensor collects data and stores it within a microcontroller prior to transmission.

The sensor was mounted on the end effector of the Kuka lightweight robotic arm (Kuka, Augsburg, Germany) which has torque sensors in each of its joints; these provide contact force estimation between the myrmex sensor and object. The slip sensing algorithm was developed for the ANN by recording a number of slip stick conditions for 5 different materials. Initial contact forces were maintained at 0.8N and secondly at 2N and slip was recorded 5 times for each contact force and each material. Data processing was performed to transfer the information from the time domain into the frequency domain using a Fast Fourier Transform (FFT).

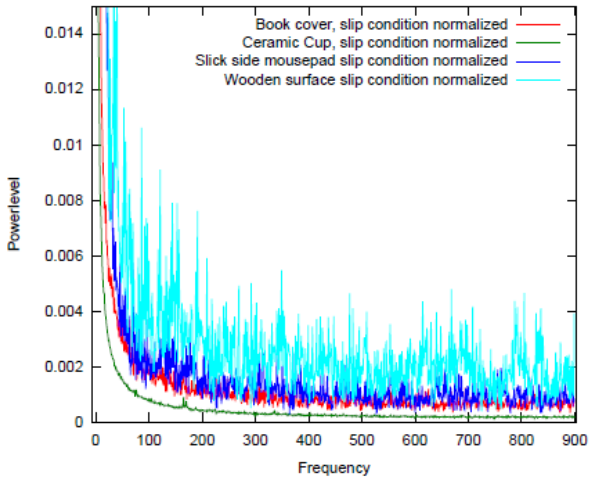

Figure 2.50: Frequency response of each of the materials when slip occurs. [75]

The frequency response of the tactile sensor showed quantitative and qualitative differences between each of the materials as shown in figure 2.50. The size of the FFT window for

determining slip was investigated. This was then used to differentiate between different materials. Although the largest window size investigated was superior, it also exhibited the largest standard deviation as seen in figure 2.51. The material classification experiments were unable to consistently determine the material component of each of the objects.

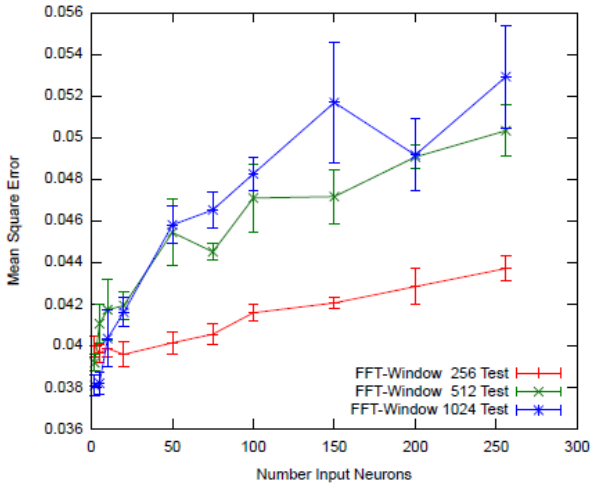

Figure 2.51: Comparison between window size of FFT for the classification of slip in the frequency domain [75].

It has been shown that the myrmex sensor is able to distinguish between slip and stick conditions based on the resistance output of the sensor investigated in the frequency domain. Within the frequency domain, the material exhibits distinctly different responses when slipping; however these responses do not enable individual distinction by the e robot. This may have been due to the relatively small training set for the ANN or possibly due to further post processing which could be addressed by a larger data set.

A biomimetic sensor for use in minimal access surgery was proposed by Hu *et al* [76]. It is based on a polyamide piezo-resistive sensors inspired by a hair follicle. The authors fabricated the sensor which comprised of a central silicon post and a thin polyamide film with 4 piezo-resistors fabricated atop the film diaphragm which functioned as strain gauges. The cylindrical central post has freedom of movement within a larger cylindrical surround which allows shear and normal forces to be detected by the transducer. Each sensor comprised of

four of these follicles, each with four strain gauges and an overall size of 9mm^2. The sensor was mounted to a PCB with etched electrodes for each of the sensing elements which also had a reference resistor connected in series.

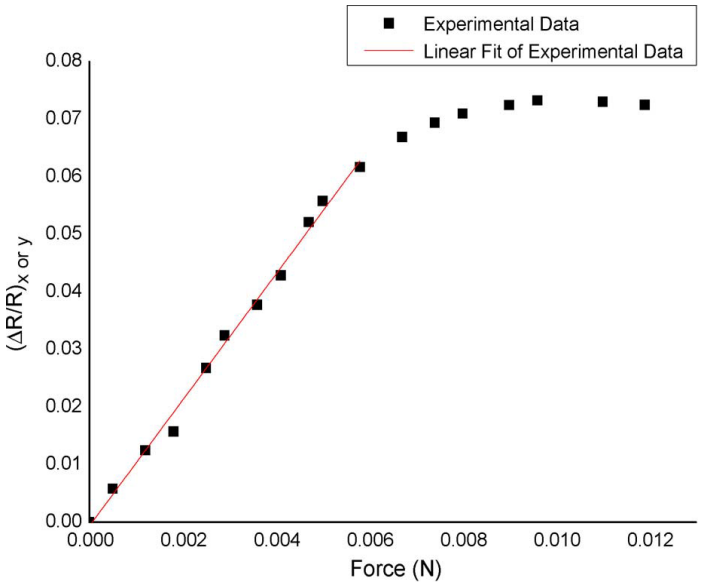

Figure 2.52: Linear response of the piezoresistive sensor on the x and y axis [76].

The force sensitivity and displacement sensitivity of the sensors were characterised by pushing on the central column of the sensor on each of the axis using a micro-needle on a nano-positioning stage. The change in resistance of each of the four surrounding resistors was recorded. There was a linear response of the change in resistance to applied load on both *x* and *z* axis as shown in figure 2.52. The saturation of resistance change when under shear is due to the central column reaching its maximum deformation. The force sensitivity was 10.8N^{-1} and 3.58N^{-1} for shear and normal forces. Minimum detectable forces were 0.017mN and 0.46mN in the shear and normal directions respectively. The resistance changes varied with the applied direction and were distinct from each other, with a similar resistance change in both *x* and *y* components when displacement force was applied in a 45 degree angle to the *x* direction.

Stimulus direction	0°	45°	90°	135°	180°	225°	270°	315°
$(\Delta R/R)_x$	-0.09709	-0.11303	0.00492	0.08991	0.04638	0.13992	-0.00910	-0.05823
$(\Delta R/R)_y$	0.00203	-0.13744	-0.08450	-0.07317	0.00337	0.14029	0.18308	0.05758
Measured direction	-1.2°	50.6°	86.7°	140.9°	184.2°	225.1°	272.8°	315.3°
difference	1.2°	5.6°	-3.3°	5.9°	4.2°	0.1°	2.8°	0.3°

Table 2.2: Theoretical and measured sensor outputs of the sensor at different angles of applied force.

Final experiments were carried out by scratching a finger at predetermined angles across the sensor and relating this to theoretical horizontal axis resistance outputs. Table 2.2 shows the measured direction and the difference between the expected and observed results. There is small difference between the two measured results, explained by the authors as an imperfection in angle control of the experiment. The team do not expand on how this 'finger scratching' experiment was controlled and thus cannot be deemed reliable from a scientific standpoint.

A piezoresistive tactile sensor with a high sensitivity for detecting forces on 3-axes has been reported[76] and which was able to detect both the magnitude and direction of slip. In this system, each sensor comprised a total of 16 resistive elements which required extensive data processing. These results are supported by a more recent publication by Alvares *et al* [77] in which a piezo-resistive sensor was developed using gold nanoparticles. Both sensors used similar testing methods and each sensing area comprised of 4 piezoresistive elements. Both are capable of multi-axial sensing and report linear changes in resistance when the applied force increases.

Thus far, piezoresistive sensors, have been shown to be able to distinguish between slip and no slip conditions with high sensitivity[76, 77]. They have also been shown to be able to detect the magnitude and direction of slip depending on the post processing of the signal from the sensor. A number have been proposed for the use in biomedical applications, MAS in particular although these studies are still at the early stage of development and have yet to

be implemented. Mirbagheri *et al* [55] reported a novel system in which strain gauges are embedded in the jaws of a triple jaw large organ grasper. Along with an actuating system this would facilitate monitoring of grasping forces.

The proposed design is a 10mm laparoscopic instrument with 3 jaws opening in a parallel fashion (by way of a four bar linker design for each jaw). Each jaw has a displacement of 42mm from the central axis of the instrument when fully opened. A strain gauge is embedded into each of the jaws midway along the active grasping area. The instrument is actuated via a DC motor housed within the handle of the device. The surgeon controls the device using a handle, or the device can be used to autonomously for grasping [55].

The efficacy of the strain gauges to measure grasping forces was studied by applying longitudinal and lateral forces ranging from 0 to 10N over a period of 60 seconds to the instrument jaws. The output of the strain gauges and digital force gauge used, were recorded for analysis. Force tracking of the instrument to provide autonomous grasping was also investigated. Forces ranged between 1 and 5N for harmonic loading of the sensor and 4 and 10N for step and ramp loading. The interface between force applied by the surgeon in hand held operation and the grasping force applied to the tissue was also investigated. A cantilever button was mounted on the handle of the instrument which applied a proportional force at the tissue-instrument interface. Finally, phantom tissue was grasped by the user in hand held operation. Grasping force was increased until visible deformation of the object occurred. This was used to characterise the grasped objects. Motor position and maximum grasping forces were recorded for evaluation[55].

Voltage output of the stain gauges exhibited a linear relationship with normal loads applied; however the system had a voltage output swing of up to 3V which changed over time. Sensitivity of the sensors varied between 0.33 and 0.51mV/V under loading of 10N. Force tacking experiments confirmed the efficacy of the system to apply a grasping force based on

a *prescribed* setting. Figure 2.53 shows that the force under one of the jaws in relation to the desired force over a range of forces. Similar results were obtained when the instrument was used in hand held operation; the relationship between the applied force on the cantilever button by the surgeon and grasping force had a maximum error of 0.7N. There was a time delay of about 100ms which instant force tracking difficult. Experiments involving grasping materials of various stiffness showed that the lower the stiffness of the material, the larger the displacement of the jaws, and the smaller the maximum grasping force[55].

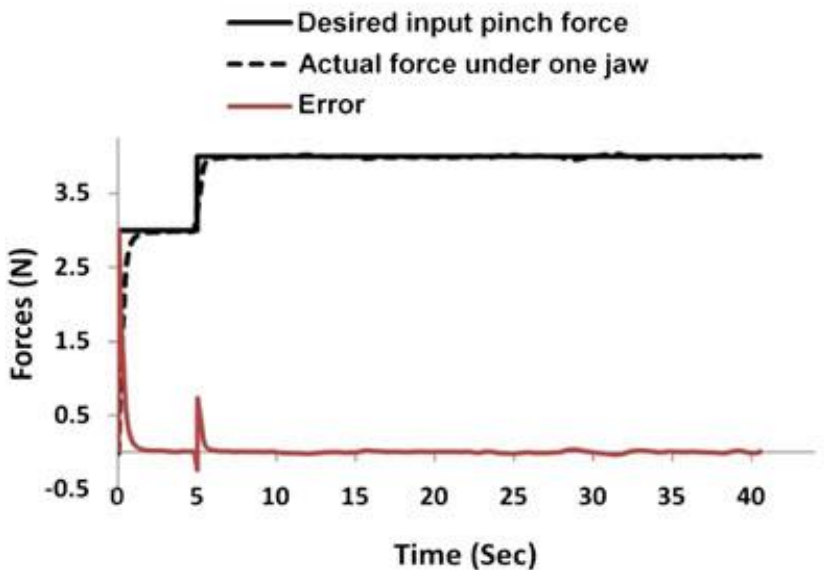

Figure 2.53: Desired and actual forces produced by the grasping jaws[55].

A grasping instrument in which strain sensors are used to detect the normal forces applied to tissue during grasping has been reported[55]. This instrument has the ability to apply prescribed loads to a grasped object with a high degree of accuracy. This is achieved by using a cantilever button to detect the force applied by the surgeon and relating this to the force detection by the strain gauge. This system is not autonomous and relies solely on the user to determine the grasping forces. The output of the sensor is also heavily time dependent with a voltage bias of up to 3V over 4 hours. As the system can only detect changes in forces on one

axis and has such a large voltage bias over time it would not be suitable for use in a closed looped autonomous system; as it would be impossible to implement any meaningful threshold.

A flexible carbon nanotube (CNT)-polymer matrix tactile sensor was developed by Engeberg *et al*[78]. The working principle is that when the CNT wires are flexed under an applied load, the length of the wire changes and this leads to a change in resistance. When coupled with a resistance of similar impedance in a half Wheatstone bridge configuration, the change in resistance will result in a proportional change in output voltage.

Multi-walled CNT's were dispersed by weight in acrylate-based monomer solution using an ultrasonic bath. This CNT-polymer solution was then extruded to a diameter of 1mm and cured. The conductive wires were then encapsulated in a polyurethane rubber. The sensor, shown in figure 2.54, comprised of ten conductive CNT-polymer elements. The sensor was investigated to see how its output voltage differed during slip and no slip conditions. For this, 100g loads were repeatedly applied and removed from the surface of the sensor as well as being slid along the surface. The signal was investigated in the frequency domain after FFT was performed. A second experiment was performed by sliding a human finger along the surface of the tactile sensor perpendicular to the alignment of the CNT wires. This was done to determine if the force can be measured at distinct locations on the sensor surface and also to establish whether the sensor was able to distinguish the direction of slip.

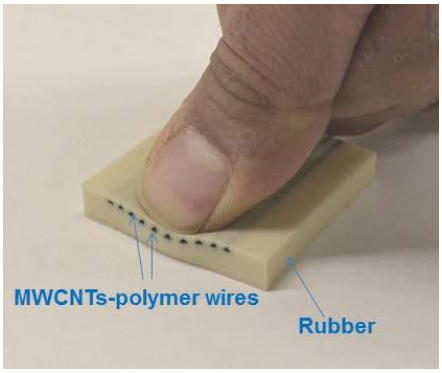

Figure 2.54: CNT wires embedded in a compliant polymer casing [78].

Slip and non-slip events in the frequency domain of the sensor output were shown to be distinctly different. Non-slip events produced a frequency of between 0 and 40Hz; whereas the frequency of a slip event ranged between 0 and 200Hz. Other experiments showed that the direction of the slip could be determined due to the time difference between voltage outputs of the individual CNT wires (figure 2.55). The author also states that the wires can determine the applied force but does not elaborate on how this can be done, the assumption being that a greater applied load would lead to a higher resistance change.

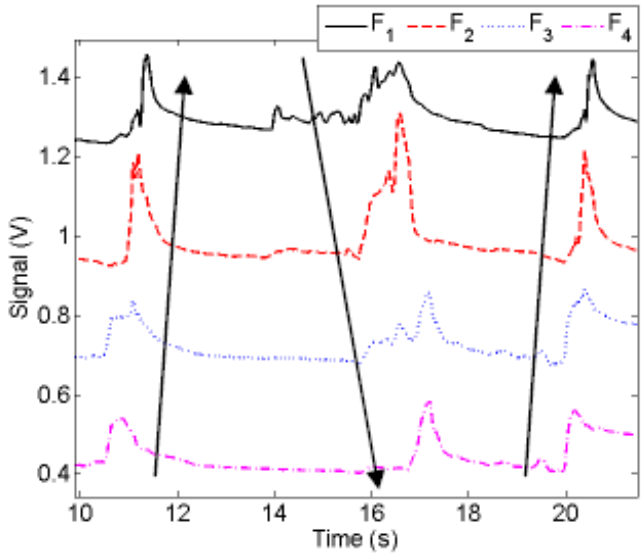

Figure 2.55; Sensor response of the various CNT wires showing the response timing [78].

A lot more work is necessary to accurately characterise this sensor to determine the applied load and the slip direction. However, given the simplicity and flexibility of the sensor design it has the potential for wide ranging applications in MAS and robotic surgery.

2.4.3 Alternate methods of slip detection

A number of other technologies have been investigated in the field of slip and force sensing which will be discussed briefly. These include capacitance based systems, optical sensing and conductive rubber-based technologies.

Optical sensing is based on changes in the detected light source. The technology comprises s a family of sensors with a wide range of design solutions; two of which are discussed because of their wide use as optical sensors. The first is a standard optical sensor often used in the mouse for a home computer and, more recently, embedded into smart phone technology. Sani *et al*[79] proposed the use of such an optical sensor for detection of slip detector, when incorporated in a prosthetic hand. The sensor used was a commercially available infrared optical sensor with built-in image acquisition and image processors capable of detecting motion rates at up to 508mm per second. The optical sensor was mounted along with the necessary lens and protective casing onto a 3 fingered robot as a prototype and experimental rig as shown in figure 2.56. During experiments a number of material properties were investigated: roughness, curvature, transparency, reflectivity and hardness.

Figure 2.56: Optical sensor mounted between two fingers of the three fingered robotic grasper as it holds a material [78].

A linear stage was used to move the selected materials across the surface of the stationary optical sensor at different distances from the sensor surface. The distance between sensor and object increased in increments of 0.5mm until the sensor ceased to detect motion. An infrared emitting LED and red light LED were both tested as a source of illumination on the assumption that both would perform equally well. The different materials used for testing the height experiments were: white paper, black paper, sheet metal, plywood, sand paper and textured, black acrylic sheet. Other materials relating to the particular investigation were used e.g. using a mirrored surface for reflectivity testing. The sensor readings, encoder readings and time between each data point were recorded for analysis.

Results showed that at a distance greater than 1mm from the surface of the optical sensor, the sensor would give a higher read out as the roughness of the material increased. When the material of the grasped object had a curvature, the sensor was able to detect motion but its output was reduced. The sensor was incapable of detecting motion through any transparent object. When the reflectivity of the object was too high (>80%) the sensor was unable to detect motion (results are summarised in table 2.3). There was no difference found between using an infrared or visible red light source.

Materials	Transparency (CPMM)	Reflectivity (CPMM)	Hardness (CPMM)
Glass	0	-	-
Acrylic	0	-	-
Acrylic with paper	0	-	-
Glass w/t textured black acrylics	254	-	-
Front silver mirror	-	0	-
CD	-	0	-
Glossy paper	-	584	-
Wood w/t wood finish	-	1448	-
Sheet metal	-	3632	-
Plywood	-	6350	-
20 Durometers	-	-	4115
35 Durometers	-	-	4191
60 Durometers	-	-	5029
80 Durometers	-	-	5105

Table 2.3: Sensor output relating to transparency, reflectivity and hardness of various materials [78].

This type of sensor has shown to be able to adequately detect slip depending on the surface textures and reflectively of the grasped material. Due to its inability to detect movements with highly reflective surface and its inability to detect incipient slip, this form of optical sensor is unsuitable for the grasping of tissue during laparoscopic surgery. The sensor is also relatively large and thus could not be incorporated in a laparoscopic instrument less than 10mm in diameter.

Photodiodes are the second most commonly used system for tactile sensing. These systems convert light intensity into a directly proportional current or voltage. Missinne *et al*[80] reported a photodiode based, ultra-thin optical shear sensor. The sensor is constructed with a light source, in this case a flexible vertical cavity surface emitting laser (VCSEL), a commercially available ultra-thin photodiode and a deformable transducer layer between the light source and sink. The sensor has an overall thickness of 260µm. Its working principle (figure 2.57) is that when a shear force is applied the photodiode will be displaced from its position directly above the VCSEL, causing a difference in detected light intensity.

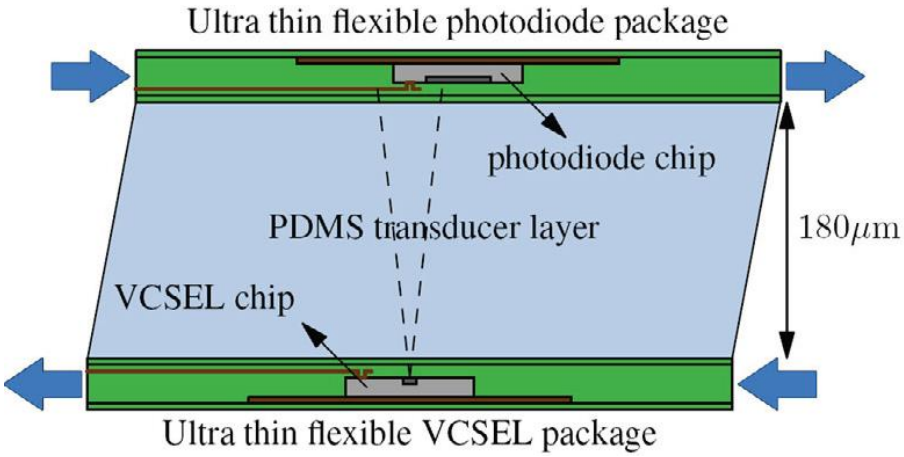

Figure 2.57: Working principle of ultra-thin photodiode based optical sensor [79].

Two studies were performed to determine the sensor response as a function of lateral displacement and the relationship between applied shear stress and lateral displacement. The bottom surface of the sensor was fixed and a prescribed displacement was applied to the upper surface. The current read out of the photodiode and the corresponding shear force were recorded. The magnitude of displacement (and corresponding shear stress) could be determined by the sensor, (figure 2.58) but the system does not sense the direction of movement. This was attributed by the author to the cylindrical nature of the photodiode. Finite element analysis of a square photodiode with a VCSEL aligned to one of the edges then showed the direction of slip were only detectable in the *x* direction. Having an additional VCSEL placed on the adjacent edge of the square would theoretically enable detection of the direction of slip in two dimensions.

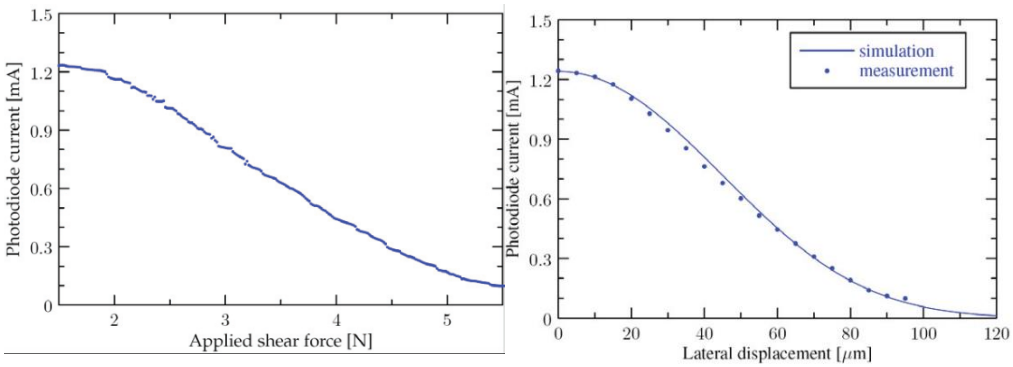

Figure 2.58: Relationship between photodiode output, shear force and lateral displacement [79]

The approach taken by Missinne shows promise but is in need of more development before it can be realised as an effective solution for slip detection. Ultimately it may be possible to determine incipient slip using this sensor if the Young's modulus and friction coefficient of the grasped object are known.

Capacitive based tactile sensors have also been proposed in the literature. Lee *et al* [81] reported a multi axial capacitance based sensor using an 8 x 8 array of polydimethylsiloxan (PDMS). Each individual sensor in the array comprised of four capacitive sensors enabling the distinction between shear forces in the *x* and *y* directions, in addition to detection of normal forces. A 3D model of the developed sensor is shown in figure 2.59. A bump is designed into the sensor along with an air gap to allow proper deformation and thus provide a better response from the sensor. Each sensor within the array measures $2mm^2$. The device is made by depositing copper electrodes then a PDMS layer atop a silicon substrate, further PDMS spacing, insulating and bumps are formed in a similar manner. Silicon substrates are then removed allowing each of the parts to be bonded together as shown in.

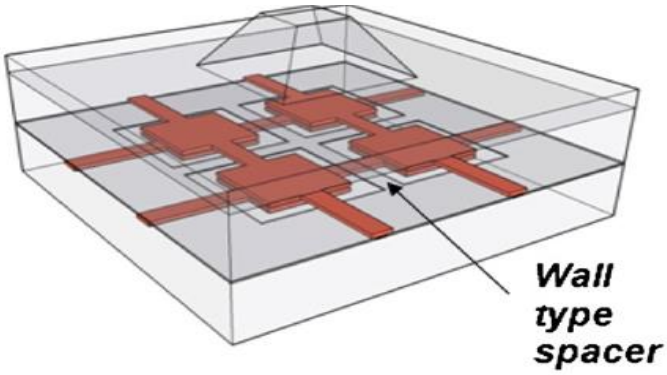

Figure 2.59: 3D model of capacitance based sensor with 4 capacitive based sensors for sensing multiple sites as well as spacers between each of them.

The device was tested by applying normal and shear forces to the bumps of the sensor by a force gauge and motorised translation stage. Initial, unloaded capacitance measurements were performed giving capacitance for each of the 4 sensors (C11, C12, C21 and C22) as 2013, 204, 190 and 205 farads respectively. The normalised capacitance for forces applied axially in each direction, are shown in figure 2.60, where it can be seen that the response for each directional loading was distinct from the others. Using this initial data the authors developed a mechanical model to calculate the force component on each axis for forces ranging between 0 and 15mN. Theoretically the responses on each axis showed a linear response and from the team estimated a sensitivity for the single unit sensor in each axis of 1.3, 1.2 and 1.2%/mN on the *x*, *y* and *z* axis respectively with a maximum response of 20mN in all directions; after this point the sensor output would saturate.

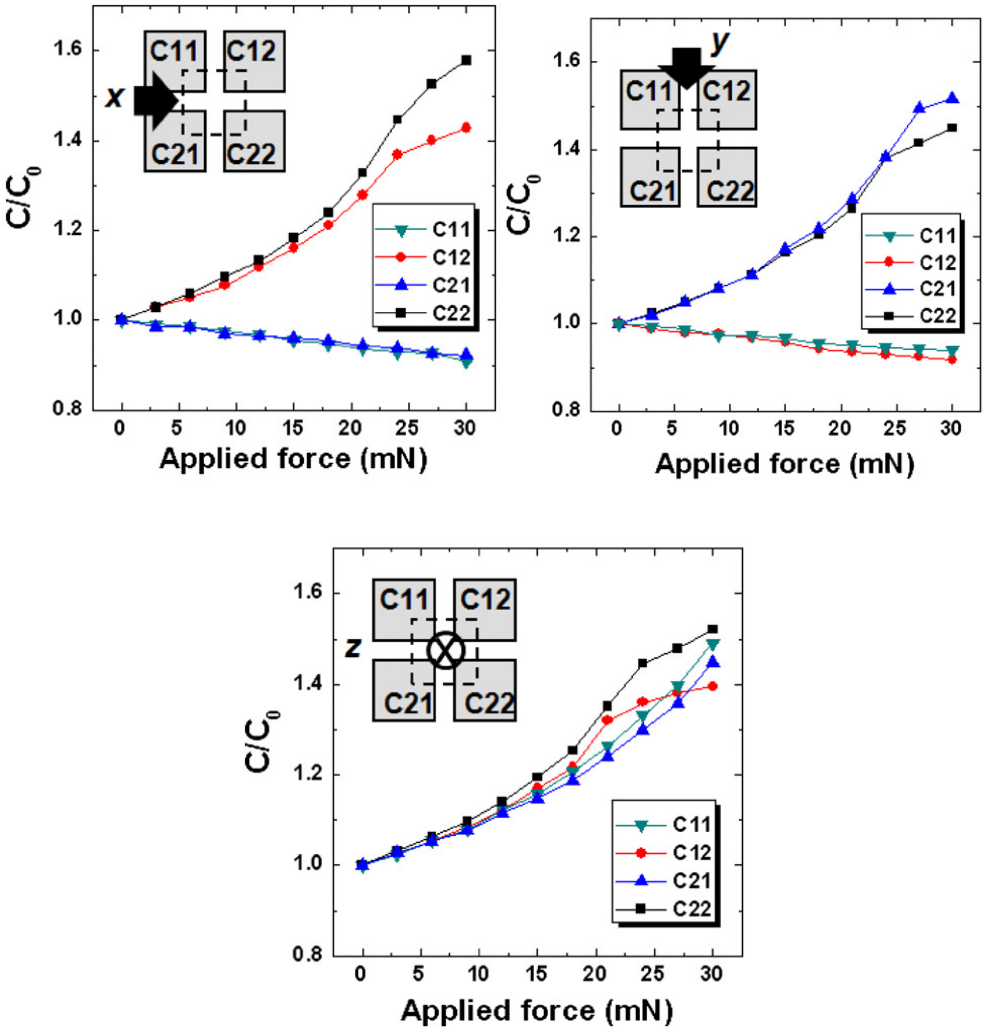

Figure 2.60: Sensor outputs according to the direction of the loading force. Shear forces are shown in the top row and normal forces below [80].

A real time measurement and display system was developed to show the capacitance of the overall 8 x 8 array sensor when it is bonded to the surface of a finger-like structure with a curvature radius of 4mm. The displayed information has 3 components, each for representing the applied forces on the different axis. Figure 2.61 shows the output of these displays when a finger applied a force *x* direction.

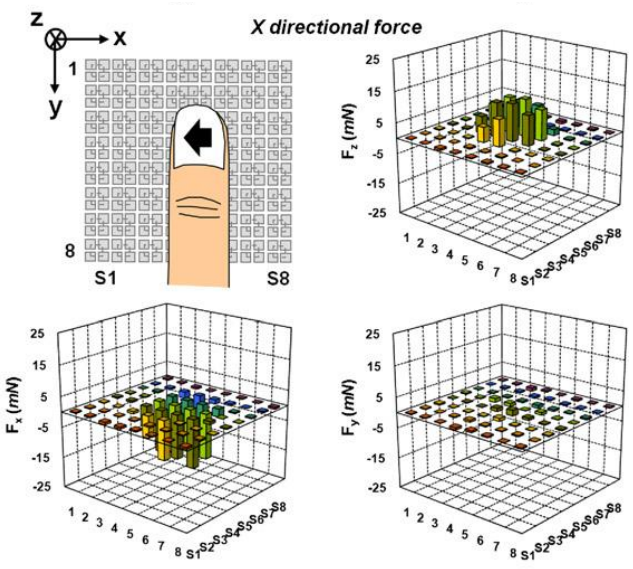

Figure 2.61: Data representation of the sensor output when a finger is rubbed across the surface [80].

Response time between the applied loading and the observation of the change in capacitance is calculated to be 160ms. The authors noted that there may be a possibility for creep due to the deformation of the viscoelastic material over time which would modify the dimensions of the air gaps in the sensor. The design proposed is of interest as it can accurately represent static and dynamic applied forces on all 3 axes within a fifth of a second. The system has not yet to undergone rigorous testing under controlled conditions and hence it is not known whether this type of sensor could detect incipient slip. The complexities in developing such a sensor also limit its use, as shown by the team in a previous article[82], since the slightest changes in the mechanical structure of the design have such a large impact on both response time and ability to detect loading forces.

3. Influence of design features in the reduction of tissue trauma by laparoscopic graspers.

3.1 Introduction

Laparoscopic tissue graspers are used to manipulate tissue during minimal access surgery (MAS). There are many variations on the basic grasper design and a number also purport to be atraumatic. Some tissue graspers contain design features such as fenestrations and surface profiling of jaws, which are supposed to aid in the retention of tissue.

Both the retention and damage of the grasped tissue resulting from these design features are poorly understood because of the limited published literature on the subject. Hence this chapter on the development of a method of testing the effects of various design features and their impact on tissue retention. In addition, the experiments investigated the design features which increase the retention of tissue in the jaws of laparoscopic graspers on application of minimum force to prevent slip. These studies will enable design of laparoscopic graspers which would provide maximal tissue retention without used of excessive applied forces that could potentially damage the tissue.

Current laparoscopic tissue graspers are small in size (5mm) and thus have a very small surface contact area with the tissue and so the loads applied to the tissue are distributed over a small area, leading to high compression pressures. This problem is exacerbated by the occlusion mechanism of the graspers. This is often a pivoting joint or 'scissor' type mechanism, which inevitably induces high pressures in the proximal opening of the jaws and at the tip of the instrument[65, 66].

It is therefore not surprising that current grasper designs have been documented to cause trauma to the grasped tissue/ organ[36] [83].

Surface profiling in the jaws of graspers is commonly used to increase grip and prevent tissue slip. The findings in the reported literature indicate that the dual objective of reduced potential for tissue damage and successful retention of the grasped tissue within the jaws of the grasper requires a large surface contact area [84, 85]. Heijnsdijk[85] also reports that a slight profile should be used to increase tissue retention during grasping.. However, many commonly used designs have significant potential to cause tissue tearing, although the ideal profile is not indicated by this author. To some extent, these observations are supported by Marucci[84] who reported that a 2mm wave profile appears to prevent damage to tissue; however it also decreases the tissue retention properties of the graspers.

Fenestrations constitute another design feature often included in laparoscopic graspers as they are thought to minimize tissue slippage due to the tissue bulging within the aperture(s). However, this perceived effect of fenestrations has not been confirmed by the only published study[51], which concluded that fenestrations have a negative effect on tissue grasping as they lead to more frequent tissue damage at lower applied loads. This study also reported that fenestrations by reducing the surface contact area between instrument and tissue produce higher local pressures and hence increased risk of damage.

Ideally laparoscopic tissue graspers should be able to safely secure tissue without causing damage or tissue slippage from the instrument. In a reported study on the forces [86] which would prevent damage including perforation during colonic laparoscopic surgery, the laparoscopic instrument required to transmit forces ranging from of 2.5 - 5N, which fortuitously approximated to the average forces trained surgeons applied to manipulate the bowel for effective dissection.

Few papers within the published literature investigate the effects of surface profiling and fenestrations with only investigation on the effects of fenestrations. In addition, there is no standardised method of reporting the outcomes of such studies, although methodology throughout the literature is relatively consistent. The present studies outlined in this chapter investigated the effect of fenestrations and surface profiling of jaws on grasping efficiency as the basis for the design of an improved laparoscopic tissue grasping instrument. It will also provide an effective method for data reporting in a consistent way which will make comparisons between fenestration and surface profile designs at the various applied loads easier to appreciate.

3.2 Methods

Three aspects of jaw geometry were investigated in three separate experiments: (i) fenestrations, (ii) ratio of contact surface to fenestration area and (iii) surface profiling.

Jaws designed for the initial two experiments did not include any surface profiling. Surface profiling along with the superior fenestration design, informed by the results of initial experiments, were investigated in the third and final experiment.

3.2.1 Manufacture of jaw designs

All of the jaw geometries were manufactured by milling the various design features from stainless steel. As an inevitable consequence of milling these shapes from a solid jaw, the rectangular apertures had a 0.5mm radius in each of the corners; and in all designs a slight

radius was manually applied to the edges to prevent excessive pressures and tissue damage[66]; these operations reflect common manufacturing practice for mass-produced surgical graspers.

3.2.2. Fenestration Designs

3.2.2.1. *Constant Surface contact area*

The first experiment investigated whether the fenestration should be either confined to one large area; or consist of a number of smaller openings. Three designs were studied: one large rectangular opening, two smaller rectangles and three circles (both equalling the area of the single large fenestration). In the only published literature on investigating the effects of fenestrations on tissue retention, various fenestration designs in the jaws of graspers were investigated in a similar manner and reported[51], although the geometries (circular) examined were not representative of those found in laparoscopic instruments.

The width of the single and twin fenestrations was 7mm and the diameter of the circular fenestrations was 6mm. A pair of featureless non-fenestrated jaws were machined and used as benchmark controls. In order to ensure that a constant pressure was exerted on the tissue, all jaw designs had the same surface contact area – 208mm^2, *i.e.,* for each 1N applied force; the pressure exerted on the tissue was 4.81kPa. The same surface contact area was used for one of the control jaws and the other control was of comparable size to the fenestrated designs. All jaw designs are shown in figure 3.1.

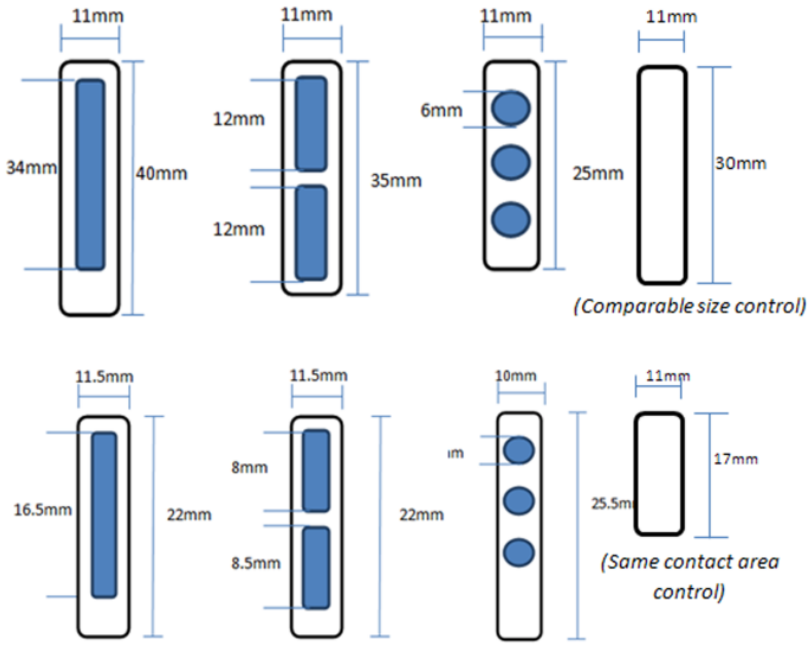

Fig 3.1.*Top Row:* Dimensions of constant surface contact area jaws.

***Bottom Row:* Dimensions of the 1:0.8 ratio fenestrated jaws.**

3.3.1.2 Surface contact area to fenestration area ratio

The second experiment investigated the optimum ratio of surface contact to fenestration area, testing the following ratios 1:0.4, 1:0.8, 1:1, 1:1.2, 1:1.6. The same three designs (single rectangle, 2 smaller rectangles and three circles) were used and the surface contact area was kept constant. All the various types were benchmarked against a pair of plain jaws of comparable dimensions.3.2.3 Profile Designs

The surface profiles investigated are shown in Figure 3.2 and were compared with smooth jaws of the same size, which served as controls. The profiles investigated had been studied and reported previously[87] but the current aim was to determine the effect of fenestration on the performance of these surface profiles. All profiles studied had an opposing jaw with

profile which inter-digitated with the opposite jaw to secure the tissue. The optimum fenestration designs, informed by the initial experiments, were also included in the jaws along with the surface profiles.

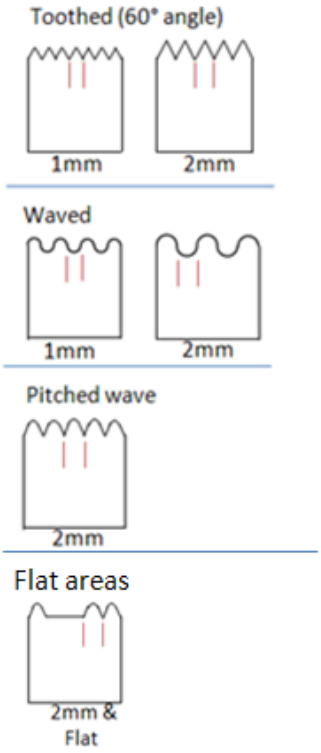

Figure 3.2: Designs of the surface profiles which were investigated.

3.2.4 Experimental procedure

Methodology for the experimental procedure was identical to that reported in the literature [84, 85].The procedure was kept consistent throughout the testing of the various design features. The jaw designs were opposed to provide parallel occlusion in a similar fashion, although not explicitly stated by, the published literature. The purpose of this was to prevent the high pinch forces found in the proximal opening of more conventional grasping jaws. Identical but opposite jaws were used throughout. This allowed the surface profile designs to inter-digitate. This was not a concern with the initial fenestration experiments which did not have any surface geometry.

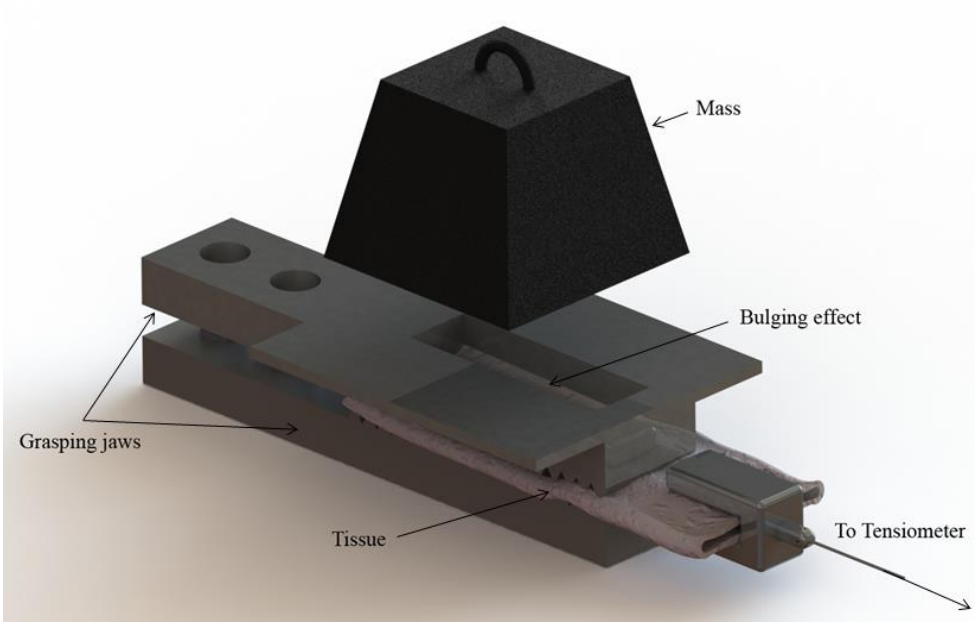

Figure 3.3: Experimental test rig for retracting tissue from the jaws of the graspers opposed in a parallel fashion.

The lower jaw was fixed in position and the upper jaw was free to move on the *y* axis along two guide pins, allowing for the grasping and equal distribution of load upon the tissue whilst also ensuring parallel movement. Thiel embalmed *ex-vivo* porcine large bowel was placed between the jaws and various loads (1N, 2N, 4N, 6N) commonly encountered during laparoscopic surgery were then applied on the upper jaw[86]. The tissue was then pulled until free from the jaws through a pulley system at an angle of 90 degrees by an Instron tensiometer (Massachusetts, USA) using traction at a rate of 3mm/s. The pulley system comprised of a free spinning wheel with negligible friction placed directly below the tensiometer head through which 8lb fishing wire was attached to tissue using a small detachable grasper. Fishing wire with a higher breaking strength than what would ever be encountered was selected and replaced at regular intervals to ensure that any stretching of the wire would not affect results. Traction force data was recorded

on a personal computer. Eight replicates for each jaw design for each loading condition was carried out.

3.2.5 Statistical analysis

All results were analysed using ANOVA and consequently the Tukey alpha post hoc test used where significance had been found. Since the means of multiple pairs were compared and all group sizes were equal this data set lent itself to the more powerful Tukey alpha post hoc test. To provide a single 'figure of merit' to aid comparisons, results are expressed as a ratio of retraction force necessary to pull the tissue from the jaws to the applied force (Rf/Af): a high value of this ratio indicates a good grasp of the tissue with minimal pressure.

3.3 Results

3.3.1 Effect of fenestrations design

At all applied forces the retraction force needed to pull tissue from any fenestration design was significantly higher than the force necessary to pull tissue from non-fenestrated jaws *($p<0.05$)*, graph 3. 1. In addition, at no point was there a significant difference in retraction forces needed to pull tissue from the two plain jaw designs (one of the same surface contact area and one of comparable size to the fenestrated jaws). No consistent significant difference was documented between the three fenestration designs studied: where significance levels were found they varied erratically with the applied force conditions and thus no strong conclusion could be made as to which fenestration design enhanced the grip.

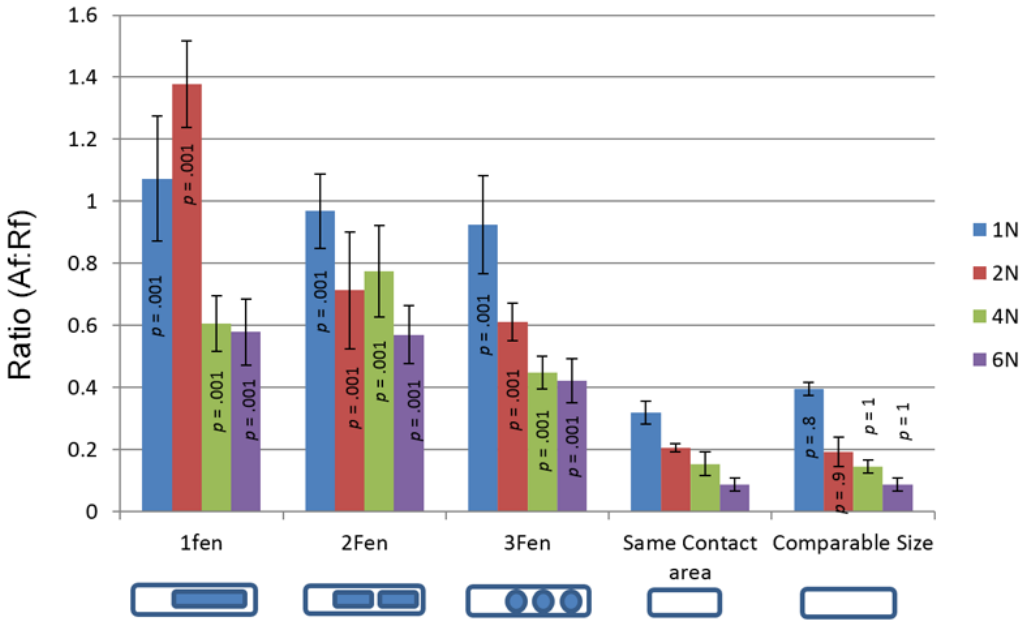

***Graph 3.1*: Ratio of retention force to applied force (±σ) for various fenestrated and plain jaws, all of which had the same contact area.**

3.3.2 Ratio of surface contact to fenestration area

The results of the second experiment for the three fenestration designs are shown in graphs 3.2, 3.3 and 3.5. The ratio of 1: 0.4 (obtained with very small fenestrations) performed significantly worse than the others ($p<.0.05$,) indicating that the ratio should exceed this, with the best tissue retention being encountered with ratios ranging from 1: 0.8 to 1.1.

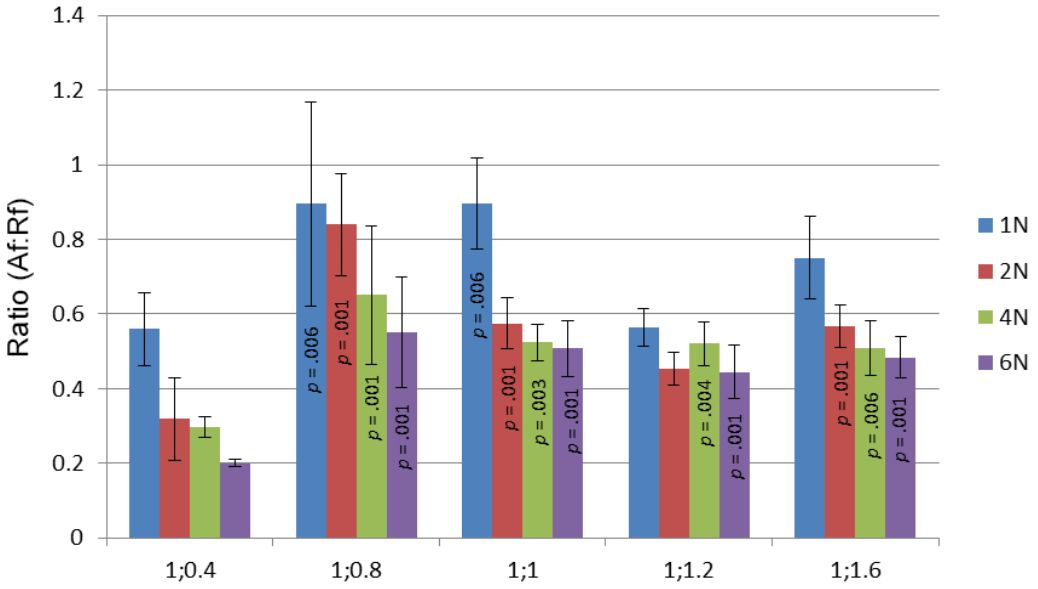

Graph 3.2: **One fenestration; Ratio of retention force to applied force (±σ).**

P **values shown are with respect to the jaws of ratio 1:0.4.**

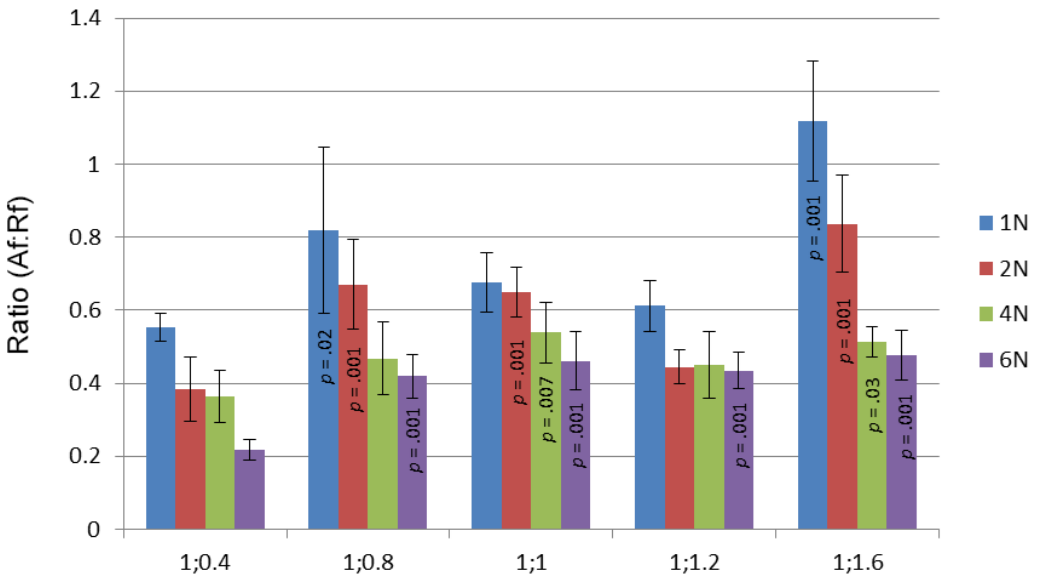

Graph 3.3: **Two fenestrations; Ratio of retention force to applied force (±σ).**

P **values shown are with respect to the jaws of ratio 1:0.4.**

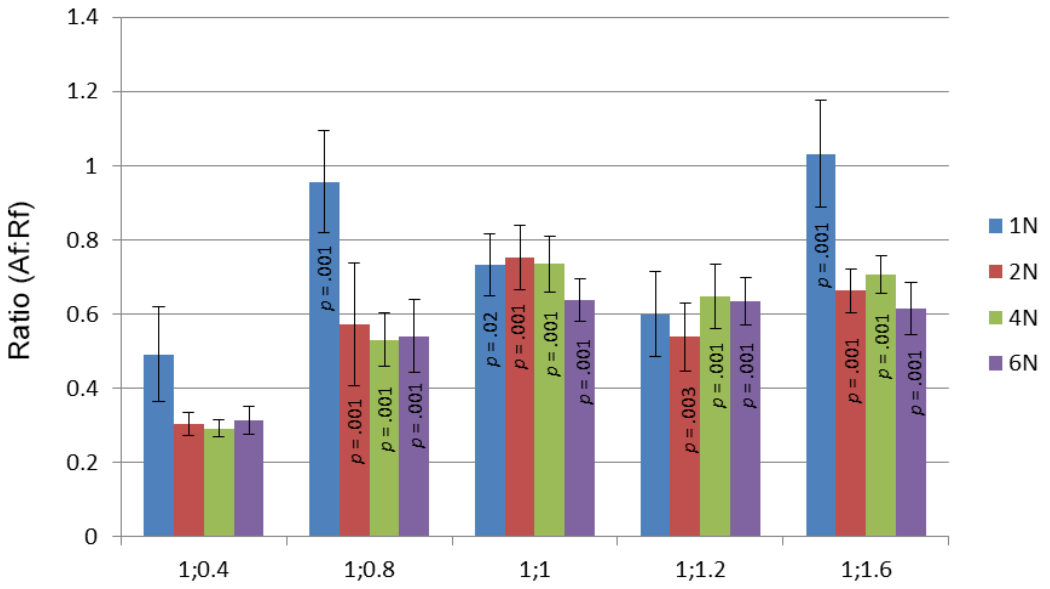

Graph 3.4: **Three fenestrations; Ratio of retention force to applied force (±σ).**

P **values shown are with respect to the jaws of ratio 1:0.4.**

3.3.3 Surface Profiling

All the profiles studied were made in jaws with a single fenestration and with a surface contact to fenestration area ratio of 1:0.8. The results of this experiment showed that all of the profile designs performed significantly better than the control ($p<0.005$) with no consistent significant differences between the profile designs with the exception of the 1mm waved profile, which performed significantly worse than the other designs ($p<0.004$), although still superior than the smooth non-profiled jaws as shown in graph 3.5. The mean and standard deviation of the retention to applied force ratio across all applied load conditions obtained by this experiment were 1.23: 1.0 for the 1mm waved profile, and 1.7:1.0 for the 1mm toothed profile with standard deviations for the corresponding retention force of ±0.45 and ±0.38 respectively. In other words with the 1mm toothed profile only 1N of clamping force is needed in order to retain tissue despite this being pulled by a force of 1.7N.

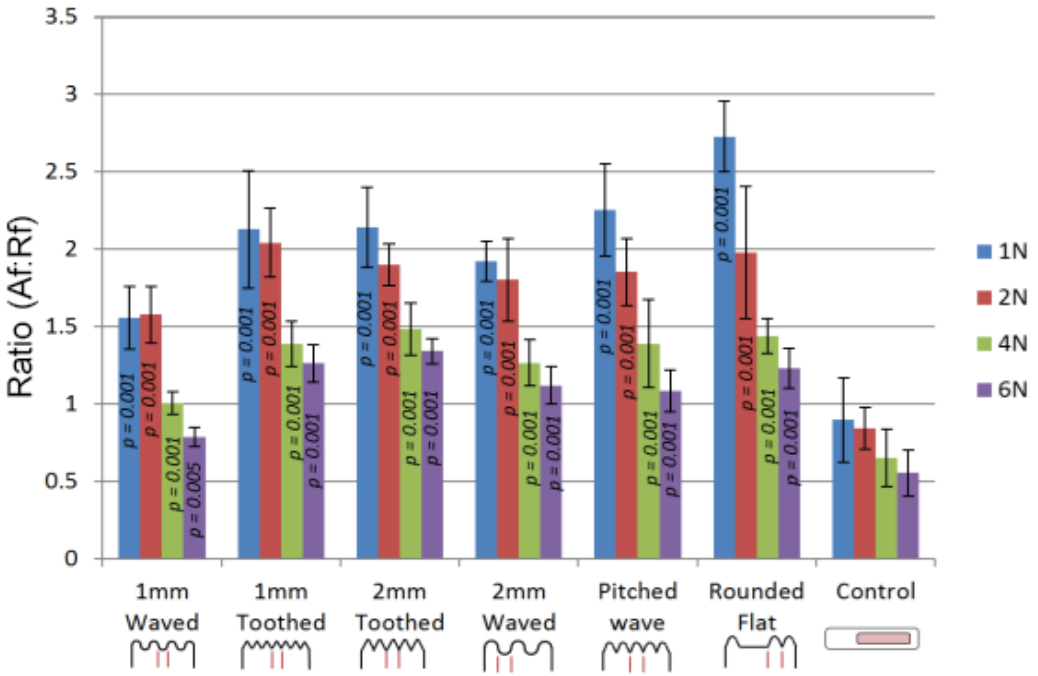

Graph 3.5: **Ratio of retention force to applied force (±σ).**

P **values shown are with respect to the control.**

3.3.4 Pressure applied to the tissue by different loading forces.

Representing the data as a ratio of applied force to retention force, enabled the determination of the amount of applied force to the tissue needed to prevent it from slipping from the jaws at various pull forces for all of the fenestration and profile designs. The results demonstrated that if the ratio was greater than 1:1, then the amount of applied force necessary to retain tissue in the jaws would be lower than the pull force, thus minimising the pressure applied to the tissue.

Table 3.1 and graph 3.6 shows the amount of applied force necessary to retain tissue against the common forces found in during laparoscopic surgery for the surface profile designs which were investigated.

	1N	2N	4N	6N
1mm Waved	0.64	1.27	3.98	7.66
1mm Toothed	0.47	0.98	2.89	4.76
Pitched Wave	0.44	1.08	2.88	5.55
Rounded/Flat	0.37	1.01	2.78	4.88
2mm Wave	0.527	1.11	3.17	5.37
2mm Tooth	0.47	1.05	2.7	4.48

Table 3.1 Applied forces needed to retain tissue against common pull forces when the Af/Rf ratio is applied.

This information can be presented as a pressure versus the applied force needed to retain tissue against the various pull forces, graph 3.7. This could provide an indication of the potential to cause trauma to the tissue being grasped when compared to published literature on the pressures necessary to cause damage to bowel tissue.

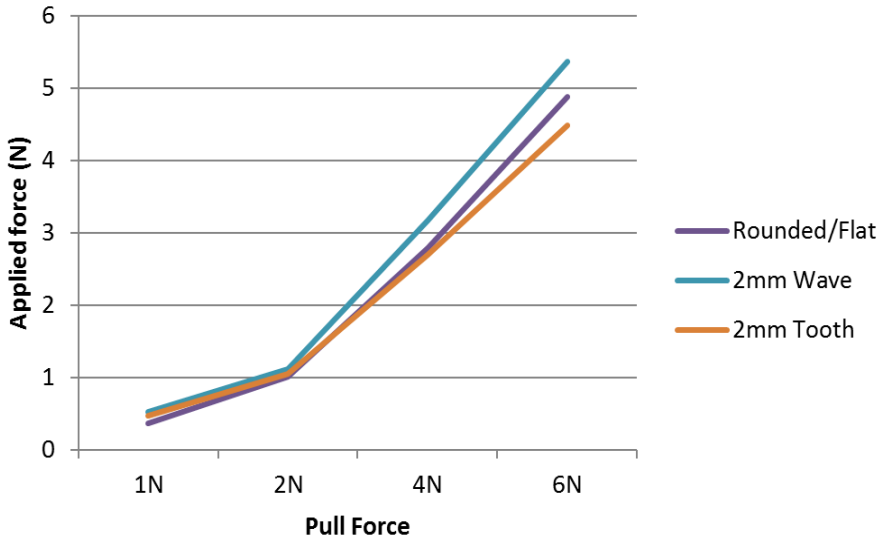

Graph 3.6: A selection of 3 surface profiles showing the amount of applied load need to retain tissue in the jaws when the Af/Rf ratio is applied.

Table 3.2 and 3.7 shows the impact of fenestrations on applied pressure when one considers the amount of force needed to retain tissue at various pull forces. As more force must be applied to the tissue to secure it within the jaws when there is no fenestration, the pressure

applied to the tissue is far greater. This is indicated by a very low ratio of retention force to applied force (>0.4:1 with the same contact area as a fenestrated jaw).

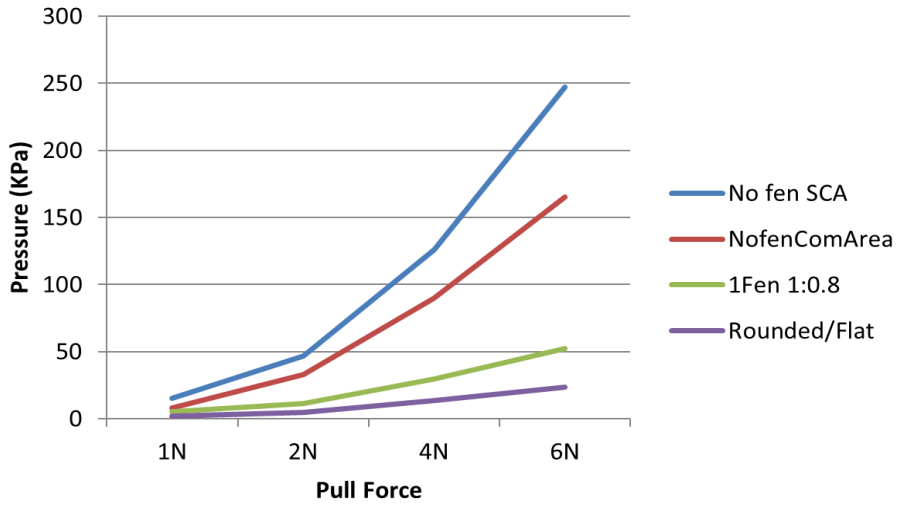

Graph 3.7 Pressure applied to retain tissue in the jaws at various pull forces when the Af/Rf ratio was applied.

	Non fenestrated (Same contact area)		Non fenestrated (Comparable size)		1 fenestration (0.8:1)		Rounded flat profile with single fenestration.	
Pull Force(N)	Applied force(N)	Pressure (kPa)	Applied force(N)	Pressure (kPa)	Applied force(N)	Pressure (kPa)	Applied force(N)	Pressure (kPa)
1	3.12	15	2.5	8	1.12	5.3	0.37	1.7
2	9.76	47	10.26	33	2.382	11.5	1.01	4.8
4	26.23	126	27.59	90	6.15	29.5	2.78	13.4
6	51.43	247	50.7	165	10.88	52.3	4.88	23.5

Table 3.2 Pressure applied to retain tissue in the jaws at various pull forces when the Af/Rf ratio was applied.

Theoretically the amount of pressure applied to tissue when it is grasped by a non-fenestrated jaw should be lower as there is a greater surface area which distributes the applied load across the tissue. As the ability to retain tissue is however hindered by the lack of fenestration, greater forces have to be applied in order to retain the tissue within the jaws. When comparing the non-fenestrated jaw to a fenestrated jaw with the same surface contact area, the force and pressure applied to the tissue could be as much as 5 times greater for the non-fenestrated jaw.

3.4 Discussion

The findings of these experiments are at variance with those reported in the published literature by Heinsdijk *et al.*[51] who concluded that fenestrations impart no benefit to the retention of tissues. The results of the present experiments clearly show the opposite, that is, the inclusion of fenestration within the jaws of the laparoscopic graspers will increase significantly the retention ability so long as the area of the aperture is greater than 40% of the tissue – instrument interface. The contrasting, mutually exclusive outcomes of the two studies may be caused by the fenestration designs used. Heinsdijk investigated the placement and number of fenestrations however the circular fenestration designs used by these researchers were not accurate reproductions of those found in laparoscopic instruments. The circular fenestrations used were also investigated in the present study which also found that they were still superior to smooth jaws and not significantly different from the other two rectangular designs.

The tissue which was used could be a possible explanation as to the disparities in the outcome of the two studies. The initial study carried out by Heinsdijk uses fresh small bowel whereas this study uses thiel embalmed large bowel. Large porcine bowel often has fatty deposits on the serosal surface of the bowel tissue, this could aid in the retention of tissue. Thiel embalming is known to alter the mechanical properties of tissue, namely increased plasticity and lower failure stress[88] when the mechanical properties of rat and human tendons were investigated.

The concern of expressed by Heinsdijk *et al.* [51] on the basis of their study is that by including fenestrations in the jaws of the instrument, the contact area will be reduced, and thus this inevitably increases the pressures applied to the grasped tissue. This is a valid concern as it is not uncommon for tissue to be grasped with excessive forces by the operating surgeon [46] which can potentially lead to tissue damage. However, the present study has demonstrated

quite unequivocally that the inclusion of fenestration in the jaws of the instrument reduces the magnitude of the applied force necessary to retain tissue at all pull forces. This is particularly important when the pressures applied to tissue are investigated. Graph 3.6 and 3.7 clearly show that due to lower applied forces needed to retain tissue in the jaws at all pull forces, the pressure applied to the tissue is greatly reduced in all instances when comparing fenestrated and non-fenestrated jaws. If the grasping forces are automated by an intelligent system so as that the forces applied to the tissue are never in excess of the force necessary to prevent slip, the pressure applied to the tissue will be less than that deemed to be dangerous and less than that needed to retain tissue with non-fenestrated jaws as shown in table 3.6 and 3.7.

The smallest fenestration with a fenestration to surface contact area ratio of 0.4:1 performed significantly worse than the other ratios investigated. No difference was found when comparing other ratios. In order to maximise the surface contact area a fenestration with a ratio of 0.8:1, will aid in reducing pressures on the tissue and still retain the benefits of added tissue retention.

Retention forces of the various profiles studied by Marucci *et al.*[46] showed the toothed profile designs to be superior in retaining tissue within the jaws. However they have the potential to cause more damage to the tissue due to the high localised pressures exerted onto the tissues. The results of the present experiments show that no significant difference can be found between the jaw designs other than the 1mm wave profile, which performed significantly worse than the others. However, as expected, all performed significantly better than jaws with no surface profile. This outcome is supported by further analysis of the data in which the same statistical analysis was carried out on the pressures applied to the tissue for the various profile designs across the range of pull forces.

3.5 Conclusions

On the basis of the results of the present experiments reported in this chapter, for parallel occlusion graspers, the ideal jaw design should employ a single fenestration with a ratio of 1:0.8 and a profile design which will have rounded off teeth and intervening flat areas. This configuration including the ratio will maximise the surface contact area with the tissue (thus minimising the pressure) while retaining the benefits which the fenestration provides. The waved profile design has less potential to damage tissue when compared to a toothed profile[87] but has a lower grasping hold. By combining these two profiles, we should be able to minimise damage with reduced high stress areas whilst retaining the high grasping force associated with a toothed profile. A 5.0 mm instrument of this design would provide a 5N retention force for an applied force of 2.8N. This would give a pressure on the tissue of 112kPa if the surface contact area is 25mm^2, i.e., well below the force known to cause bowel perforation [89].

The major drawback of the current study is the lack of histological assessment of the damage caused to tissue by the various graspers and surface profiles. Differences between the two studies on fenestrations should be addressed with further investigation to eradicate any methodological differences and to provide histological studies of tissue damage.

Chapter 4: PVDF for slip and incipient slip detection.

4.1 – Introduction

The design and development of polyvinylidene fluoride (PVDF) sensors as a method to detect slip and incipient slip of biological tissue from the jaws of parallel laparoscopic graspers will be presented in this chapter. The development of PVDF sensors and accompanying circuitry and signal processing is described. Experiments, data analysis and results are presented in later sections of the chapter.

PVDF is a piezoelectric polymer which when mechanically deformed develops a surface charge proportional to the stress on the film. Constitutive equations governing the piezoelectric effect of PVDF film are shown in equation 1.

$$\begin{bmatrix} D \\ \varepsilon \end{bmatrix} = \begin{bmatrix} e^{\sigma} & d^{d} \\ d^{c} & s^{E} \end{bmatrix} \begin{bmatrix} E \\ \sigma \end{bmatrix} \tag{4.1}$$

Where vector D is the electric displacement (C/m^2), ε is the strain vector, E is the applied electric field vector (V/m) and σ is the stress vector. The piezoelectric constants (e^{σ}, d^{d}, d^{c} and S^{E}) are the dialectric permittivity (F/m), piezoelectric coefficients (C/N) and the elastic compliance. The superscript d or c denotes whether operating in the direct or converse piezoelectric mode. The matrix values for each of the necessary properties can be found in the literature[90].

PVDF is a thin flexible polymer which makes it suitable for the detection of vibrations and is easily deformed. With a Youngs modulus approximately 10 times less than comparable piezoelectric ceramics making it much more compliant under loading however the

piezoelectric constants for PVDF are also about 10 times less than comparable piezoceramics as summarised in table 4.1. [91]

	PZT-5H	PVDF
Young's modulus (GPa)	71	4–6
d_{31} (pC/N)	–274	18–24
d_{32} (pC/N)	–274	2.5–3
d_{33} (pC/N)	593	–33
e_{33} (nF/m)	30.1	0.106

Table 4.1: Youngs modulus and piezoelectric constants for PZTand PVDF [91].

PVDF sensors have also been found to perform superiorly to standard foil strain gauges, requiring less signal conditioning and no excitation voltage[91]. Piezoelectric transducers can only detect dynamic loading and thus are unsuitable for the continual monitoring of applied load. The application of PVDF will be to detect small strains transmitted to the surface of the sensor through a compliant silicon casing. As PVDF is highly sensitive to these dynamic changes it makes it particularly suitable for the application at hand.[92]

The efficacy of PVDF to be used as a transducer to distinguish between slip and no slip conditions has been shown in the literature [67, 68]. The ability to determine incipient slip has also been investigated with varying degrees of success [69, 70]. PVDF has been implemented into the jaws of minimally invasive surgical instruments however the aim of the project was to determine the amount of force applied to tissue when grasping material and provide force feedback. This would also allow the surgeon to detect hidden anatomical features such as lumps and arteries[73].

The design and development of PVDF sensors will be described. As the sensors will be used to detect slip when housed within a surgically grasper, experimentation is designed to replicated these conditions. Investigations into the use and design of the PVDF sensor are carried out including Rate of slip, surface geometry of the silicon casing investigation and

determining the efficacy of detecting incipient slip with the described signal processing methods.

4.2 – Methods and Materials

4.2.1 – Fabrication of PVDF transducers

Transducers were developed to fit on the tip of a 10mm laparoscopic grasping instrument. Uni-axially, poled PVDF film of 52µm thick (Precision acoustics, Dorchester, United Kingdom) was cut into 8mm x 8mm squares. Both sides of the PVDF film had been metallised with a 250nm gold coating atop a 40nm coating of chrome. Surfaces and edges of the sensors were cleaned by rubbing using a dilute acetone to remove any impurities.

Aluminium tape with a conductive adhesive backing was attached to each surface of the PVDF film to act as electrodes. The contact area of the electrodes was $7mm^2$ which covered the most part of the active area of the PVDF film to ensure the best possible electrical connection.

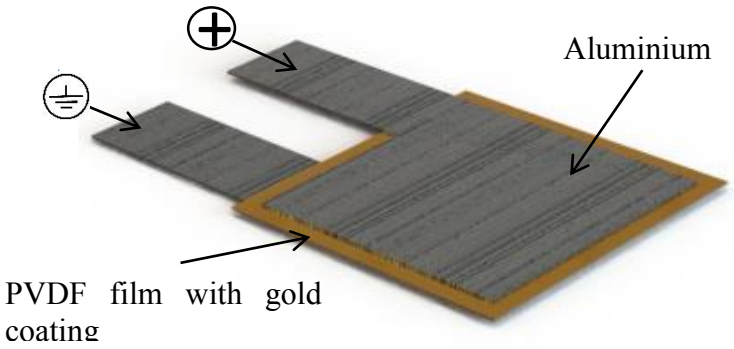

Figure 4. 1: Fabricated PVDF transducer

The sensors were then potted in silicone (Rhodorsil RTV 2450) with a shore hardness of 50 (scale A) which was cured at 60°C. The silicone casing provided a compliant backing for the deformation of the sensor predominantly in thickness mode (d_{33}) when under strain. It also acted to protect and waterproof the sensor.

At a loading force of 1N in the *y* plane over the area of the sensor, under ideal conditions, the PVDF sensor would have a surface charge of 2.2*pC* and a capacitance of 130*pF* given by the governing piezoelectric equations of PVDF[93].

$$D = QA = d_{3_n}\sigma_n \tag{4.2}$$

Where *D* is the charge density developed, *Q* is the charge developed, *A* is the active area of the PVDF film, d_{3n} is the appropriate piezoelectric coefficient for the axis of applied strain and σ_n being the stress applied in the relevant direction.

$$C = \varepsilon \frac{A}{t} \tag{4.3}$$

Where *C* is the capacitance of the film, ε the permittivity, *A* the active area of the PVDF and *t* being the thickness of the film.

4.2.2 Signal conditioning and data acquisition

As the charge developed by the PVDF film is proportional to the change in mechanical deformation thus the first stage in signal conditioning is to develop a suitable charge amplifier. The output voltage of the charge amplifier is dependent on the feedback capacitance as opposed to the input capacitance therefore making it independent of any cable capacitance.

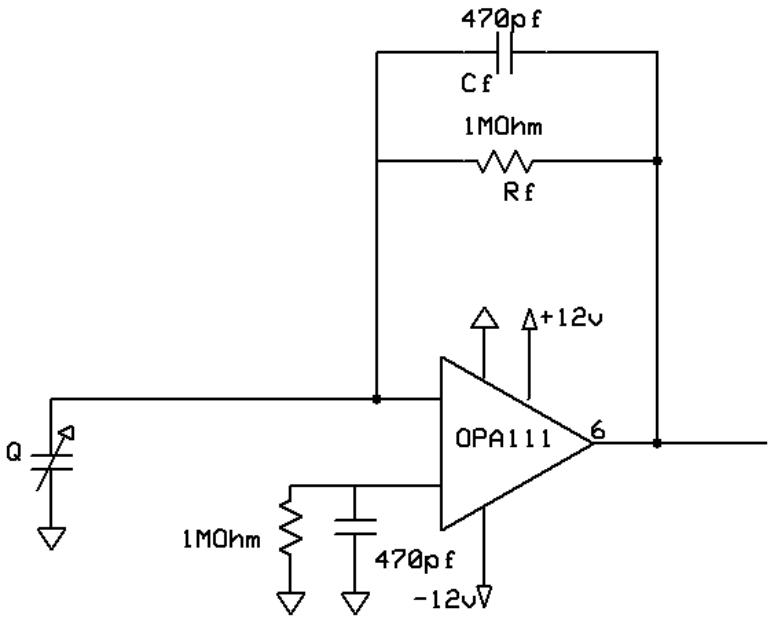

Figure 4.2; Charge amplifier schematic.

The charge amplifier comprises of an operational amplifier with a high input resistance and low bias current. The operational amplifier chosen within this circuit is a Burr-Brown OPA111 (Texas Instruments, Texas, USA), providing low noise and low drift. The feedback capacitor (Cf) absorbs the charge build up on the electrodes and thus the film exhibits no time constant however the addition of the feedback resistor (Rf) causes a time constant independent of the film capacitance and can be accurately controlled. The feedback resistor is used to compensate for drift in the signal.

Sensor data is acquired using data acquisition hardware (National Instruments, Texas, USA) at rate of 3KHz. Digital signal conditioning of the charge amplifier signal is then performed within the Labview environment (National Instruments, Texas, USA) . A 4^{th} order low pass filter of Butterworth topology at 5Hz is applied to the signal along with a gain of 100. The signal was then detrended using an exponential smoothing filter to assure there was no remnant drift in the system caused by the feedback resistor. Finally the signal was digitally

rectified which presented the final signal as a DC signal. Waveform information was recorded to a personal computer at a rate of 30Hz.

4.2.3 Optimisation and investigation of PVDF sensor.

4.2.3.1 Surface geometry

Surface geometry of the silicone casing was investigated to determine the best suited design to transmit the tangential forces of tissue slipping to the surface of the transducer, causing mechanical deformation. Patterning of the silicone casing of a tactile sensor has been reported briefly by Goeger *et al.*[68] in which it is stated that a cylindrical protrusions were found to be superior when compared to surface with no geometry when investigating PVDF in the frequency domain however no data or experimental procedure is given to show how this was determined. Cylindrical protrusions have also been included in the design of PVDF sensors elsewhere; Jockusch *et al.*[94] used a similar cylindrical protrusion design when developing a fingertip with a both piezoelectric and piezoresistive sensors to detect static and dynamic loading, again with no comparison to any other design. Chuang *et al.*[70] investigated the stress state of a PVDF sensor under a micro-column applied directly onto the surface of the transducer. The sensor was encased in a compliant silicone rubber, with no surface geometry, and subject to various loading conditions. It was found that the micro structures on the PVDF created large areas of stress which translated to high electrical potential output of from the sensor.

Figure 4.3: Surface geometry of PVDF sensors.

Three surface geometries will be investigated to determine which will be the most suitable for the detection of tissue slippage. The three surface geometries to be investigated, figure 4.3, will be; A flat unadorned profile, cylindrical protrusions and a column structure protruding in a transverse direction to the direction of slip. A further two sensors will be developed to investigated how inserting metal structures into the cylindrical and column protrusions will affect the output voltage of the PVDF sensor, as shown in figure 4.4.

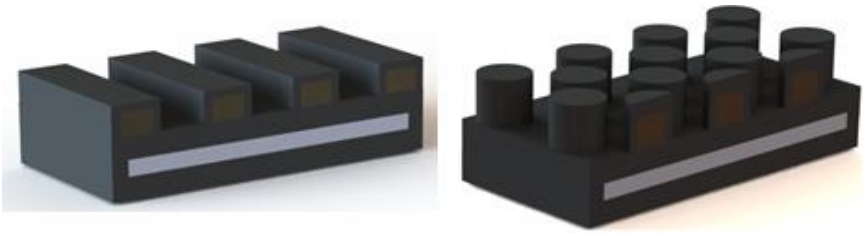

Figure 4.4: Metal inserts in surface geometries of PVDF sensors.

Sensors where adhered to a fixed lower jaw. Tissue was apposed between the lower and upper jaw. Various loads, commonly encountered during surgery (1N, 2N, 4N and 6N), were applied to the upper jaw and the tissue was pulled at a rate of 1.5mm/s by tensiometer (Instron, MA, USA) until the peak load reduced by 20%, indicating that slip had occurred. The jaws were opposed in a parallel fashion. The voltage signal of the charge amplifier was conditioned and the data was recorded to file for analysis at a later time. The experimental test rig is shown in figure 4.5.

4.2.3.2 Rate of slip

The sensor design which was found to be superior after data analysis was then tested to determine how the rate at which tissue was slipping would affect the output signal. As there is no established literature on the rate at which tissue slips from the jaws of laparoscopic graspers a large range would have to be investigated. Slip rates investigated were; 0.75mm/s,

1.5mm/s, 3mm/s and 6mm/s. The assumption being that tissue would not slip at a rate slower than 0.75mm/s.

Rate of slip experiments were carried out in the same manner however the jaws of the apparatus were profiled and fenestrated using the chosen profile from the previous chapter. This was to test the PVDF sensor under conditions most accurately replicating those of the final instrument.

4.2.3.3 Incipient slip detection

Waveforms recorded during the rate of slip experiments were investigated to develop a method for determining incipient slip. Two components of the waveform were investigated in the 1.5 seconds prior to a slip event and compared to a segment of the waveform in which no slip is evident over the same timeframe.

Components to be investigated were the derivative of the signal and the average peak voltage of the signal in the time investigated. The derivative of the signal was determined over a period of 100ms and recorded to a personal computer.

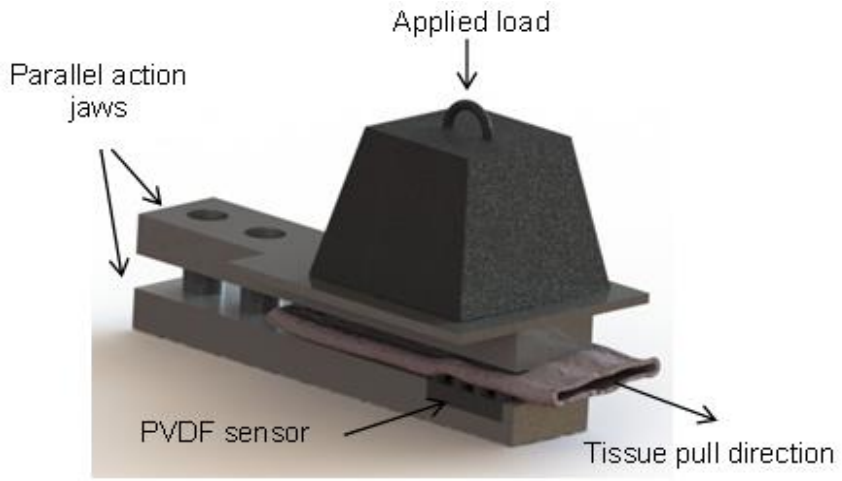

Figure 4.5: PVDF experimental test rig.

4.2.4 – Data analysis

One way Kruskal – Wallis non-parametric analysis of variance (ANOVA) statistical test was used for data analysis. This statistical test was performed rather than the a standard ANOVA test as it was often found that data was not normally distributed and would thus fail a homogeneity of variance test (Levene's statistic) which is a prerequisite of the standard ANOVA method. This is not an assumption made by the Kruskal-Wallis test however as the data is ranked prior to testing. The test is not as robust as a standard ANOVA, it is still more robust than other alternatives and lends itself to multiple comparisons.

Post hoc analysis of the data was performed where a significant difference had been found by the ANOVA. Dunn's multiple comparison test indicates where amongst the dataset that the ANOVA had found a significant difference within the data.

All statistical analysis was performed using Graphpad Prism 6 (California, USA).

4.3 – Results

4.3.1 – Surface Geometry

Surface geometries are initially compared by grouping according to the applied load and comparing the voltage output of each sensor to determine any consistent trends within the data. Data was then analysed to investigate how the applied loading force affects the output voltage of the PVDF. As the voltage output of the charge amplifier is directly proportional to the strain on the transducer therefore the higher the voltage output, the larger the deformation of the sensor.

Graphs 4.1 to 4.4 show the output voltages of the PVDF sensor across the surface geometries investigated, under the various load conditions (1N, 2N, 4N and 6N). Output voltages of the PVDF sensors with a protruding surface geometry were found to be

significantly different than the flat sensor design under all loading conditions with the exception of one as reported in graph 1. Therefore *p* values comparing surface geometries to the flat sensor are not included unless significance was *not* found. All other reported *p* values indicate where a significant difference was found between sensor casings with a protruding design. Surface designs which include metal inserts are annotated by the inclusion of MI in the sensor name.

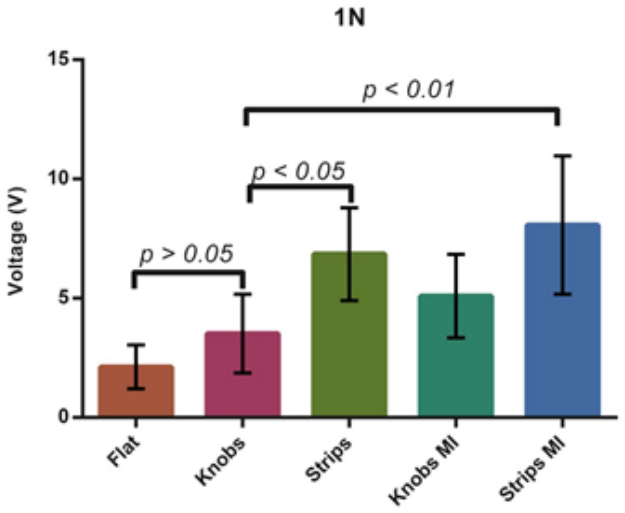

Graph 4.1: Voltage output comparison between surface profiles for 1N applied load. Showing the only instance where a significant difference was not found between a surface design and the flat design.

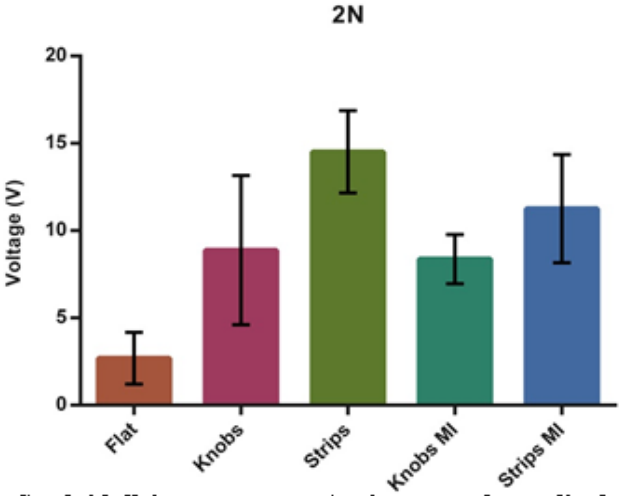

Graph 4.2: Voltage output comparison between surface profiles for 2N applied load. The flat sensor had a significantly lower voltage output than its counterparts in all instances with no difference found amongst other geometries.

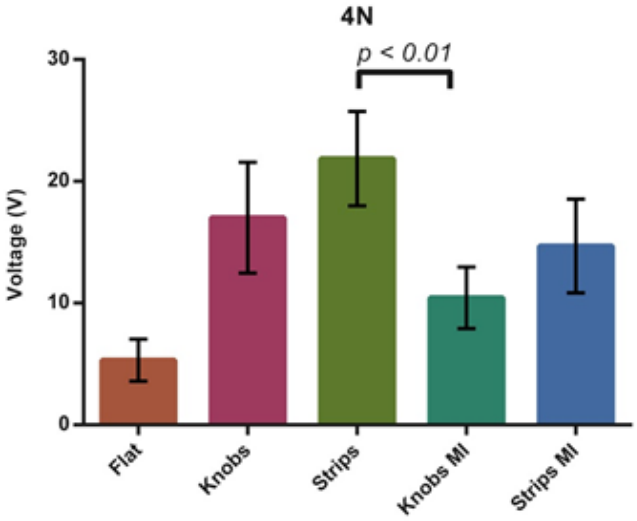

Graph 4.3: Voltage output comparison between surface profiles for 4N applied load. Significant difference is found on one occasion between surface geometries.

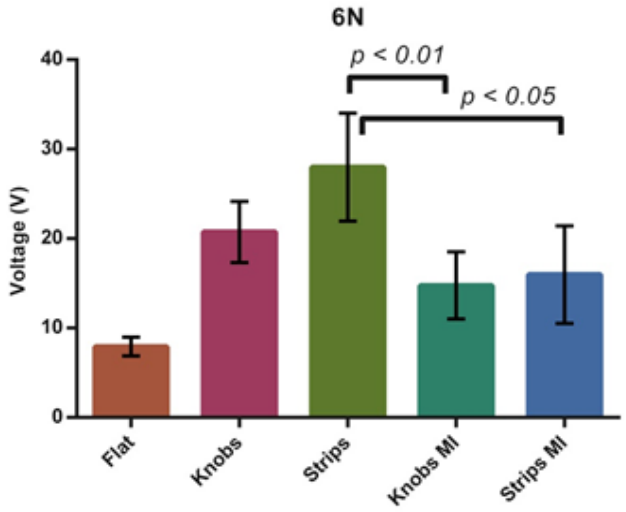

Graph 4.4: Voltage output comparison between surface profiles for 6N applied load. Significance is found between the strip geometry and the two profiles with metal inserts.

Analysis of the voltage output of the various sensor designs when the first instance of slip occurs indicates that all surface profiles would be adequate for determining when slip had occurred. Sensor designs with a protruding geometry perform consistently significantly better than the flat sensor design. All sensor designs show a steady increase in output voltage as the applied load increase. This is caused by a larger pull force needed to displace the tissue when grasped between the two jaws which in turn increases the amount of strain, as expected.

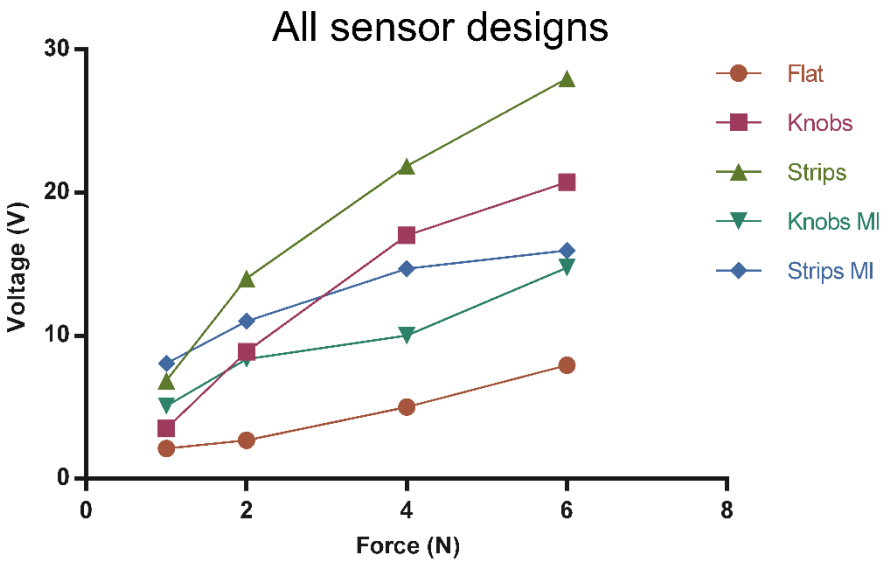

Graph 4.5: All data graphed against applied load. Indication a trend that voltage output of designs without metal inserts have a more consistent output as the applied load increases. It can also be noticed that the flat designs perform poorly in comparison.

Comparisons between surface geometries with and without metal inserts shows that as the applied load increases, the voltage output of the sensors *without* metal inserts increases at a greater rate than those with metal inserts, as shown in graph 4.5. This indicates that the inclusion of the metal structures within the silicone casing inhibit the deformation of the silicone, thus diminishing the amount of stress applied to the PVDF film. Statistical significance of this is effect is rarely found within the data but does appear to be more apparent at higher applied loads and a general trend supporting the effect can be seen in graph 4.5.

The surface geometry selected to progress with is the cylindrical protrusions without metal inserts (knobs). The reason for this is that the strip design did not perform significantly better and because of the design the column-like protrusions would only deform when a force is acting perpendicular to alignment of the columns. The cylindrical protrusions have one more degree of freedom and thus will deform on both the *x* and *z* and so will be able to detect tissue slipping from the jaws of a grasper in any direction.

4.3.2 – Rate of slip

Various slip rates were investigated to determine if the increase in rate of slip would correlate with an increase in voltage output from the PVDF film. The conical protrusion geometry will be the only sensor design to be investigated. Surface profiling and fenestrations design features (Fenestration with a ratio of 1:0.8 and a blunt tooth interspaced with flat areas surface profile) were also included in the experiment to closer replicate a final grasping instrument.

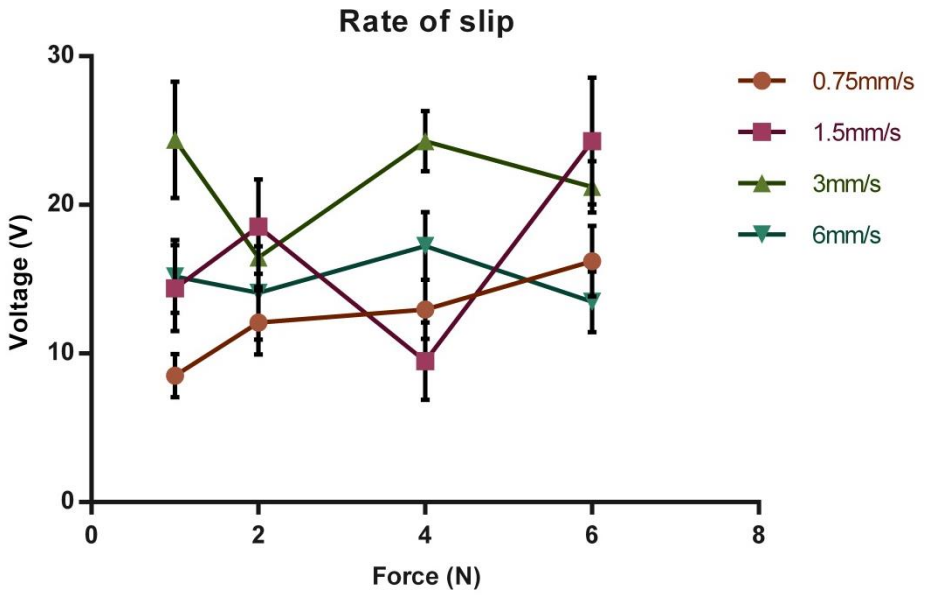

Graph 4.6: Rate of slip cross the various applied loads.

As graph 4.6 shows, there is no discernible relationship between rate of slip and voltage output of the sensors. The data also shows large standard deviation within data sets. This indicates that with the inclusion of the surface profiling of the jaws, there is a larger variation in the amount of stress transmitted onto the surface of the sensor than seen in previous experiments. This could be caused by the slip-stick effect caused by the jaw profiles in which

a number of smaller slip events occur comparatively to an unadorned jaw in which one large instance of slip is seen, followed by continuous slip.

This is supported when we look at how the voltage output changes across loading conditions grouped by the rate of slip as shown in graph 4.7, previously a trend was noticed when investigating surface geometries of sensors which showed that with an increase in applied load, there was an increase in voltage output of the sensor. When we look at graph 4.6 and 4.8, we see that this relationship has been lost with the introduction of fenestrations and surface profiling of the grasper jaws.

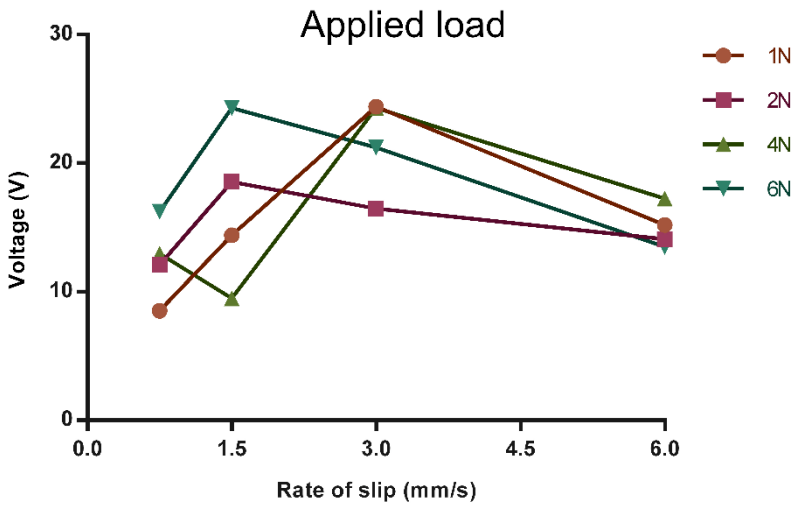

Graph 4.7: Voltage change across applied loading conditions for various rates of slip

4.3.3 – Incipient Slip detection

4.3.3.1 Derivative Analysis

Analysis of the first derivative of the waveform was undertaken to determine if it was a viable method for determining incipient slip. No slip and incipient slip conditions were investigated. A no slip condition is defined by averaging 1.5s of the waveform during a period in which no slip occurred when compared to the tensiometer load cell data. An incipient slip

condition is defined by averaging the 1.5s prior to the occurrence of a slip event, again defined by tensiometer load cell data.

Data is compared by grouping the values according to the applied load and comparing between the two conditions, graph 4.8. On all occasions the incipient slip condition was significantly greater than the no slip condition ($p = <.05$), often the mean the two groups differed by at least one order of magnitude as shown in table 4.2. Unusually large values can be noticed for 0.75mm/s slip rate at 1N incipient slip these can be accounted for by the occurrence of two replicates with uncharacteristically high values prior to the occurrence of slip and the same is evident in graph 4.9. The cause of which went unnoticed during experiments but indicate a high amount of deformation of the piezoelectric sensor, when discounting these two values the data is more homogeneous with the rest of the data acquired and still significantly different from the no slip values however with the cause of these two anomalies being unclear, it would not be pertinent to exclude them from the dataset.

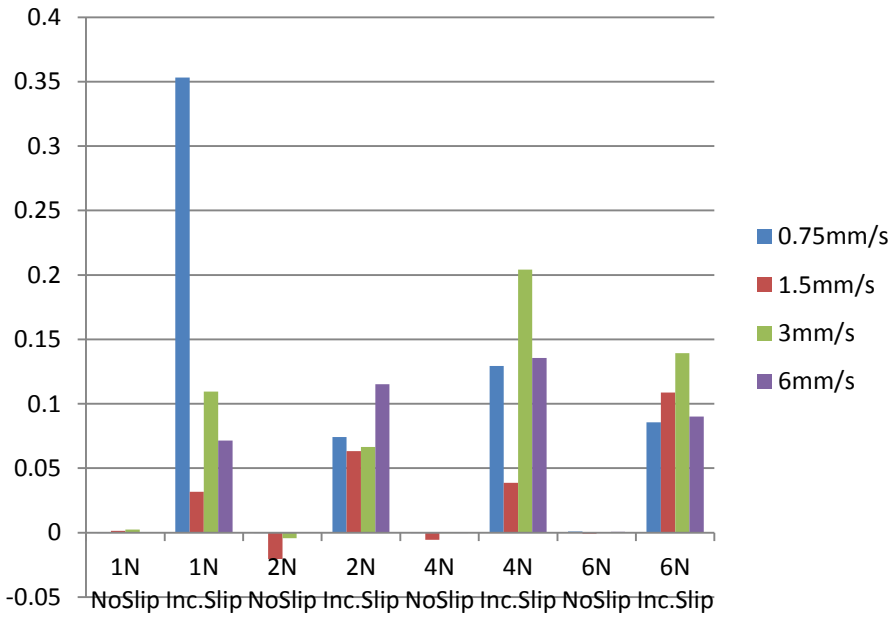

Graph 4.8: Derivative comparison between no slip and incipient slip conditions.

Incipient slip can be detected by the analysis of the first derivative in the seconds leading up to a slip event. Determining a threshold for incipient slip by analysis of the derivative will be undertaken in chapter 5.

4.3.3.2 Peak Voltage analysis

Voltage output of the PVDF sensor prior to a slip event was investigated in the same fashion as the derivative above. Similar to the derivative analysis, there is a large difference between the no slip and incipient slip conditions, graph 4.9. Statistical significance (*p = <.05)* was found on all but two occasions.

The incipient slip condition exceeded 50mV on all occasions other than one. This could be a starting point for further investigation when determining a threshold for incipient slip based on voltage fluctuations prior to a slip event.

Rate (mm/s)	1N NoSlip (V)	1N InSlip (V)	2N NoSlip (V)	2N InSlip (V)	4N NoSlip (V)	4N InSlip (V)	6N NoSlip (V)	6N InSlip (V)
0.75	-2.5E-4	0.35	-8.2E5	0.07	-3E-4	0.12	1E-3	0.09
1.5	-1.4E-3	0.03	-0.025	0.06	-6E-3	0.04	-8E-4	0.11
3	2E-3	0.11	-4E-3	0.07	-1E-4	0.2	1E-4	0.14
6	2E-4	0.07	7E-5	0.12	3E-4	0.14	6E-4	0.09

Table 4.2: No slip and incipient slip conditions compared for derivative analysis**.**

Rate (mm/s)	1N NoSlip (V)	1N InSlip (V)	2N NoSlip (V)	2N InSlip (V)	4N NoSlip (V)	4N InSlip (V)	6N NoSlip (V)	6N InSlip (V)
0.75	6E-4	0.32	2E`-3	0.08	2E-3	0.08	0.01	0.09*
1.5	4E-3	0.07	0.03	0.07	0.02	0.04*	3E-3	0.41
3	4E-3	0.14	0.02	0.12	4E-3	0.17	9E-3	0.14
6	0.02	0.12	9E-3	0.14	7E-3	0.14	0.01	0.09

Table 4.3: No slip and incipient slip conditions compared for voltage analysis.

*Denotes where significance was not found (p>0.05).

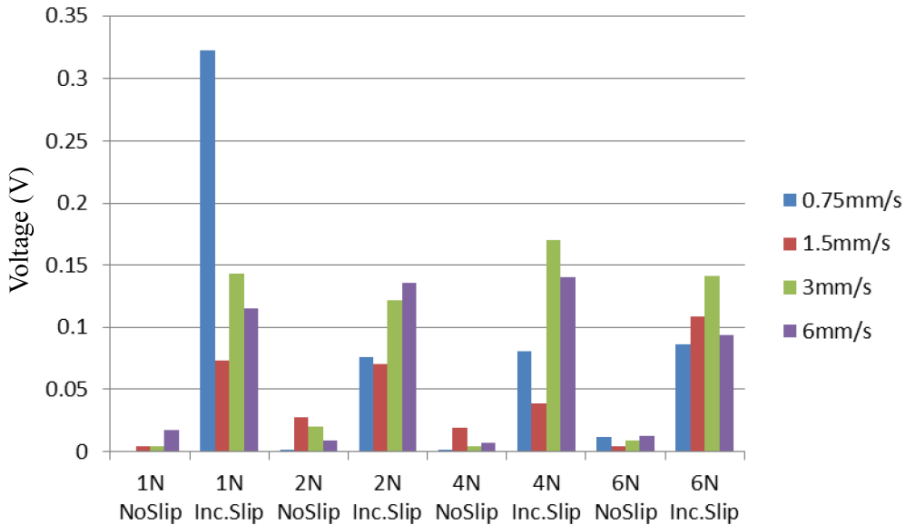

Graph 4.9: Voltage analysis of incipient slip and no slip conditions.

4.4 Discussion

It has been shown that it is possible to distinguish between no slip, slip and incipient slip conditions by. Initial investigation showed that the output voltage of the transducer was dependent on both the grasping force and the surface geometry of the protective silicone casing. Both of these were impacting factors on how much stress the PVDF sensor was subject to. It would be more accurate to say that the increase in voltage output associated with the increase in applied load to the upper grasping jaw was actually caused by the higher pull forces necessary to displace the tissue and cause an instance of slip. As the applied load is a static force throughout experiments, it should not have much of an effect on the voltage output as the PVDF sensor will not detect static forces. As the applied load increases, the force necessary to overcome this static load will inevitably increase also, this would account for the increase in output voltage as the applied load increases.

All surface geometries investigated, including flat, would have been suitable for the detection of slip as the signal to noise ratio for a flat sensor at 1N applied force was 21dB. Protruding surface geometries were found to be significantly superior to the flat profile as expected. A trend appeared to suggest that as the applied load increased, sensors without metal inserts had a higher voltage output, although not statistically relevant. As the output voltage of the PVDF film is directly proportional to the strain applied, it can be concluded that the metal inserts prevented the deformation of the silicone and in turn less stress was acting upon the film.

The sensor design with cylindrical protrusions was selected to proceed with experiments. Reasons for the selection were that it was not significantly different from the design incorporating rectangular protrusions but it would be more readily able to detect slip in any direction as the protrusions could deform in both the *x* and *z* axis, unlike the column like

structures which would deform as expected only when a load is applied transversely to the geometry.

Subsequent studies included surface profiling and fenestrations within the jaw designs. With this introduction the voltage output of the sensor seemed to become independent of both the rate of slip and the applied load. No apparent trend or statistical consistency would be found when grouping and comparing across these variables. This indicates that surface profiling of the grasper jaws has an overwhelming effect on the way in which tissue slips. The surface profile creates a slip-stick effect in which the tissue is pulled free from an individual tooth and stopped by the next. In such a case, the rate at which the tissue is pulled from the jaws would be negated and would not translate beyond the first tooth in the jaw profile ultimately leading to erratic and unpredictable voltage outputs from the sensor which is observed in graph 4.6.

The efficacy of using both derivative analysis and voltage analysis to determine the number of upcoming or incipient slip event is clear. At all times the two conditions of no slip and incipient significance was found when examining the first derivative. There were only two occasions when these conditions were not significantly different when inspecting the voltage output of the sensor.

4.5 Conclusions

It has been shown that PVDF can be used to distinguish between 3 different slip conditions; No slip, Incipient slip and Slip. The surface geometry selected to proceed with development of the instrument is one which will detect slip occurring in multiple directions and provides a large and easily distinguishable signal when slip occurs.

With the introduction of design features in the jaws of the grasper, the magnitude of the voltage signal cannot be used to determine the rate or force at which the tissue is slipping.

The next stage will be to determine thresholds for the three signal components which will discriminate between the slip conditions. This will provide Boolean conditions which the rest of the autonomous grasping system will be developed upon.

Chapter 5: Autonomous grasping of bowel tissue to prevent slip

5.1. Introduction

The previous chapter described the development and initial investigation of the PVDF sensors. This chapter addresses the incorporation of these PVDF sensors within a closed loop control system/ device which will autonomously detect and inhibit slip occurring by modulating the force which is applied to the tissue.

A number of laparoscopic graspers have been proposed which employ to provide haptic feedback of the tissue that is being grasped[95] or to provide the surgeon with information on forces acting on the tissue[73]. This haptic feedback is often provided via auditory or visual signals to the operation surgeon. The proposal behind the work outlined in this chapter is to develop a proactive system by which events such as excessive grasping forces and tissue slippage are anticipated and prevented as a more effective means compared to the reactive system based on haptic feedback.

To date there is no instrument which uses sensory feedback to control the force being applied to the tissue autonomously has been described or reported. This is described in this chapter. A PVDF sensor is used to detect incipient slip or slip events; and corresponding Boolean triggers are then used to control the state machine on which the closed loop control system is built.

In the first section, the Boolean thresholds which will be used to indicate the onset of slip will be studied. These will then be used in a closed loop system which will react to the occurrence of what is defined as occurring incipient slip or slip. These studies will involve use

of increasing the force applied to the tissue by engaging a DC motor which is used to actuate a parallel action grasping instrument.

5.2 Methods and materials

5.2.1 Closed loop control system

A closed loop control program was developed using Labview (National Instruments, USA) visual programming. A closed loop control system must have sensory feedback in order to ascertain whether the aim of a certain process has been achieved; within the system the PVDF sensor will provide this information in the context of tissue slippage.

The data from the PVDF sensor was acquired using data acquisition hardware (National Instruments, Texas, USA) at rate of 3 KHz. Further analogue and digital signal processing was performed on the signal as described in the previous chapter. Thresholds for both incipient slip and occurring slip were determined through experimentation.

These thresholds were then used within the state machine architecture of the programme to determine between each activity and output of the closed loop control system. State machine programming comprised an initial state, a number of transitional states and a final state. The state machine is ultimately a sequential logic system and progression between states is determined by whichever input occurs *and* has been defined as a trigger for progress to a pre-determined state. The benefit of using state-machine architecture is its simplicity. Additionally, it also only uses the computational power necessary to run whichever current state is present Ultimately this increases the reaction time of the system as the programme needs investigate continually only loops through the current state for a trigger for its transition.

The state machine developed for the autonomous grasping of tissue comprises of 8 states which are triggered by user input and predetermined thresholds. Below is a short description of each state.

1) *State selection (Initial state)* - This is the initial state of the programme when first turned on. User inputs (manual mode, engage tissue, disengage) and sensory inputs (thresholds, applied force, inactivity) are used in a Boolean manner to determine which state the machine will progress to. This initial state is the most active as it is continuously called after transitional states have completed their action. This allows for the continuous monitoring of the input triggers.
2) *Manual node* – via a small button on the handle of the instrument the surgeon can select to use the system for manual or autonomous grasping of the tissue. Actuation of the instrument is controlled using a potentiometer within the handle to replicate a standard laparoscopic grasper.
3) *Incipient slip* – When the threshold for incipient slip has been met (derivative ***and/or*** peak detection) the instrument automatically increases force applied by small increments based on motor rotations to the tissue to prevent slip occurring.
4) *Slip occurring* – If the threshold for an occurrence of slip is met, force is increased (not beyond a safe amount which could cause damage to tissue) to prevent tissue slipping further.
5) *Engage tissue* – This is another user input in which the surgeon selects to engage the grasping instrument with the tissue. After this action is carried out, the instrument will be in autonomous mode.

6) *Disengage tissue* – this state is selected by a button input and automatically fully opens the jaws of the instrument when the surgeon decides to remove the instrument or free the tissue from the autonomous grasp.
7) *Decrease force* – the instrument will reduce the amount of force applied to the tissue after a period of 45 seconds without any occurrences of slip or incipient slip occurs. This prevents tissue being grasped with excessive pressures for extended periods of time.
8) *Warning* – A warning occurs when tissue has slipped from the graspers or when a slip event is occurring despite the tissue being grasped by the maximal allowable force.

5.2.2 Grasping and actuation

The physical components of the closed loop control system comprised of (i) a PVDF sensor mounted on the distal end of the lower jaw of the grasping instrument, (ii) a DC motor with a 10mm diameter (Maxon, Sachsein, Switzerland) and (iii) a parallel action grasper with a stationary lower jaw. The arrangement of the components for the autonomous grasping experiments is shown in figure 5.1

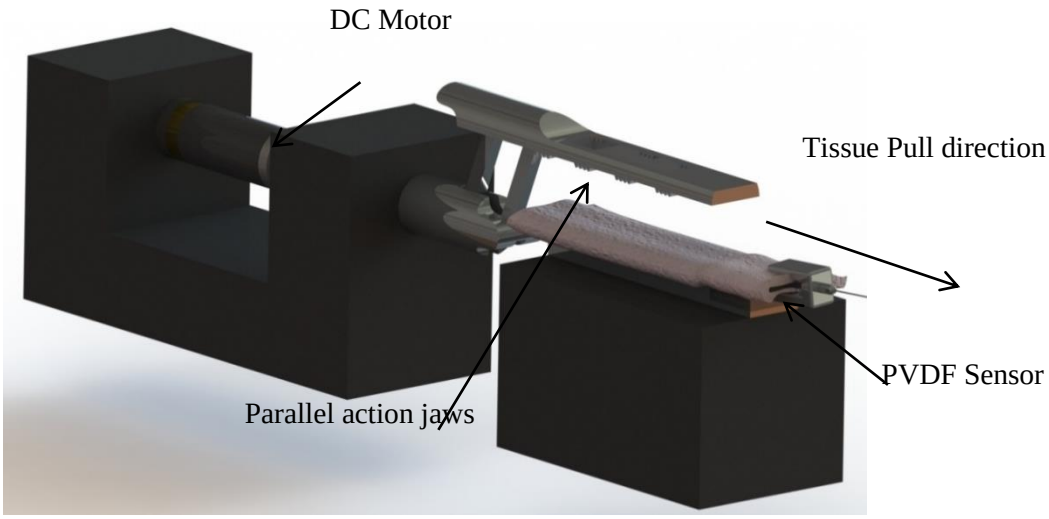

Figure 5.1: Experimental test rig showing a parallel action grasper being actuated by a DC motor. This will increase the applied force on the tissue which is pulled at varying forces by a tensiometer.

The jaws of the graspers were patterned with a pitched-wave style profile with a fenestration according to the conclusions of chapter 3. The PVDF sensor was connected to the charge amplifier and then to the National Instruments (NI) data acquisition hardware. A Pololu (Las Vegas, USA) motor controller, in combination with timed outputs from the NI hardware, was used to control the DC motor.

The grasping action was controlled by accurately timed outputs from the NI hardware, which actuated the motor in incremental steps to modulate the force applied to the tissue. In order to calibrate this applied force a capacitive based pressure sensor (Tekscan, Boston, USA) was mounted on the distal tip of the upper jaw, directly opposite from the PVDF sensor. The data from this pressure sensor were calibrated against the number of rotations of the motor when grasping tissue in order to estimate force.

5.2.3 Experimental Procedure

5.2.3.1 Slip and Incipient slip threshold determination

Results from the previous chapter demonstrated ability of the PVDF sensor to detect both slip and incipient slip. The average voltage output and average derivative results during

the 1.5 second time-frame prior to a slip event indicated a starting point for investigating a threshold for determining incipient slip. The same was true for determining a threshold for the occurrence of slip.

Four thresholds for each of the 3 conditions (peak detection, derivative analysis and peak voltage) were investigated. Thresholds are summarised in table 5.1. Peak detection was set to detect 3 peaks of the determined voltage over 25ms and derivative was determined over a period of 25ms also.

Condition	Threshold 1	Threshold 2	Threshold 3	Threshold 4
Derivative	0.025	0.5	0.1	0.2
Peak detection	10mV	20mV	40mV	80mV
Peak Voltage	0.1V	0.2V	0.5V	1V

Table 5.1. Threshold for the three different Boolean conditions which were investigated.

Experiments were carried out in the same manner as previously described, i.e., tissue was grasped between two parallel action jaws with surface profiling and fenestrations. A PVDF sensor was distally mounted on the lower jaw and the voltage was recorded on a personal computer via NI data acquisition after signal processing had been performed. Boolean conditions were set within the Labview environment to determine when each of these thresholds had been triggered and was recorded in a binary format along with the actual value. Loads (1N, 2N, 4N and 6N) were applied to the upper jaw to simulate common grasping forces and tissue was pulled from the jaws of the grasper at a rate of 0.75mm/s to induce slip. No force modulation was used throughout threshold determination. Twelve replicates were carried out for each threshold at each of the applied loads.

Data were analysed to determine the number of times thresholds had been triggered and then these were determined to be either correct slip or incipient slip detection or false positives. This was done by scrutinizing the 1.5 second interval prior to a slip event as indicated by a

significant change in the gradient of pull force as recorded by the Instron tensiometer. The number of times in which a slip event occurred but thresholds were not triggered was also recorded. The purpose of this was to determine which threshold for each of the three conditions was the most accurate in determining a slip event. In this scenario, a minimal number of false positives and maximal number of slip events detected was considered the most desirable outcome. Each threshold was investigated independently with 18 replicates of each threshold at each applied load.

5.2.4.2 Pressure sensor calibration

The flexi-force pressure sensor was calibrated by mounting the active area of the sensor upon the distal tip of the upper jaw of a parallel action grasper. Tissue was grasped between the jaws and a load was applied to the upper jaws (1N – 6N) in increments of 1N. A flexi-force adaptor was used for signal conditioning and the data was recorded to a PC for analysis. Six replicates were performed for each applied load. Pressure data from the sensor was averaged between loading groups and plotting against the applied force to determine the live of best fit.

5.2.4.3 Pressure and motor rotation calibration

To determine the increase of force upon the tissue the number of timed rotations would be investigated and related to the information provided by the flexi-force pressure sensor with the aim of being able to increase the load on the tissue by 0.5N with each timed motor response in the event of a slip or incipient slip threshold being triggered.

Tissue was grasped in parallel action jaws which were actuated by the use of a Maxon DC motor. The motor was initiated for a pre-determined time which was controlled by a Labview programme. Each of these timed outputs related to a fraction of one full motor rotation. The

number of times the motor was initiated was recorded along with the force which was being applied to the tissue after each rotation as indicated by the flexi-force pressure sensor.

Three timed motor timings were investigated; 0. 05s (1/10 of a full rotation), 0.1s (1/7) and 0.15s (2/9). Number of rotations to engage the tissue and how subsequent rotations related to increases in applied force were of most interest. Data were recorded on a PC for analysis.

This would inform the timed responses in the closed loop control system so applied forces were never excessive and small increments in force increases were made as often as possible. A cubic growth of force to number of rotations was expected and the viscoelastic response of the tissue would be almost impossible to account for and so this method will only be able to provide a good estimate of applied force by counting the motor rotations however it should be accurate enough to ensure excessive forces are never applied to the tissue.

5.2.3.4 Autonomous Grasping

The closed loop control system was used in conjunction with a motorised parallel action grasper in order to evaluate the efficacy of autonomous grasping using PVDF to detect incipient slip and the occurrence of slip. Thresholds for peak detection, derivative and maximal voltage were selected based on prior investigation. Prior research also informed the design of the autonomous grasper, including PVDF sensor design as well as surface profile design of the grasping jaws (including fenestrations) as shown in figure 5.3.

Ex vivo porcine bowel tissue was placed within the grasping jaws and engaged until a grasping force of 2N was applied (as indicted by the motor rotation experiments). Tissue was retracted by the Instron tensiometer using a cyclic tension test. This cyclic tension test comprised of retracting at various rates, increases and decreases in force as well as holding forces for set periods of time. A graph of the cyclic test is shown in figure 5.5. The duration of each cyclic test was 25 minutes relating to expected length of grasping surgical times for colectomies and

cholecystectomies as reported by Heijnsdijk et al [10]. as well as the maximum recommended grasping duration[46]. This would represent all of the expected pull forces which the grasping device would be subject to for the duration of grasping or retraction.

If a trigger for a slip event occurs the grasping force will be increased by sending a timed output to engage the actuating motor for a certain period of time based upon prior experiments. A small pause in trigger detection of 25ms after a force increase is used to prevent false positives and to allow the PVDF sensor to relax as an increase in grasping force will undoubtedly cause mechanical deformation of the sensor.

All PVDF sensor data including; peak detection, derivative of the signal and peak voltage of the signal was recorded along with a Boolean value for each trigger and the time at which the trigger occurred. Motor rotations and the flexi-force output was also recorded to compare to the retraction force which was recorded by the tensiometer. The distance which the tissue was pulled from the jaws of the grasper throughout the cyclic testing was also recorded.

5.3 Results

5.3.1 Slip and Incipient slip threshold determination

Incipient slip and slip thresholds were investigated to determine the most accurate thresholds to use in later experiments. A low number of false positives while accurately detecting slip on as many occasions is possible was the most desirable result for each of the thresholds.

Derivative				
Threshold	Number of events detected	False positives	Slip not detected	% false positives
0.025	490	140	29%	30%
0.05	603	105	17%	18%
0.1	**696**	**67**	**10%**	10%
0.2	361	32	9%	**9%**

Table 5.2: Results for each of the derivative thresholds investigated.

During the analysis of the derivative threshold data with an increase in threshold value, the false positives reduced, as expected. The final threshold, although exhibiting the lowest false positives, failed to detect slip in 9 of the 72 occasions as well as detecting the least number of events. The data shows that a derivative of 0.1 was the most accurate for detecting incipient slip (failing to detect slip on only one occasion) while also reducing the number of false positives.

Peak Detection				
Threshold	Number of events detected	False positives	Slip not detected	% false positives
10mV	1771	536	0	30%
20mV	2970	536	0	18%
40mV	2012	211	0	10%
80mV	**1340**	**121**	**0**	**9%**

Table 5.3: Results for each of the peak detection thresholds investigated.

Analysis of the peak detection threshold (table 5.2) shows a similar trend to that of the derivative analysis. As the threshold is increased the number of false positives decrease with the lowest percentage of false positives being 9%. At no point did the peak detection threshold fail to detect the onset of slip. The threshold of 80mV will be used for further experimentation of the autonomous grasping system as it produced the lowest percentage of false positives whilst always detecting upcoming slip events.

Peak Voltage				
Threshold	Number of events detected	Number of slip events	% of slip detected	% false positives
0.1V	64	41	87%	49%
0.2V	81	60	78%	57%
0.5V	90	66	93%	42%
1V	45	63	60%	11%

Table 5.4: Results for each of the slip thresholds investigated

Table 5.3 shows the analysis of the thresholds investigated for the occurrence of slip, as distinct from incipient slip which the derivative and peak detection thresholds are used to determine. The data show a large percentage of false positives, most probably due to the threshold being triggered after a slip event had occurred. The final threshold of 1V shows the lowest percentage of false positives, but it also detects the least number of slip events. Comparison of this with the previous threshold shows the inverse with a high percentage of slip events being detected but also a large number of false positives. This indicates that a threshold for the detection of slip would be somewhere in between these two thresholds. Hence a threshold of 0.75V was set for further experiments. This should minimise the number of false positives whilst also detecting a large percentage of the actual slip events.

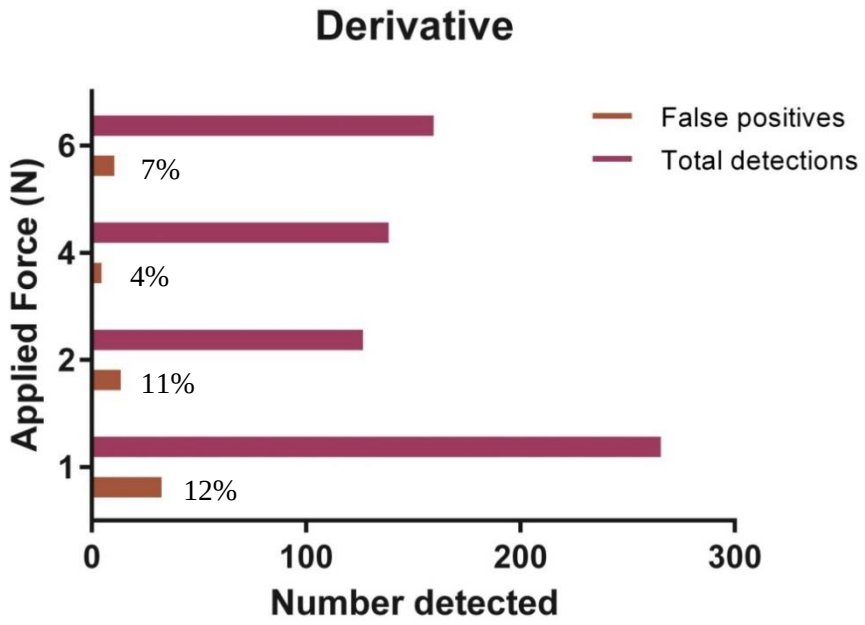

Graph 5.1: Incipient slip detections of the selected derivative threshold (0.1) for different loading conditions.

The chances of detection of incipient slip using the derivative threshold (graph 5.1) seemed to be slightly affected by the loading condition because a weak correlation was found, indicating that at the lower applied loads the threshold for incipient slip is triggered more regularly than at higher applied loads. Multiple comparison ANOVA established significantly more detections ($p<0.05$) at 1N applied force when compared to any of the other loading forces. There were no significant differences in the occurrence of false positives across different applied loads.

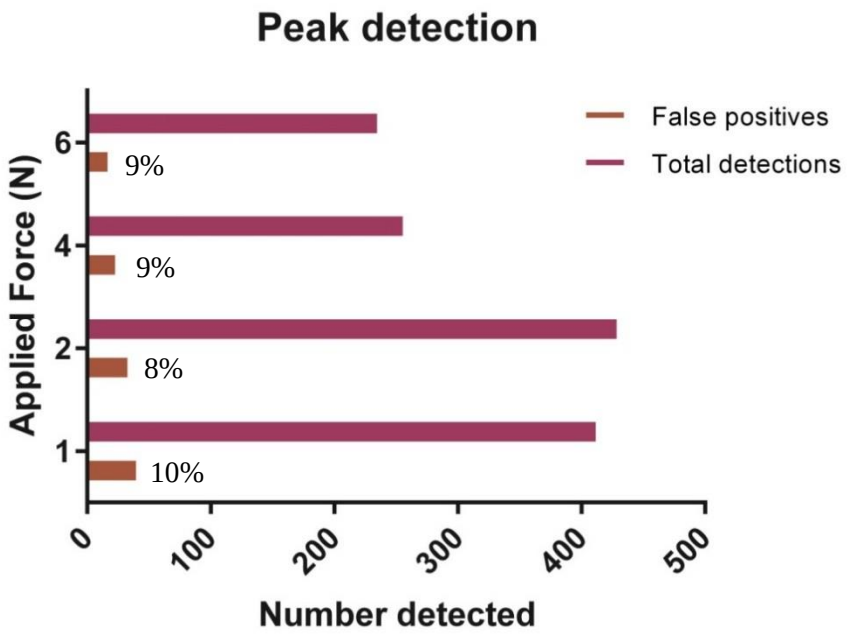

Graph 5.2: Incipient slip detections of the selected peak detection threshold (80mVmV) for different loading conditions

The number of threshold detections again seems to show a correlation between loading conditions and the number of detected incipient slip events when investigating the peak detection threshold. Significant difference was found on two occasions when comparing 1N and 2N against 6N applied force ($p < 0.05$). Again there were no significant differences between the occurrences of false positives across loading conditions.

Being able to determine the applied force to the tissue due to the number of slip events detected would be useful in the development of the autonomous grasping instrument. However the relationship only seemed to be able to determine differences between the lowest and highest applied forces and would only be available post hoc so would therefore be almost useless as loading conditions may be continually changing around an incipient slip or slip event.

5.3.2 Pressure sensor calibration

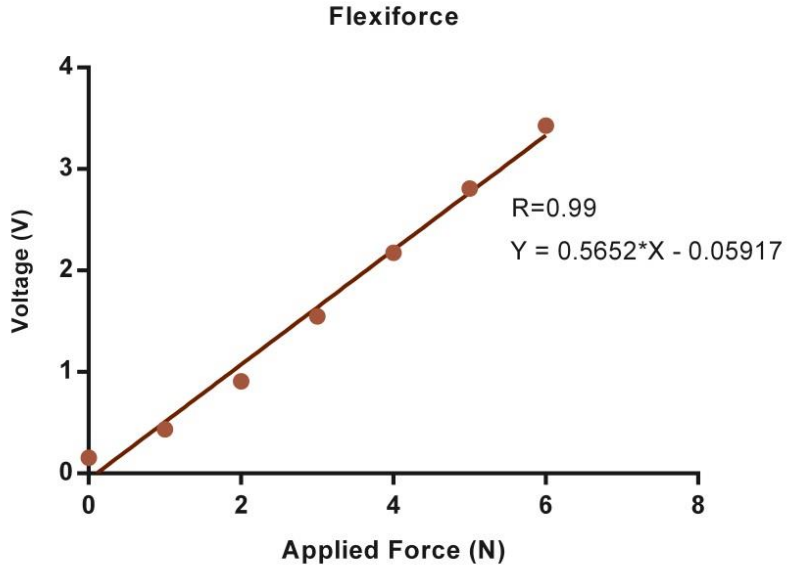

Graph 5.3: Relationship between applied force and voltage output of the Flexi-force pressure sensor.

The flexi-force pressure sensor was calibrated according to the manufacturer instructions in which a known value was applied to the surface of the pressure sensor and the voltage output was recorded. Graph 5.3 shows the linear relationship between applied force and voltage output. This information is then used to determine how the number of timed motor rotations affects the force applied to the tissue.

5.3.3 Pressure and motor rotation calibration

As a method of estimating the amount of force being applied to the tissue, the number of timed rotations were counted and the force applied to the tissue was recorded by the flexi-force pressure sensor.

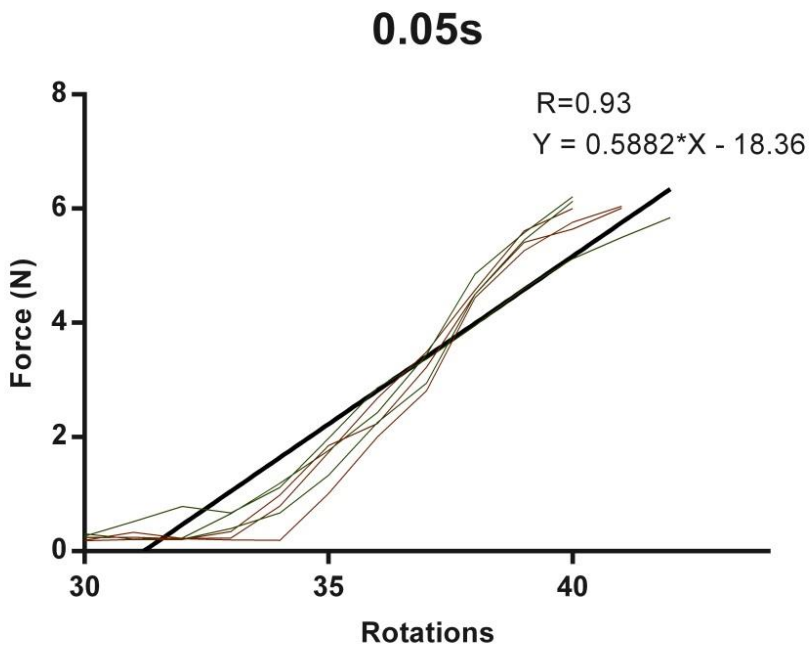

Graph 5.4: Increase in force according to the number of motor rotations for the tied output of 0.05s.

Three timed rotations were investigated (0.05s, 0.1s and 0.15s). The lowest timed output was selected as this produced the smallest average increase in force per rotation. Graph 5.4 shows the force increase according to rotations for a timed output of 0.05s. Although the resulting graph is not particularly linear it is only used to provide an estimate of the applied force. Any attempt to decrease the timed rotation to less than 0.05s was unsuccessful due to the constraints of the national instruments hardware used, in which accurately timing an output of less than 0.05s was impossible.

5.3.4 Autonomous Grasping

Cyclic testing of the autonomous grasping instrument was performed 22 times for duration of 25 minutes on each occasion. The length of the tissue which was grasped in the jaws of the instruments was 65mm. The tissue was successfully grasped for the complete

cyclic test in 20 of the replicates with the tissue being pulled free on two occasions (9%). Disregarding the two occasions in which grasping failure occurred, the average displacement of the tissue was 20.5(±6) mm or about 31% of the overall tissue length as shown in table 5.5 along with other initial analysis.

	Derivative	Peak detection	Peak Voltage	Tissue ΔD
Total recorded	1629	10912	10	349mm
Average per rep	86 (±35)	574(±211)	0.42	N/A
Average value	0.19 (±0.05)	0.12(±0.03)	1.6V	20.5(±6)mm
Maximum	0.35	0.23V	2.9V	31mm
Minimum	0.11	0.09V	0.75V	11mm

Table 5.5: Collated results of the autonomous grasping experiments showing outputs from each of the Boolean conditions of incipient slip and slip and the length of tissue which was pulled from the grasper.

Force which was being applied to the tissue throughout the cyclic testing was investigated. The percentage difference between the pull force as recorded by the tensiometer and the estimated applied force according to motor rotations was calculated for the period of each replicate. An illustration of this is presented in graph 5.5. The peak voltage threshold was only triggered during two replicates in which grasping failure occurred, slip was recognise while the tissue was being pulled from the jaws.

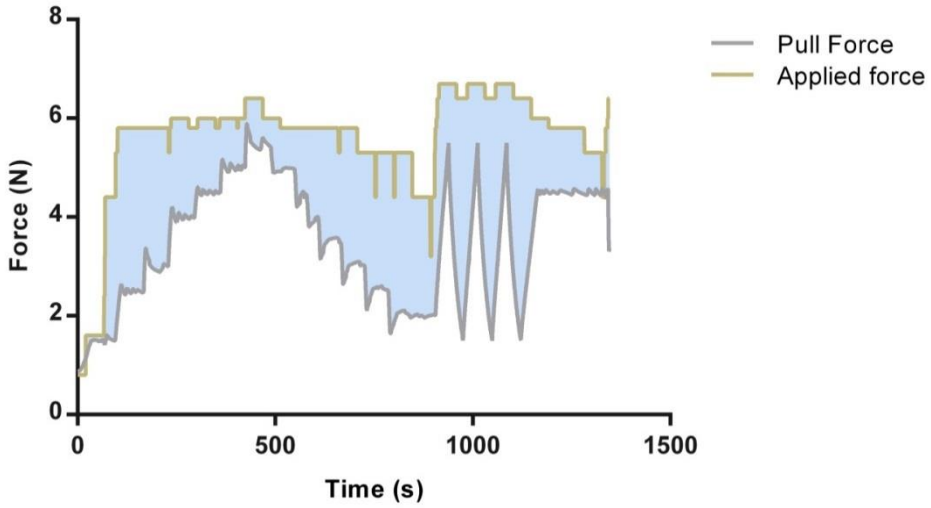

Graph 5.5: Shaded area of the graph indicates the percentage difference between the pull force and applied force.

The force applied by the grasping instrument was found to be, on average, 71.81(± 24.4)% greater than the amount of pull force. The average maximal percentage difference during experimentation was found to be 331(±63) % greater applied force than pull force. This indicates that the reduction in applied force which occurs every 45 seconds is not sufficient to more accurately modulate the applied force. The large percentage differences within the data sets are most often found in the region of 500 to 900 seconds. This may be due to the change in strain acting upon the PVDF sensor causing a false positive and thus preventing the reduction in applied force or 45 seconds being too large a period of time to wait before reducing the applied force.

The number of applied force increases per replicate was 28±7 with the number of force decreases being 20± 6. The number of applied force increases were investigated in 3 minute intervals as shown in graph 5.6. The data was analysed using the multiple ANOVA statistical method. Significantly more force increases ($p < 0.05$) were found to have occurred within the first 3 minutes of the cyclic testing than at any other point throughout and no other statistical significance was found between other time intervals. This implies that although there is

sufficient applied force to overcome the pull force that there is still disturbance being detected by the PVDF sensor which is causing the motor to further engage the tissue.

This is most likely due to the tissue being brought fully into tension and overcoming the viscoelastic properties of the bowel tissue when stress relaxation occurs. Bowel tissue has been reported to have a percentage elongation of between 9% and 13% depending on area of the colon under strain[96]. This would also account for a percentage of displacement of tissue which was found during the experiments.

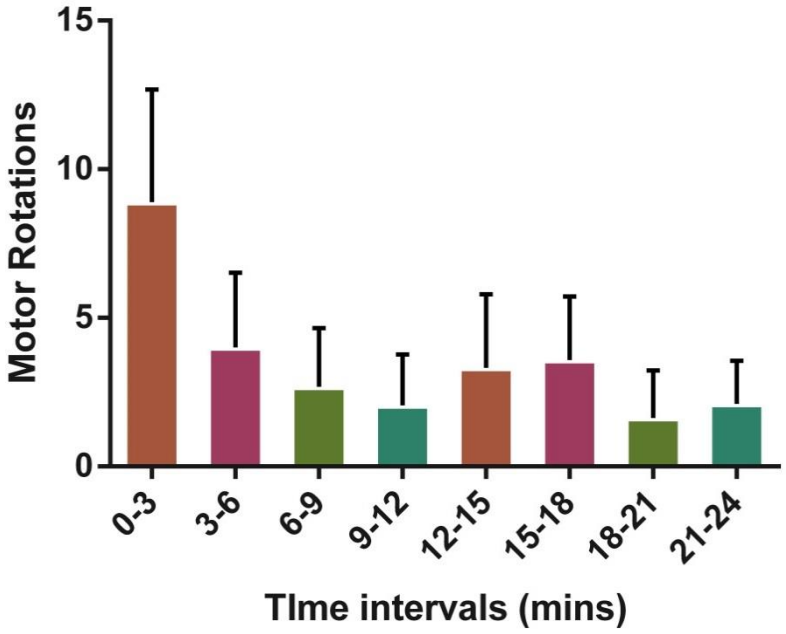

Graph 5.6: Distribution of applied force increases in 3 minute intervals throughout testing.

Failure to successfully grasp the tissue for the duration of the cyclic test occurred on two occasions. Figure 5.2 shows the two graphs of applied force vs. pull force for these two failures. On both occasions failure occurs at or towards the peak when the rate of change of pull force is at its highest, this coupled with the reduction in applied at or just prior to the tissue being pulled from the grasper.

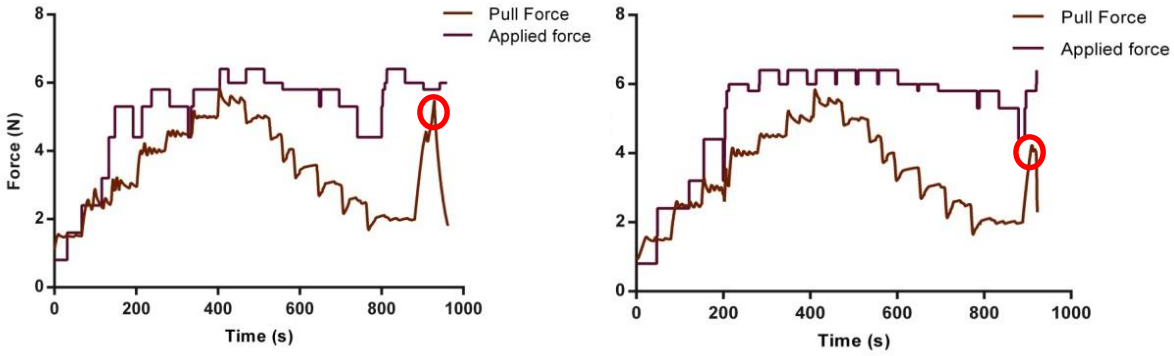

Figure 5.2: The two graphs in which failure to grasp tissue occurred. Grasping failure is highlighted by a red circle and can be seen to be precluded by a decrease in the applied force.

5.4 Discussion

It has been shown that the use of PVDF in a closed loop control system can secure tissue within the jaws of a laparoscopic tissue grasper while the force applied to the tissue is modulated. Within this chapter thresholds which determine incipient slip and slip have been shown to be viable to produce Boolean indicators for the onset and occurrence of slip. Failure to secure the tissue within the grasping jaws occurred on two occasions and was caused by a combination of a high rate of increase in force and a brief reduction in the applied force by the grasping device.

While counting the rotations of the motor has provided an estimate of the grasping force of the instrument, it has been shown to be insufficient in providing the accuracy necessary to modulate the force applied to the tissue. As has been reported, the average applied

force throughout experiments was found to be 72% greater than the pull force. This method of estimating force according to number of rotations would not be suitable if the instrument was being used to grasp tissue with large variances in thickness.

As the maximum grasping force is pegged to *x* number of rotations it is difficult to imagine that the grasping instrument would exert excessive forces upon the tissue which would damage it as the pressure being applied to the tissue (288KPa for a 5mm instrument) would still be lower than the pressures known to cause bowel perforation and similar to the lower pressures commonly exerted onto tissue via standard instruments[11]. However upon further iterations of the device it would be wiser and easier to implement a dedicated force sensor so that the normal force to the grasping jaws can easily be determined. There would be scope to implement this in an array format using MEMS technology along with the PVDF sensors.

Bringing the tissue into tension during the initial stages of the experiments is thought to create a number of false positives, shown by the large number of motor rotations within the first minutes, which ultimately leads to a disproportionately high applied force. This would unlikely be an issue during a surgical procedure as the tissue would be in full tension before the instrument would be set to automate the force and react to incipient slip and slip events but in relation to these experiments it could account for up to 13% of the recorded tissue displacement.

5.5 Conclusions

An autonomous grasping system has been presented which has been shown to effectively detect and prevent slip occurring while automating the force applied to the tissue. Successful grasping was performed for the duration of the experiments in 91% of the occasions. When compared to the literature where tissue slipping from the grasping jaws has been shown to occur in up to 38% of incidences[97] and grasping success rates of 63%[10] it

can be said that the closed loop grasping system presented is more successful at grasping tissue whilst also modulating the applied force to prevent dangerous levels of pressure being exerted upon the tissue. Average tissue displacement (33%) would indicate that there is some slip occurring however up to 13% of this could be explained by the viscoelastic properties of the tissue when under strain leaving an actual tissue displacement around 20% which could be seen as acceptable considering the high degree of grasping success.

Although the forces applied to the tissue during experiments is often significantly greater than the force at which the tissue is being retracted this can be explained by the way in which force is modulated by motor rotations in an open loop manner. For this reason a more refined system of modulating applied force is required and called for. This would have to be realised with direct force measurement, distinct from force measurement methods which have been reported regarding tissue graspers in which strain gauges fixed to linkages[98] or torque sensors[99] within the motor housing are used to indirectly measure force as these indirect measurements have been shown to wrongly estimate grasping force by up to an order of magnitude[100].

It would be necessary to implement this force sensor into the closed loop control system in order to provide the accurate force control which would be necessary. This would also negate the usage of timed outputs to the motor.

Chapter 6: Parallel action tissue grasping.

6.1 Introduction

Parallel action grasping for surgical instruments is preferable over the more conventional pivoting style graspers which are predominant in most surgical instruments. This pivoting action creates an uneven distribution of pressure upon the tissue when grasping which leads to high stresses acting upon tissue in the proximal opening of the grasping jaws. Parallel grasping has been reported previously[49, 50] however almost all of the proposed mechanisms have been variations on the standard parallel linkage or 4-bar linkage system, illustrated in figure 6.1.

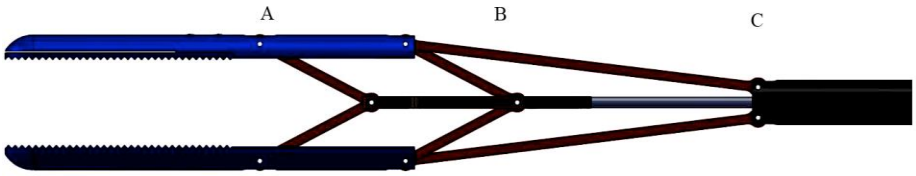

Figure 6.1: Example of proposed parallel mechanisms for laparoscopic instrument. The overall length of the mechanism (A-C) is longer than the active grasping area.[50]

There are a number of concerns when selecting this parallel linkage for use in a surgical instrument. Firstly, as the linkages are rigid and only pivot around the hinges within the upper and lower jaw, the length of each link must at least match the opening distance between the two jaws creating a very large active area at the distal end of the instrument. These linkages must then be a sufficient distance apart along the length of the jaw to prevent horizontal motion (tip deviation) when a force is acting upon it. Ultimately the space required to employ such a mechanism becomes 2.5 to 3 times the opening distance of the jaws. Secondly, due to the

collapsing of the parallelogram to provide the grasping force a translational movement of the upper jaw occurs along the *x* axis. This becomes a concern for surgeons as the line of sight when performing laparoscopic surgery is along the length of the shaft with limited depth perception this could lead to high incidences of repeated grasping.

There have been mechanisms proposed on a variation of the 4-bar linker in which two parallelograms are combined into a 10-bar linkage which is actuated through the central link and the mechanism closes in upon itself. This design reduces but does not eliminate the translational movement of the upper jaw and it also increases the amount of space that the mechanism uses within the jaw which is out with the shaft.

To overcome the issues associated with current parallel action tissue graspers a design specification was developed for which a number of mechanisms were investigated. Two designs were selected for further investigation for the attributes which they possessed. The first design to be investigated is based upon the pantograph mechanism; the "X" pattern mechanism is often commonly used in stair lifts and other applications. The planar mechanism can be actuated centrally creating an outward motion in both directions along the *y* axis or by a sliding connection along the bottom fixed body. The benefit of this mechanism is that it produces a purely parallel motion.

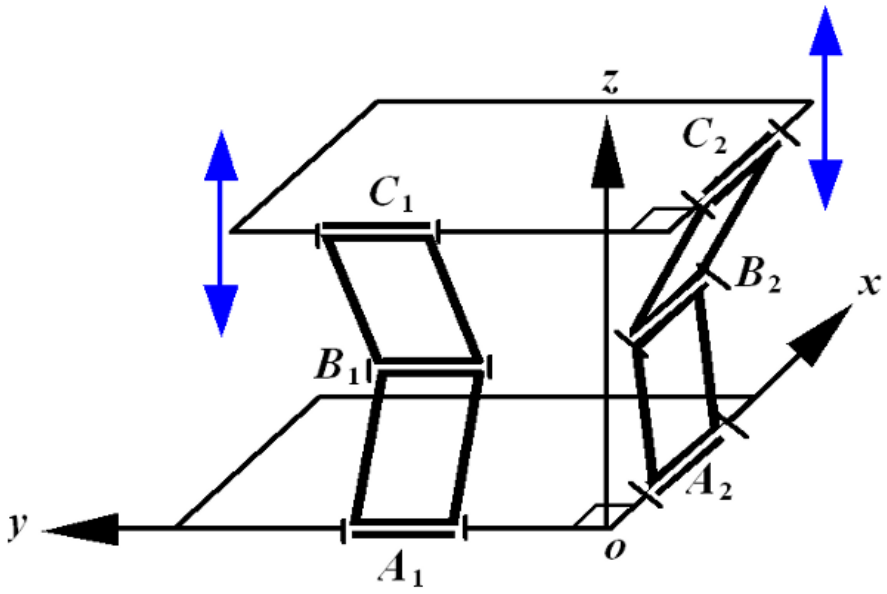

Figure 6.2 Free body diagram of the sarrus mechanism.

The second mechanism invented is the over-constrained Sarrus mechanism, first proposed in 1853 by Pierre Frédéric Sarrus and is recognised to be the first straight line mechanism invented. It is a spatial mechanism in which the two linkages are perpendicularly aligned and are connected by two parallel plates. The rotational movement of the hinges creates a parallel motion along the *y* axis. Recently the Sarrus mechanism has been implemented into crawling microrobots[101] as well as being proposed for a new style of automotive suspension[102].

Firstly the designs to be investigated will be presented. Stress analysis of the designs is performed using finite element analysis software and results will be discussed.

6.2 Methods and materials

6.2.1 Design specification

The design of a novel parallel grasping instrument was undertaken to reduce the potential to cause damage to tissue while grasping whilst also addressing a number of issues which are currently found within the limited selection of current parallel action instruments.

A six point design specification was developed and is ordered by weight of importance below in a descending manner.

1) The grasper must provide a purely parallel motion with no translational movement along the *x*-axis for the benefit of the surgeon when working in a small space envelope with limited spatial and depth perception.

2) The device should have a stationary lower jaw to account for the surgeons line of sight along the length of the instrument. A jaw which actuates outwards from a central position will make grasping accurately difficult as the surgeon will not be able to see the lower moving jaw.

3) The mechanism length to jaw opening ratio must be lower than 5:2. Reducing the space envelope which the parallel mechanism needs to open will prevent the device being prohibitive to use.

4) Mechanism must be able to be manufactured by standard techniques in surgical instrument development whilst also using common materials found within surgical instruments.

5) The instrument must be suitable for development as a hand actuated or motor actuated instrument.

6) The device should be designed as a 5mm instrument, following current user driven trends.

6.2.2 Pantograph mechanism

The mechanism design is shown in figure 6.3. The design is actuated by applying a pull force to the lower proximal pin which is a sliding mechanism allowing for the parallel motion. The mechanism is mirrored around the central axis. A free body diagram of the pantograph mechanism is shown in figure 3.

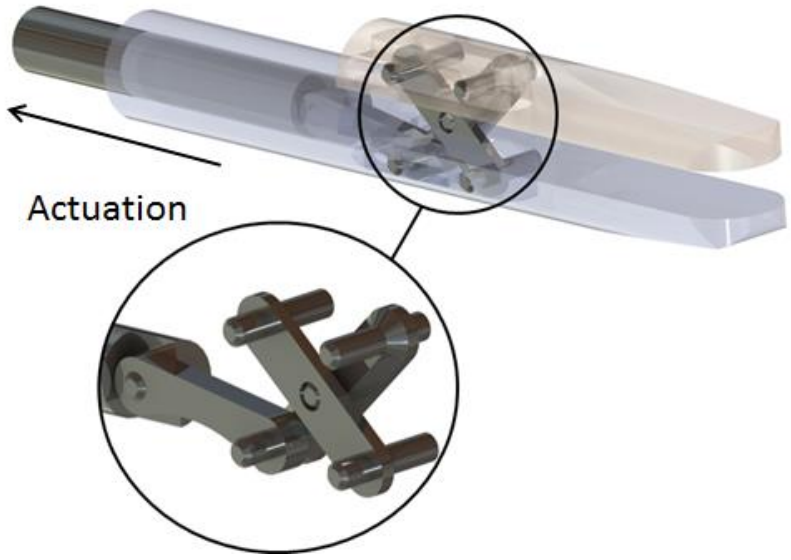

Figure 6.3: 3D rendering of the pantograph mechanism incorporated into the instrument. The two proximal pins are free to rotate and move along the *x*-axis whilst the distal pins are fixed and act as hinge joints.

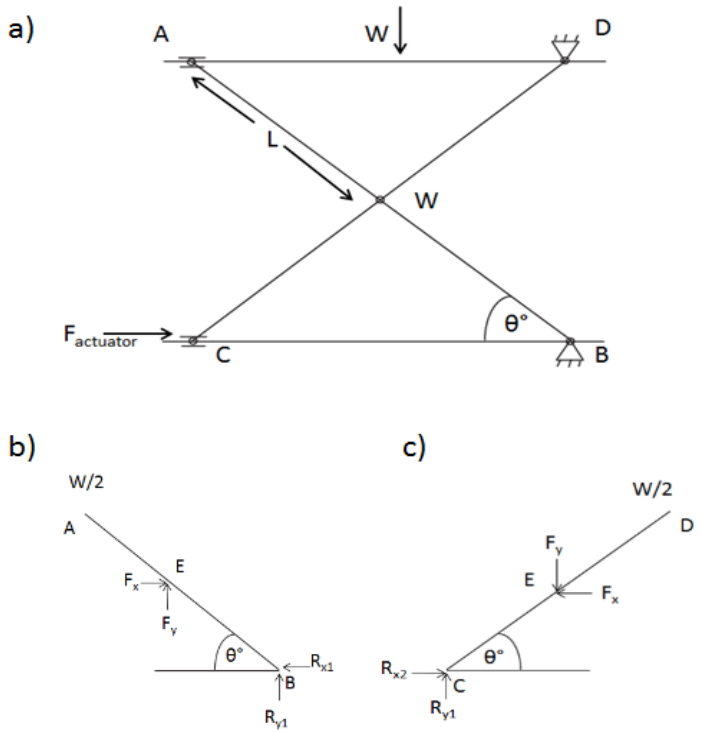

Figure 6.4: A; Free body diagram of the pantograph mechanism. B&C: Diagrams between points A and B, C and D to help determine equations for the actuation force.

Static analysis of the mechanism was performed relating to the free body diagrams in figure 6.3 for which the equations shown (6.1 to 6.8) where derived.

$$\emptyset = \frac{W}{2} 2Lcos(\theta) - F_y Lxcos(\theta) - F_x Lxsin(\theta)$$

$$F_y = \frac{\left(-\frac{W}{2} 2Lcos(\theta)\right)}{(Lcos(\theta))} + \frac{(F_x Lsin(\theta))}{(Lcos(\theta))}$$

$$F_y = -WF_x \tan(\theta)$$

(6.1-6.3)

$$\emptyset = -\frac{W}{2} 2Lcos(\theta) - F_y Lxcos(\theta) - F_x Lxsin(\theta)$$

$$F_y = \frac{\left(\frac{W}{2} 2Lcos(\theta)\right)}{(Lcos(\theta))} + \frac{(-F_x Lsin(\theta))}{(Lcos(\theta))}$$

$$F_x = \frac{W F_x}{\tan(\theta)} - \left(-\frac{W}{\tan(\theta)} - \frac{F_y\, tan(\theta)}{\tan(\theta)}\right)$$

(6.4-6.6)

The amount of force necessary to achieve a certain applied force upon the can be shown by the equation 6.8 which is derived from the equations 6.1 to 6.7. F_x being the actuation force and W being the desired applied force upon the tissue.

$$F_x = \frac{2W}{\tan(\theta)} + F_y$$

$$F_x = \frac{W}{\tan(\theta)}$$

(6.7 & 6.8)

6.2.3 Sarrus mechanism

6.2.3.1 Stationary jaw Sarrus design

The original Sarrus mechanism design generally uses two hinged linkages sitting in a perpendicular fashion to provide parallel motion through the changing angle between the linkages. With this arrangement, developing a grasping instrument with a stationary lower jaw becomes problematic. For this reason the mechanism was modified so that the proximal linkage would become one part and would be retracted into the shaft of the instrument to create a downward motion. The transverse linkages would not be modified and would act to constrain the upper jaw in the *x* and *z* directions.

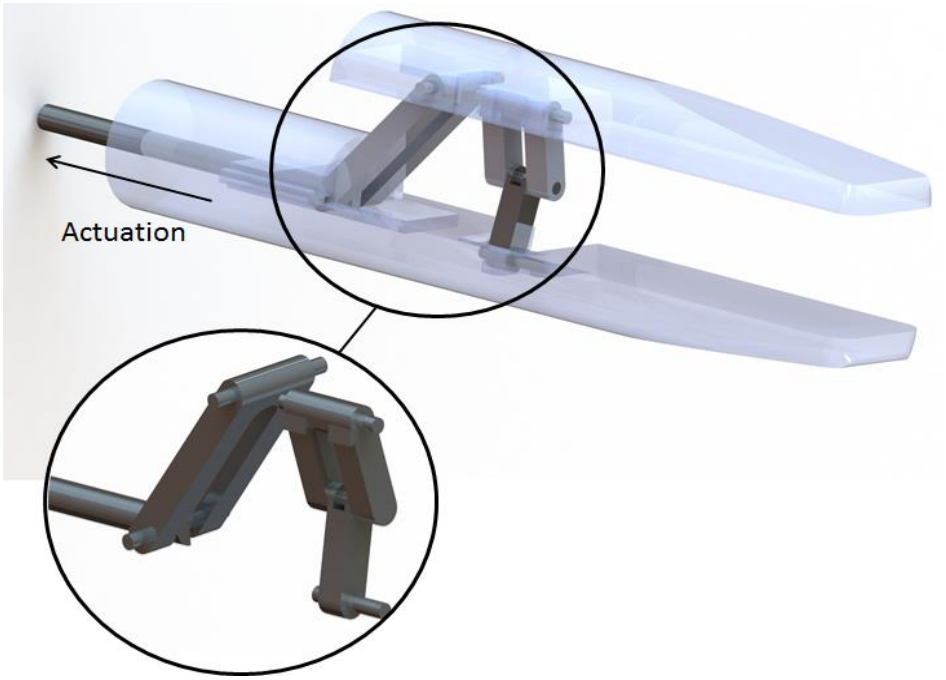

Figure 6.5: Modified Sarrus mechanism replacing the hinged linkages at the proximal end with one long link to be retracted into the shaft of the instrument.

For the purpose of simulation a spring, although not modelled in figure 6.5, was applied between the upper and lower jaws centrally between the two linkages. This is necessary to open the jaw after it had been closed and the actuation force had been relaxed.

6.2.3.2 Centrally actuated Sarrus mechanism

Although more conventional actuation of the Sarrus mechanism does not meet the design specification, it was thought pertinent to investigate it as it may be useful for other applications such as vascular occlusion.

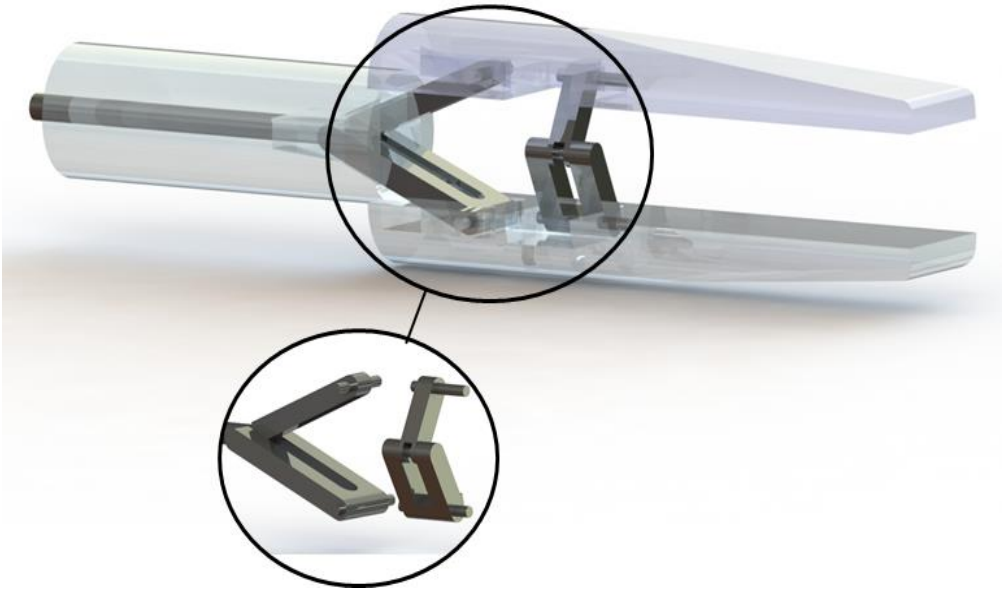

Figure 6.6: Sarrus mechanism with extended proximal links. The motion of the device is controlled by drawing these links into the shaft which acts as a sheath.

To actuate the device the proximal links were extended to provide a method of actuation. These links would be drawn into the instrument shaft and the resulting forces acting at the mid-point of these along the *x* axis would force the jaws of the instrument together. This sheathing of the links could also be performed inversely by keeping the links and jaws stationary and forcing the shaft over the links. This would prevent to occurrence of a translational movement.

6.2.4 Finite element analysis

Finite element analysis (FEA) of each of the components within each of the three models were performed. Material properties of stainless steel 440C were applied to all of the components. This is a surgical steel which is the most commonly used in surgical instruments. Actuation was provided by a prescribed displacement which would mean there would be no upper limit on the amount of force which was necessary to actuate the device.

Simulations were performed over a 5 second time frame for which the model was solved 8 times a second. A loading force of up to 10N was applied to the active grasping area of the upper jaw at a rate of 3N/s with the onset of loading occurring approximately 2.5 seconds into the simulation to replicate engaging tissue.

This method was used for all of the simulations with the exception of adding a spring force between the jaws of both of the Sarrus designs as well as a secondary applied force acting normal to the lower jaw of the centrally actuated Sarrus design, again to accurately replicate tissue grasping.

Stress (σ), deformation (μ) and the factor of safety were all solved by the finite element software. Areas of high stress, potential mechanism failure or anything exceptional will be discussed within the results. Reaction forces around each of the joints were also investigated. Due to the high number of individual parts investigated, any parts which are not discussed can be assumed to have performed as expected, fall within the material limits of the device or are unremarkable.

6.2.5 Prototypes

A prototype of each of the designs was developed. Sarrus mechanism prototypes were, in the most part, manufactured using 3D printing however some integral parts which were expected to come under large amounts of stress were manufactured using stainless steel 440C. The pantograph prototype was initially manufactured using 3D printing and subsequently in SS440C.

6.3 Results

6.3.1 Pantograph mechanism

Actuation forces were theoretically estimated using the equation 6.8. This was compared to the actuation forces computed by the FEA software. This acted as a verification to confirm the mechanics and solver of the model under FEA. The results plot of this is shown in graph 6.1. Both the computed actuation force and calculated actuation force match which confirms that the pantograph model under investigation performs under loading as expected.

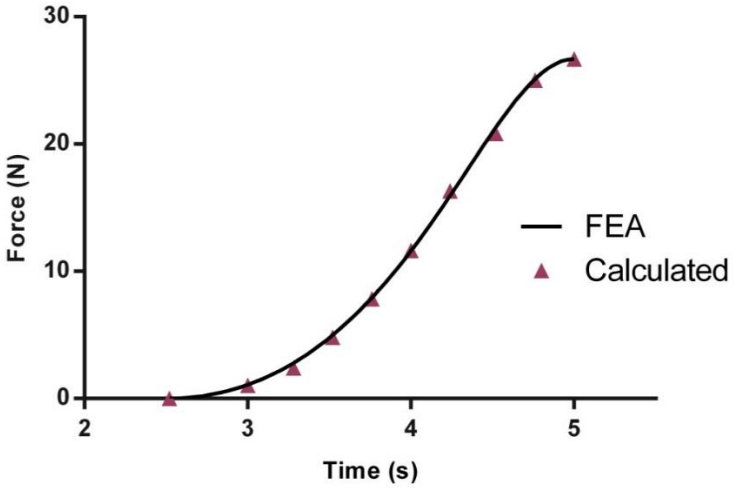

Graph 6.1: Calculated and computed actuation forces for the pantograph model.

The matching plots indicate that the FEA model is acting as expected.

The actuation force is plotted against the applied force in graph 6.2. This shows the actuation forces necessary to grasp tissue at the desired force. It can be seen that the actuation force increases as a function of both the increase in applied or grasping force and a decrease in the angle (θ°). Actuation forces reported by graph 6.2 will not be constant due to variances in tissue thickness which will ultimately change the angle (θ°) at which the forces act over. It would be safe to say that a force which can apply a force of up to 20N would be sufficient to apply the desired 5N grasping force upon the tissue. Current miniature (5.8mm diameter) linear DC motors would be sufficient to provide this actuation force however it would not be able to be mounted within the 5mm diameter instrument and thus would need to be housed within the proximal region of the shaft or in the handle of the instrument.

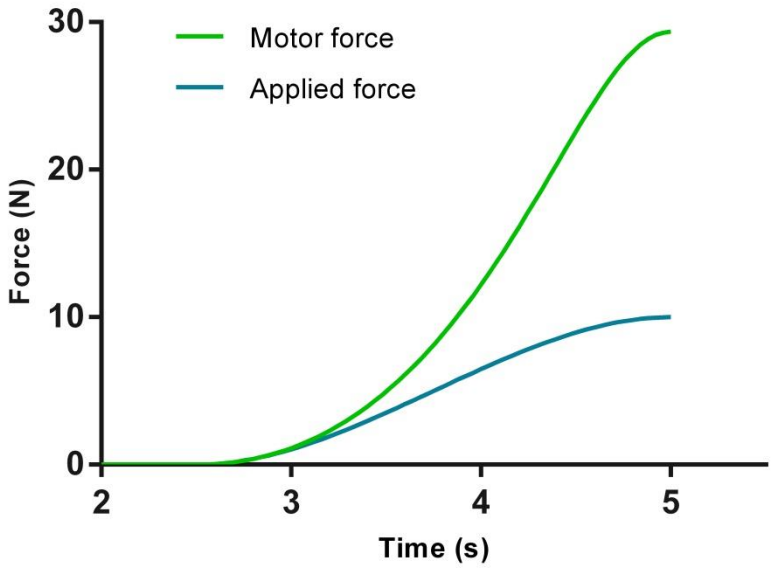

Graph 6.2: Actuation forces necessary translate to desired grasping forces.

The highest stress areas within the design were found on the design features which allowed for the lower proximal links to slide. The highest recorded stress at a grasping force of 10N

was 1120Mpa (figure 6.7) which gives the device a factor of safety of 1.6. This is sufficient as the suggested maximal grasping force would be 5N however it is good practice to design for the extremes in cases such as this.

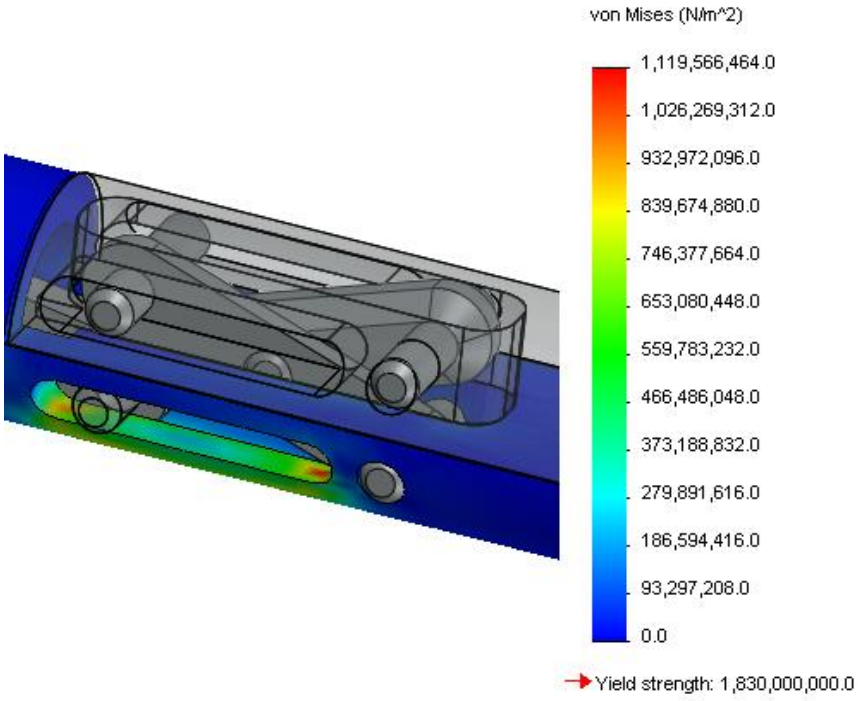

Figure 6.7: Stress plot of the lower jaw at a grasping force of 10N. The areas of red indicate the highest concentrations of stress within the pantograph design. Sufficiently lower than the yield strength of the material.

The forces acting on the tangential between the pin and slot feature were investigated due to the high concentration of stresses in this area. The *x* component of the forces acting was found to be similar to that of the actuation force as expected. A 13N force was found to be acting in the *y* direction (graph 6.3) which would account for the concentrated areas of stress in this region.

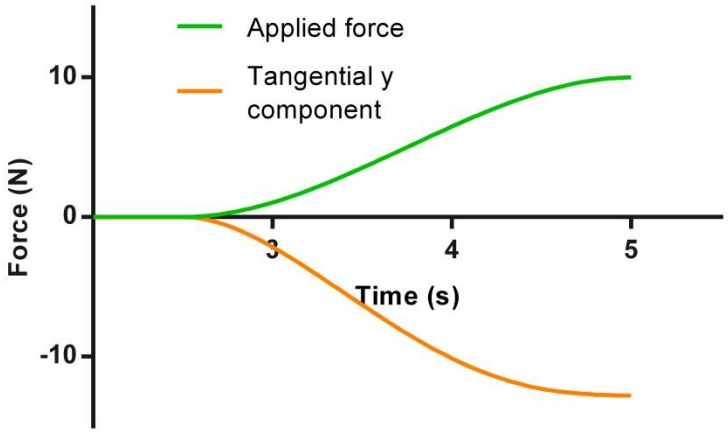

Graph 6.3: Force acting on the *y* axis between the lower sliding pin and the slot feature plotted against the grasping force. This force creates the highest areas of concentrated stress within the design.

An initial prototype of the pantograph style parallel action grasper is shown in figure 6.8. This shows the full range of motion of a 5mm design of the instrument. This prototype was actuated by hand using a small pull rob in a similar fashion to the simulations. There was a small amount of resistance but it was easily overcome by pulling on the transmission rob by hand. Further testing to establish the actuating and grasping forces are necessary.

Figure 6.8: Prototype of the pantograph grasping instrument showing the full range of motion from closed to fully open.

6.3.2 Sarrus mechanism

Both Sarrus mechanism designs resulted in failure with the FEA model being unable to resolve when small loading forces being applied due to the linkages within each of the designs seizing. The initial FEA results are analysed to determine where the failure occurred.

To determine which area of the mechanism was seizing the forces acting concentric to each of the pins was investigated. The model was only able to solve for 0.2s after the initial load was applied due to the forces acting on certain areas of the design (particularly the rotating pins) which caused massive failure. The area of interest was found to be with the transverse pin on the upper and the connected link. Graph 6.4 shows the forces acting on the pin at the time of failure.

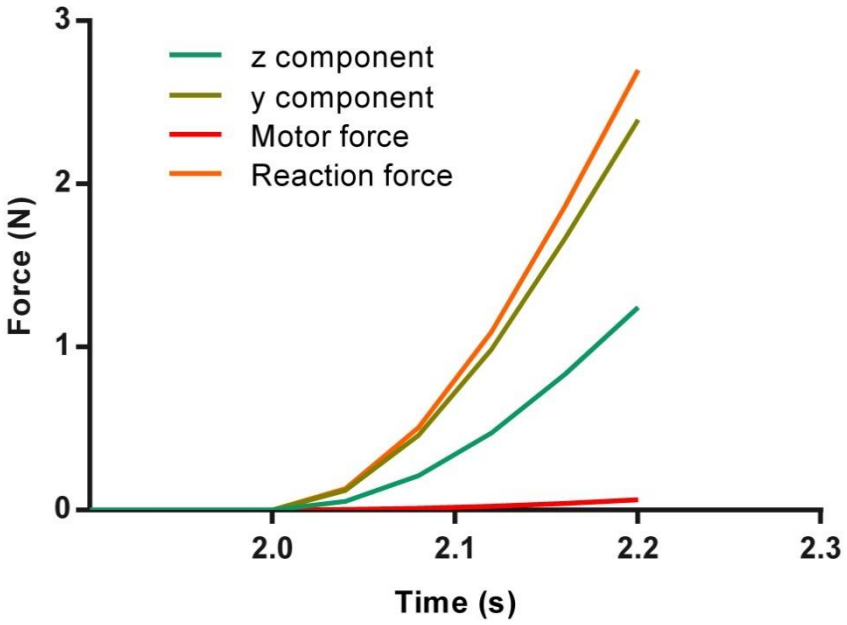

Graph 6.4: Forces acting on the concentric mate of the transverse upper pin.

A low applied force has resulted in total reaction force on the pin.

Both the *y* and *z* components are plotted.

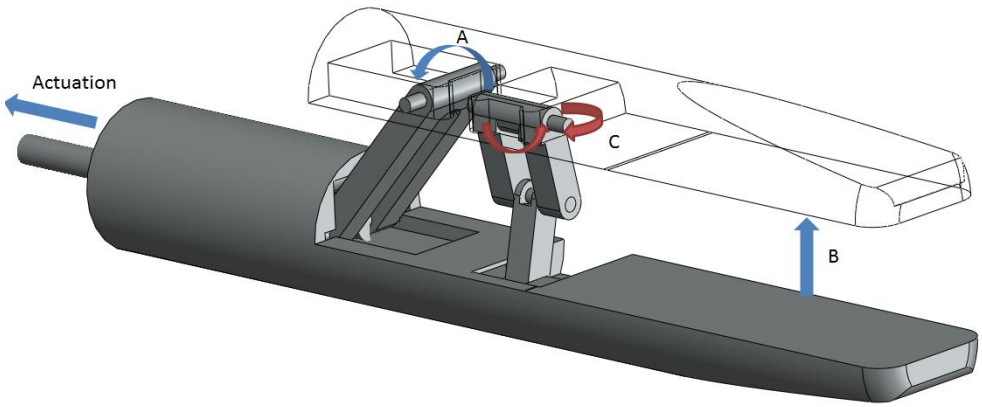

Figure 6.9: Forces acting upon the instrument (blue) which causes the reaction forces around the pin (red) ultimately leading to the failure of the mechanism.

It would appear from graph 6.4 that even at very low grasping forces the reactive forces around this pin, create a torsion acting around the centre of the pin in the *z* axis which causes the linkage to seize. This is illustrated in figure 6.9 along with the forces caused by actuation which contribute to the moment around the concentric mate.

As the actuation force creates a pull force acting downwards in the *y* axis and along the length of the jaw in the *x* axis. As the transverse link is constrained to one side of the jaw the forces acts unevenly across the length of the jaw which leads to a torque. Combined with the grasping force acting on the jaw leads to large reaction force acting on the pin, which if the instrument didn't seize would ultimately succumb to failure.

Figure 6.10: Rapid prototype of centrally actuated Sarrus mechanism showing the jaws out of parallel alignment and failure at the lower transverse pin connection. The design was made to 10mm diameter.

The same outcome as found with the centrally actuated Sarrus mechanism with loads acting on the lower transverse pin created by the connected link which created the same moment, causing the joint to seize and preventing further motion. A prototype of this design in which the applied force has caused the jaws to go out of parallel alignment and eventually to the failure of the lower transverse pin as predicted by the FEA is shown in figure 6.10

6.4 Discussion

From the designs which have been investigated to be implemented to create parallel motion in the jaws of a laproscopic tissue gasper the pantograph style design is the option which would be used in further development of this instrument. The design meets all of the 6 design specifications points. The mechanism length to jaw opening ratio is found to be 2.2:1 however with design optimisation this could be reduced slightly further. The factor of safety could also be increased with slight design optimisation however reported stress plots are for grasping forces higher than which would occur within the proposed autonomous grasping system.

The pantograph style design is capable of producing purely parallel motion for the even distribution of pressure when grasping tissue. The space envelope of the mechanism, although larger than those found in conventional graspers, is a reduction on the currently proposed 4-bar parallel systems in the literature. Further experimentation is required to ensure the efficacy of the mechanism for grasping tissue and to measure the real-world actuation and reaction forces of the device as only theoretical results are reported here however a working prototype has been developed which can be easily actuated using a pull rod.

Regretfully the Sarrus mechanism designs did not perform as well as the pantograph. Both designs failed under loading caused by a seizing of the mechanism when a force acting normal to the grasping area was applied. Exhaustive prototyping of these designs has been undertaken with minimal success and so the only recommendation would be that the arrangement of the Sarrus mechanism is improbable to be successfully used as a mechanism to actuate a surgical instrument. An actuating force acting normal to the surface on one axis seems to be the only way to create parallel motion.

6.5 Conclusions

Three parallel action mechanisms to be used within the jaws of a laparoscopic grasper have been proposed. The pantograph mechanism has been shown to be an option for further development into both this project to create an autonomous grasping instrument which grasps tissue in a parallel manner as well as being a viable solution to create a hand standard hand actuated surgical grasper which will reduce the trauma caused by grasping by evenly distributing the grasping tissue across the whole of the grasping area.

Integration of this mechanism into the autonomous grasping system which has been previously described will be the next stage. This will allow the mechanism to be tested for the necessary actuation forces and resultant grasping forces.

Chapter 7: Discussion & Conclusions

This thesis has presented a number of methods to reduce the potential to cause trauma when grasping tissue during laparoscopic surgery. A number of the chapters focus on a mechanical design approach in order to minimise high stress areas and provide even pressure distribution across the surface of grasped tissue whilst the other half of the thesis focuses on developing an autonomous grasping system with a closed loop control system. Firstly mechanical considerations when designing laparoscopic graspers will be discussed and then on the outcomes of the investigation into slip detection and autonomous grasping. Finally an overall discussion combining these disparate fields of study will be reported.

Investigation into a number of design features commonly found to adorn the surfaces of laparoscopic graspers have expanded the literature in these fields. This work was presented alongside the investigation into using a piezoelectric film (PVDF) to detect and prevent slip occurring when grasping tissue

Chapter 3 builds upon the published literature to investigate the effect which common design features found on the jaws of laparoscopic instruments have on the grasping of tissue. An extensive study of previously investigated[45, 87] and novel surface profiles was undertaken. It was found that the more aggressive the profiling was, the better that it would be at retaining tissue. However, aggressive surface profiles such as large toothed designs would inevitably cause more damage to the tissue when exposed to high grasping forces or high pull forces. A novel design incorporating blunt teeth interspaced with flat regions which would allow tissue to bunch and resist pull forces was selected.

A large study on the impact of fenestrations in the jaws of the grasper indicated, contrary to the published literature[51], that fenestrations played a large role in retaining tissue within the

jaws of the grasper. A standardised method for reporting studies on laparoscopic graspers is also proposed. Although the literature in the field is currently lacking, it is difficult to compare the results of separate studies. For this reason it would be good practice to disseminate findings in the convention found here in which the ratio of applied force to retention force is reported. The combination of both the surface profile and fenestration investigations resulted in what was seen to be the optimal grasping jaw which had a high retention force to applied force ratio, ultimately this meant that the amount of force needed to retain tissue within the jaws was significantly reduced which resulted pressures acting on the tissue as relatively low[11] and certainly too low to cause perforation[89].

Histological analysis of the grasped tissue is the major drawback of this study. Further investigation, focusing on the histological assessment of grasped tissue samples similar to those performed by Marucci *et al*[46]. would be the logical and desired next step. Ultimately further investigation into the design features along with informed decisions on specific design features can help to reduce high stresses acting on tissue which will in turn, reduce the potential to cause trauma under excessive loading.

All studies were carried out in a manner which would replicate the tissue being grasped in a parallel fashion to ensure even distribution of pressure. The action of parallel grasping is the best method to prevent excessive pressures being applied to a small area of tissue. Within conventional laparoscopic graspers which employ the pivoting mechanism create a large and uneven pressure distribution of pressure at the proximal opening. Cuschieri *et al*[48] proposed a mechanism in which bowel tissue would be encompassed by two grasping arms akin to a thumb and forefinger. Regardless of the obvious benefits which parallel grasping and atraumatic holding of tissue provides the uptake of such devices has been remarkably low, reasons for which are discussed in chapter 6.

To address these issues, 3 designs have been developed and reported on with varying success. A parallel action mechanism in which the motion is provided through a pantograph inspired mechanism proved to be most successful. The device provides purely parallel grasping whilst keeping the overall size of the grasping instrument to a minimum. It has a stationary lower jaw and so will not feel dissimilar to a conventional scissor-like grasper when in operation. Finite element analysis of the design showed that using stainless steel 440C the areas of concentrated stress were not enough to cause permanent deformation even when simulated grasping was at levels which would be described as excessive[45].

A prototype of the pantograph grasping mechanism was developed as a 5mm instrument. It was found that it was easily actuated by hand through the pull rod with minimal tip deviation in both the *y* and *z* axis. However as this is anecdotal, further investigation into the real world performance of the parallel mechanism is necessary to measure actual actuation forces and the resulting grasping force.

It is proposed that the pantograph mechanism will be integrated into the autonomous grasping system which was developed using PVDF within a closed loop control system to detect and prevent tissue slipping from the jaws of the grasper. Actuation would be performed using a DC motor to incrementally increase the grasping force when slip was detected. The device would apply just enough force upon the tissue to prevent it falling from the instrument but never excessive forces which could damage it.

Piezoelectric sensors have been investigated for the use in laparoscopic instruments previously [73, 95] however the focus has been on determining grasping forces or anatomical features such as tumours. Outwith the field of surgery it has been widely reported as a slip sensor for use in prosthetics and industrial applications [67-70, 103] with the number of reported studies using PVDF to detect the onset of slip or incipient slip reported only an rare occasions with varying degrees of success.

Chapter 4 investigates PVDF sensors for the detection of incipient slip and slip of bowel tissue from jaws of a laparoscopic grasper. By analysing the output signals prior to slip events occurring it was found that both the number of peaks over a certain voltage occurred in small clusters, it was also found that the average derivative of the signal was significantly different to that outwith this timeframe prior to a slip event.

These were then used as Boolean conditions in a closed loop control system which employed a simple state machine architecture to reduce the computation power necessary which ultimately increases the reaction time of such a system. Testing of the autonomous grasping instrument showed that the device could accurately determine slip and incipient slip events and react to prevent these events. Tissue grasping was successful for the duration of experiments 92% of the time with a tissue displacement of 20% (accounting for tissue elasticity). These results are comparable to the literature in detecting, reacting and preventing slip[104, 105]

The autonomous grasping instrument did not provide sufficient force feedback to accurately actuate the forces with a disparity of 78% between the grasping force and pull force. This is an area for future development. Incorporating another sensor to detect the normal force acting on the tissue and encompassing it into the closed loop control system would help to more accurately control the applied force to the tissue.

When the outcomes of each of the chapters is amalgamated a proactive, instrument for detecting and preventing incipient slip with design features to minimise tissue trauma during surgery emerges. By investigating the individual design features a number of areas have been identified in which improvements can be made to instrument design which will ultimately improve patient outcome whilst also reducing stress upon the surgeon as repetitive and strenuous actions such as grasping or tissue retraction can be automated.

Chapter 8: Future work

Further development of the system proposed within this thesis is of course necessary. Ideally histological analysis of tissue, incorporation of a secondary force sensor for detecting grasping force and testing of the pantograph parallel action grasper would be the next stage of the project to realise the goal of developing a deployable tissue grasping and retraction system which would apply the necessary force to the tissue without damaging it.

As the published literature relating to tissue trauma caused by design features is still relatively small with a number of areas still not fully understood, further research is certainly necessary. This research could begin to encompass such effects as the influence of material coatings and material selection and the relationship to tissue retention. This would ideally be expanded to include not only histological assessment of *ex vivo* tissue but also harvested *in vivo* tissue.

Development of the presented device would require a multi-axial force sensor. This could be provided by the combination of both PVDF and another sensing technology (such as those described in chapter 2) in an array sensor to detect slip and applied forces.

Developing the device into a deployable autonomous grasper would require wireless data transmission as well as low power components to make the device as efficient as possible. This could be combined with novel data compression methods to reduce power consumption. This would lead to large, bulky components such as batteries being reduced in size and with the advancement in actuation technologies, could mean the reduction in size of DC motors with sufficient torque output to realise the development of a compact autonomous sensing and grasping system.

References

1. Reynolds, W., Jr., *The first laparoscopic cholecystectomy.* Jsls, 2001. **5**(1): p. 89-94.
2. Berguer, R., *Surgical technology and the ergonomics of laparoscopic instruments.* Surgical Endoscopy, 1998. **12**(5): p. 458-462.
3. Dunker, M.S., et al., *Cosmesis and body image after laparoscopic-assisted and open ileocolic resection for Crohn's disease.* Surgical Endoscopy, 1998. **12**(11): p. 1334-1340.
4. Korolija, D., et al., *Evaluation of quality of life after laparoscopic surgery: evidence-based guidelines of the European Association for Endoscopic Surgery.* Surgical Endoscopy And Other Interventional Techniques, 2004. **18**(6): p. 879-897.
5. Rao, P.P., P.P. Rao, and S. Bhagwat, *Single-incision laparoscopic surgery - current status and controversies.* J Minim Access Surg, 2011. **7**(1): p. 6-16.
6. Berguer, R., D.L. Forkey, and W.D. Smith, *Ergonomic problems associated with laparoscopic surgery.* Surgical Endoscopy, 1999. **13**(5): p. 466-468.
7. Maeso, S., et al., *Efficacy of the Da Vinci Surgical System in Abdominal Surgery Compared With That of Laparoscopy: A Systematic Review and Meta-Analysis.* Annals of Surgery, 2010. **252**(2): p. 254-262 10.1097/SLA.0b013e3181e6239e.
8. Piccigallo, M., et al., *Design of a Novel Bimanual Robotic System for Single-Port Laparoscopy.* Mechatronics, IEEE/ASME Transactions on, 2010. **15**(6): p. 871-878.
9. Alonso, O., et al. *Control electronics integration toward endoscopic capsule robot performing legged locomotion and illumination*. in *VLSI System on Chip Conference (VLSI-SoC), 2010 18th IEEE/IFIP*. 2010.
10. Heijnsdijk, E., J. Dankelman, and D. Gouma, *Effectiveness of grasping and duration of clamping using laparoscopic graspers.* Surgical Endoscopy, 2002. **16**(9): p. 1329-1331.
11. Cartmill, J.A., et al., *High pressures are generated at the tip of laparoscopic graspers.* The Australian and New Zealand journal of surgery, 1999. **69**(2): p. 127-130.
12. *National Institutes of Health Consensus Development Conference Statement on Gallstones and Laparoscopic Cholecystectomy.* The American Journal of Surgery, 1993. **165**(4): p. 390-396.
13. Sherwinter, D.A. *Laparoscopic Cholecystectomy*. (2013) [cited 2013 22/11/2013]; Available from: http://emedicine.medscape.com/article/1582292-overview#aw2aab6b2b5.
14. Rao, P.P. and S. Bhagwat, *Single-incision laparoscopic surgery - current status and controversies.* J Minim Access Surg, 2011. **7**(1): p. 6-16.
15. Aimaq, R., G. Akopian, and H.S. Kaufman, *Surgical site infection rates in laparoscopic versus open colorectal surgery.* Am Surg, 2011. **77**(10): p. 1290-4.
16. Garrard, C.L., et al., *Adhesion formation is reduced after laparoscopic surgery.* Surg Endosc, 1999. **13**(1): p. 10-3.
17. Salimath, J., et al., *Comparison of return of bowel function and length of stay in patients undergoing laparoscopic versus open colectomy.* Jsls, 2007. **11**(1): p. 72-5.
18. Huscher, C.G., et al., *Laparoscopic versus open subtotal gastrectomy for distal gastric cancer: five-year results of a randomized prospective trial.* Ann Surg, 2005. **241**(2): p. 232-7.

19. Nguyen, N.T., et al., *Comparison of minimally invasive esophagectomy with transthoracic and transhiatal esophagectomy.* Archives of Surgery, 2000. **135**(8): p. 920-925.
20. Schwenk, W., B. Bohm, and J.M. Muller, *Postoperative pain and fatigue after laparoscopic or conventional colorectal resections. A prospective randomized trial.* Surg Endosc, 1998. **12**(9): p. 1131-6.
21. Veldkamp, R., et al., *Laparoscopic surgery versus open surgery for colon cancer: short-term outcomes of a randomised trial.* Lancet Oncol, 2005. **6**(7): p. 477-84.
22. Cali, R.L., et al., *Effect of Morphine and incision length on bowel function after colectomy.* Dis Colon Rectum, 2000. **43**(2): p. 163-8.
23. Huang, C., et al., *Laparoscopic and open resection for colorectal cancer: an evaluation of cellular immunity.* BMC Gastroenterology, 2010. **10**(1): p. 127.
24. Allendorf, J.F., et al., *Better preservation of immune function after laparoscopic-assistedvs. open bowel resection in a murine model.* Diseases of the Colon & Rectum, 1996. **39**(10): p. S67-S72.
25. Keus, F., et al. *Laparoscopic versus open cholecystectomy for patients with symptomatic cholecystolithiasis*. Cochrane Database of Systematic Reviews, 2006. DOI: 10.1002/14651858.CD006231.
26. Guller, U.M.D.M.H.S., et al., *Laparoscopic Versus Open Appendectomy: Outcomes Comparison Based on a Large Administrative Database.* Annals of Surgery, 2004. **239**(1): p. 43-52.
27. Dowson, H., et al., *Systematic Review of the Costs of Laparoscopic Colorectal Surgery.* Diseases of the Colon & Rectum, 2007. **50**(6): p. 908-919.
28. Velanovich, V., *Case-control comparison of laparoscopic versus open distal pancreatectomy.* Journal of Gastrointestinal Surgery, 2006. **10**(1): p. 95-98.
29. Tian, H.L., et al., *The effects of laparoscopic vs. open gastric bypass for morbid obesity: a systematic review and meta-analysis of randomized controlled trials.* Obesity Reviews, 2011. **12**(4): p. 254-260.
30. Christopher, R.W., et al., *The Benefit of Force Feedback in Surgery: Examination of Blunt Dissection.* Presence: Teleoper. Virtual Environ., 2007. **16**(3): p. 252-262.
31. Meijden, O.A.J. and M.P. Schijven, *The value of haptic feedback in conventional and robot-assisted minimal invasive surgery and virtual reality training: a current review.* Surgical Endoscopy, 2009. **23**(6): p. 1180-1190.
32. Eleonora Patricia Westebring-van der, P., *The Effect of Augmented Feedback on Grasp Force in Laparoscopic Grasp Control.* IEEE Transactions on Haptics, 2010. **3**(4): p. 280-291.
33. Crothers, I.R., et al., *Experienced Laparoscopic Surgeons are Automated to the "Fulcrum Effect": An Ergonomic Demonstration.* Endoscopy, 1999. **31**(05): p. 365-369.
34. Prasad, S.M., et al., *Surgical robotics: Impact of motion scaling on task performance.* Journal of the American College of Surgeons, 2004. **199**(6): p. 863-868.
35. Berguer, R., W.D. Smith, and Y.H. Chung, *Performing laparoscopic surgery is significantly more stressful for the surgeon than open surgery.* Surg Endosc, 2001. **15**(10): p. 1204-7.
36. van der Voort, M., E.A.M. Heijnsdijk, and D.J. Gouma, *Bowel injury as a complication of laparoscopy.* British Journal of Surgery, 2004. **91**(10): p. 1253-1258.
37. Ballantyne, G.H., *The Pitfalls of Laparoscopic Surgery: Challenges for Robotics and Telerobotic Surgery.* Surgical Laparoscopy Endoscopy & Percutaneous Techniques, 2002. **12**(1): p. 1-5.

38. Romanelli, J. and D. Earle, *Single-port laparoscopic surgery: an overview.* Surgical Endoscopy, 2009. **23**(7): p. 1419-1427.
39. Inoue, H., et al., *Peroral endoscopic myotomy (POEM) for esophageal achalasia.* Endoscopy, 2010. **42**(4): p. 265-71.
40. Cuschieri, A., *Single-incision laparoscopic surgery.* J Minim Access Surg, 2011. **7**(1): p. 3-5.
41. Canes, D., et al., *Transumbilical Single-Port Surgery: Evolution and Current Status.* European Urology, 2008. **54**(5): p. 1020-1030.
42. Romanelli, J.R. and D.B. Earle, *Single-port laparoscopic surgery: an overview.* Surgical Endoscopy And Other Interventional Techniques, 2009. **23**(7): p. 1419-1427.
43. Emam, T.A., G. Hanna, and A. Cuschieri, *Comparison of orthodox versus off-optical axis endoscopic manipulations.* Surgical Endoscopy, 2002. **16**(3): p. 401-405.
44. Galvao Neto, M., A. Ramos, and J. Campos, *Single port laparoscopic access surgery.* Techniques in Gastrointestinal Endoscopy, 2009. **11**(2): p. 84-93.
45. Heijnsdijk, E.A.M., et al., *Slip and damage properties of jaws of laparoscopic graspers.* Surgical Endoscopy, 2004. **18**(6): p. 974-979.
46. Marucci, D.D., et al., *Grasper trauma during laparoscopic cholecystectomy.* Australian and New Zealand Journal of Surgery, 2000. **70**(8): p. 578-581.
47. Stewart, L. and L.W. Way, *Bile duct injuries during laparoscopic cholecystectomy: Factors that influence the results of treatment.* Archives of Surgery, 1995. **130**(10): p. 1123-1128.
48. Frank, T.G. and A. Cuschieri, *Prehensile atraumatic grasper with intuitive ergonomics.* Surgical Endoscopy, 1997. **11**(10): p. 1036-1039.
49. Frank, T., G.J. Willetts, and A. Cuschieri, *Detachable clamps for minimal access surgery.* Proc Inst Mech Eng H, 1995. **209**(2): p. 117-20.
50. Vakili K, F.M.S., G S L Teo, Sepp T R, *Design and testing of a pressure-sensing laparoscopic grasper.* Paper presented at Design of Medical devices Conference, 2011.
51. Heijnsdijk, E.A.M., et al., *Fenestrations in the jaws of laparoscopic graspers.* Minimally Invasive Therapy & Allied Technologies, 2005. **14**(1): p. 45-48.
52. Rizzoni, G., *Principles and Applications of Electrical Engineering*. 2005: McGraw-Hill Education.
53. Liu, D.K.-C., J. Friend, and L. Yeo, *A brief review of actuation at the micro-scale using electrostatics, electromagnetics and piezoelectric ultrasonics.* Acoustical Science and Technology, 2010. **31**(2): p. 115-123.
54. B, F.M.B.D.-M.S., (Faulhaber, 2006).
55. Mirbagheri, A. and F. Farahmand, *A triple-jaw actuated and sensorized instrument for grasping large organs during minimally invasive robotic surgery.* The International Journal of Medical Robotics and Computer Assisted Surgery, 2013. **9**(1): p. 83-93.
56. Doğan*, A. and E. Uzgur, *Piezoelectric Actuator Designs*, in *Piezoelectric and Acoustic Materials for Transducer Applications*, A. Safari and E.K. Akdoğan, Editors. 2008, Springer US. p. 341-371.
57. Kenji, U., *Piezoelectric ultrasonic motors: overview.* Smart Materials and Structures, 1998. **7**(3): p. 273.
58. Saedi, S., A. Mirbagheri, and F. Farahmand. *Conceptual design of a miniaturized hybrid local actuator for Minimally Invasive Robotic Surgery (MIRS) instruments*. in *Engineering in Medicine and Biology Society,EMBC, 2011 Annual International Conference of the IEEE*. 2011.

59. Byungkyu, K., et al. *An earthworm-like locomotive mechanism for capsule endoscopes*. in *Intelligent Robots and Systems, 2005. (IROS 2005). 2005 IEEE/RSJ International Conference on*. 2005.
60. Schlaak, H.F., et al., *A Novel Laparoscopic Instrument with Multiple Degrees of Freedom and Intuitive Control*, in *4th European Conference of the International Federation for Medical and Biological Engineering*, J. Sloten, et al., Editors. 2009, Springer Berlin Heidelberg. p. 1660-1663.
61. Otsuka, K. and C.M. Wayman, *Shape Memory Materials*. 1999: Cambridge University Press.
62. Kim, B., et al., *An earthworm-like micro robot using shape memory alloy actuator.* Sensors and Actuators A: Physical, 2006. **125**(2): p. 429-437.
63. Gorini, S., et al. *A Novel SMA-Based Actuator for a Legged Endoscopic Capsule*. in *Biomedical Robotics and Biomechatronics, 2006. BioRob 2006. The First IEEE/RAS-EMBS International Conference on*. 2006.
64. Yan, S., et al., *Tactile feedback control for a gripper driven by SMA springs.* AIP Advances, 2012. **2**(3): p. -.
65. Thomann, G., G. Chen, and T. Redarce, *Design and control of an autonomous bendable tip for colonoscopy.* Journal of Micro-Nano Mechatronics, 2008. **4**(3): p. 103-114.
66. Moers, A.J.M., M.F.L. Volder, and D. Reynaerts, *Integrated high pressure microhydraulic actuation and control for surgical instruments.* Biomedical Microdevices, 2012. **14**(4): p. 699-708.
67. Sasaki, K., et al., *Signal processing for slip and contact sensing and its application to a two-fingered robotic hand.* Integrated Computer-Aided Engineering, 2001. **8**(4): p. 283-291.
68. Goeger, D., N. Ecker, and H. Woern. *Tactile sensor and algorithm to detect slip in robot grasping processes*. in *Robotics and Biomimetics, 2008. ROBIO 2008. IEEE International Conference on*. 2009.
69. Fujimoto, I., et al., *Identification of Incipient Slip Phenomena Based on the Circuit Output Signals of PVDF Film Strips Embedded in Artificial Finger Ridges.* Transactions - Society of Instrument and Control Engineers, 2004. **40**(6): p. 648-655.
70. Chuang, C.H., Y.R. Liou, and C.W. Chen. *Detection system of incident slippage and friction coefficient based on a flexible tactile sensor with structural electrodes*. in *Solid-State Sensors, Actuators and Microsystems Conference (TRANSDUCERS), 2011 16th International*. 2011.
71. Yamada, Y., H. Morita, and Y. Umetani, *Slip phase isolating: impulsive signal generating vibrotactile sensor and its application to real-time object regrip control.* Robotica, 2000. **18**(01): p. 43-49.
72. Shirafuji, S. and K. Hosoda. *Detection and prevention of slip using sensors with different properties embedded in elastic artificial skin on the basis of previous experience*. in *Advanced Robotics (ICAR), 2011 15th International Conference on*. 2011.
73. Qasaimeh, M.A., et al., *PVDF-Based Microfabricated Tactile Sensor for Minimally Invasive Surgery.* Microelectromechanical Systems, Journal of, 2009. **18**(1): p. 195-207.
74. Okada, H., et al. *A membrane type Si-MEMS tactile imager with fingerprint structure for realization of slip sensing capability*. in *Micro Electro Mechanical Systems (MEMS), 2010 IEEE 23rd International Conference on*. 2010.

75. Schoepfer, M., et al. *Using a Piezo-Resistive Tactile Sensor for Detection of Incipient Slippage*. in *Robotics (ISR), 2010 41st International Symposium on and 2010 6th German Conference on Robotics (ROBOTIK)*. 2010.
76. Yating, H., et al., *Bioinspired 3-D Tactile Sensor for Minimally Invasive Surgery.* Microelectromechanical Systems, Journal of, 2010. **19**(6): p. 1400-1408.
77. Alvares, D., et al., *Development of nanoparticle film-based multi-axial tactile sensors for biomedical applications.* Sensors and Actuators A: Physical, 2013. **196**(0): p. 38-47.
78. Engeberg, E.D., M. Vatani, and C. Jae-Won. *Direction of slip detection for a biomimetic tactile sensor*. in *Control, Automation and Systems (ICCAS), 2012 12th International Conference on*. 2012.
79. Sani, H.N. and S.G. Meek. *Characterizing the performance of an optical slip sensor for grip control in a prosthesis*. in *Intelligent Robots and Systems (IROS), 2011 IEEE/RSJ International Conference on*. 2011.
80. Missinne, J., et al., *Ultra Thin Optical Tactile Shear Sensor.* Procedia Engineering, 2011. **25**(0): p. 1393-1396.
81. Lee, H.-K., et al., *Real-time measurement of the three-axis contact force distribution using a flexible capacitive polymer tactile sensor.* Journal of Micromechanics and Microengineering, 2011. **21**(3): p. 035010.
82. Hyung-kew, L., et al., *Normal and Shear Force Measurement Using a Flexible Polymer Tactile Sensor With Embedded Multiple Capacitors.* Microelectromechanical Systems, Journal of, 2008. **17**(4): p. 934-942.
83. Heijnsdijk, E.A.M., J. Dankelman, and D.J. Gouma, *Effectiveness of grasping and duration of clamping using laparoscopic graspers.* Surgical Endoscopy And Other Interventional Techniques, 2002. **16**(9): p. 1329-1331.
84. Franco, M.L., et al., *An integrated pneumatic tactile feedback actuator array for robotic surgery.* The International Journal of Medical Robotics and Computer Assisted Surgery, 2009. **5**(1): p. 13-19.
85. Heijnsdijk, E.A.M., et al., *Slip and damage properties of jaws of laparoscopic graspers.* Surgical Endoscopy And Other Interventional Techniques, 2004. **18**(6): p. 974-979.
86. Visser, H., et al., *Forces and displacements in colon surgery.* Surgical Endoscopy, 2002. **16**(10): p. 14263-1430.
87. Marucci, D.D., et al., *Patterns of Failure at the Instrument–Tissue Interface.* The Journal of surgical research, 2000. **93**(1): p. 16-20.
88. Fessel, G., et al., *Suitability of Thiel embalmed tendons for biomechanical investigation.* Annals of Anatomy - Anatomischer Anzeiger, 2011. **193**(3): p. 237-241.
89. Heijnsdijk, E.A.M., et al., *Inter- and intraindividual variabilities of perforation forces of human and pig bowel tissue.* Surgical Endoscopy And Other Interventional Techniques, 2003. **17**(12): p. 1923-1926.
90. Yongrae, R., V.V. Varadan, and V.K. Varadan, *Characterization of all the elastic, dielectric, and piezoelectric constants of uniaxially oriented poled PVDF films.* Ultrasonics, Ferroelectrics and Frequency Control, IEEE Transactions on, 2002. **49**(6): p. 836-847.
91. Sirohi, J. and I. Chopra, *Fundamental Understanding of Piezoelectric Strain Sensors.* Journal of Intelligent Material Systems and Structures, 2000. **11**(4): p. 246-257.
92. Francomano, M.T., D. Accoto, and E. Guglielmelli, *Artificial Sense of Slip—A Review.* Sensors Journal, IEEE, 2013. **13**(7): p. 2489-2498.
93. Specialties, M. *Piezo Film Sensors Technical Manual*. Piezo Film Sensors Technical Manual]; Available from: http://www.meas-spec.com. [25/02/2012]

94. Jockusch, J., J. Walter, and H. Ritter. *A tactile sensor system for a three-fingered robot manipulator*. in *Robotics and Automation, 1997. Proceedings., 1997 IEEE International Conference on*. 1997.
95. Sokhanvar, S., M. Packirisamy, and J. Dargahi, *A multifunctional PVDF-based tactile sensor for minimally invasive surgery.* Smart Materials and Structures, 2007. **16**(4): p. 989.
96. Watters, D.A., et al., *Mechanical properties of the colon: comparison of the features of the African and European colon in vitro.* Gut, 1985. **26**(4): p. 384-92.
97. Westebring-van der Putten, E.P., et al., *Force feedback requirements for efficient laparoscopic grasp control.* Ergonomics, 2009. **52**(9): p. 1055-66.
98. Moradi Dalvand, M., et al., *An actuated force feedback-enabled laparoscopic instrument for robotic-assisted surgery.* Int J Med Robot, 2014. **10**(1): p. 11-21.
99. Lee, D.H., et al., *An implementation of sensor-based force feedback in a compact laparoscopic surgery robot.* Asaio j, 2009. **55**(1): p. 83-5.
100. Tholey, G., et al., *Design, Development, and Testing of an Automated Laparoscopic Grasper with 3-D Force Measurement Capability*, in *Medical Simulation*, S. Cotin and D. Metaxas, Editors. 2004, Springer Berlin Heidelberg. p. 38-48.
101. Hoover, A.M. and R.S. Fearing, *Analysis of off-axis performance of compliant mechanisms with applications to mobile millirobot design*, in *Proceedings of the 2009 IEEE/RSJ international conference on Intelligent robots and systems*. 2009, IEEE Press: St. Louis, MO, USA. p. 2770-2776.
102. Yu, Z., et al. *Mobility analysis of a Sarrus Linkage-like 7-R single closed loop mechanism*. in *Robotics and Automation (ICRA), 2013 IEEE International Conference on*. 2013.
103. Fujimoto, I., et al. *Development of artificial finger skin to detect incipient slip for realization of static friction sensation*. in *Multisensor Fusion and Integration for Intelligent Systems, MFI2003. Proceedings of IEEE International Conference on*. 2003.
104. Xu, W., et al. *Development of a Tactile and Slip Sensor Controlled Prosthetic Hand System*. in *International Conference on Power Control and Optimization*. 2008.
105. Roberts, L., G. Singhal, and R. Kaliki. *Slip detection and grip adjustment using optical tracking in prosthetic hands*. in *Engineering in Medicine and Biology Society,EMBC, 2011 Annual International Conference of the IEEE*. 2011.

Relevant Publications

Surg Endosc (2014) 28:1277–1283
DOI 10.1007/s00464-013-3323-7

Impact of fenestrations and surface profiling on the holding of tissue by parallel occlusion laparoscopic graspers

Andrew W. Brown · Stuart I. Brown · Donald Mclean · Zhigang Wang · Alfred Cuschieri

Received: 13 May 2013 / Accepted: 6 November 2013 / Published online: 24 December 2013

Abstract
Background Despite the importance of efficient grasping during laparoscopic surgery, the published literature on jaw features, e.g., fenestrations and surface profiling on grasping efficiency defined as resistance to slip without inflicting trauma, is limited.
Methods Various surface geometries of the jaws were tested with respect to (i) inclusion of fenestrations; (ii) surface contact to fenestration area ratio, and (iii) surface profiling of the jaws. Various loads were applied to the tissue which was subsequently pulled at a constant rate until free from the jaws. The maximal force necessary to pull the tissue free was recorded. The jaws were designed for use in parallel-occlusion graspers to avoid the well documented high pinch forces encountered with pivoted occlusion.
Results At all applied forces the force needed to pull tissue from any fenestration design was significantly higher than the force necessary to pull tissue from non-fenestrated jaws ($p < 0.05$) with no significant differences between the three fenestration designs. The ratio of surface contact to fenestration area must exceed 1:0.4 to achieve a significant increase in the tissue retention. All the profiles studied were made using a single fenestration and with a surface contact to fenestration area ratio of 1:0.8. All such profile designs studied performed significantly better than the control ($p < 0.005$). The ratio of the mean retraction to applied force across all load conditions tested were 1.23:1.0 and 1.7:1.0 for the waved and toothed profile respectively, with standard deviations for the corresponding retraction force of ±0.45 and ±0.38 respectively.
Conclusions The retention efficiency of laparoscopic graspers is improved by fenestration which must, however, exceed a certain ratio (>1.0:0.4). Likewise surface profiling of the jaws enhances retention efficiency and its design (tooth, waved, mixed) directly influences the amount of pressure needed to retain tissue.

Keywords Laparoscopic graspers · Fenestrations · Surface contact to fenestration area · Surface profiling · Parallel occlusion

A. W. Brown · S. I. Brown · D. Mclean · Z. Wang · A. Cuschieri (✉)
Surgical Technology and Robotics Group, Institute for Medical Science and Technology, University of Dundee, 1, Wurzburg Loan, Dundee DD2 1FD, Scotland, UK
e-mail: a.cuschieri@dundee.ac.uk

A. W. Brown
e-mail: a.w.y.brown@dundee.ac.uk

Laparoscopic tissue graspers incorporate design features which enhance retention of tissue within the approximated jaws, thereby reducing slip without inflicting trauma to the tissue. However, because of the small size of these instruments (usually 5 mm), high pressures are often inevitably applied to the tissue especially at high stress areas [1, 2], rendering efficient grasping without some tissue damage difficult. Heijnsdijk et al. [3] reported that during the performance of laparoscopic colectomy, tissue is grasped 117 ± 48 times [3] only 63 % of these grasping actions being successful. In 7 %, tissue slip is encountered during grasping, and although rare, 1–3 % of grasping manoeuvres result in trauma to the gasped tissues. A systemic review of the literature [4] comprising 273 full-thickness and partial bowel injuries during laparoscopic surgery indicated that only 1 % are caused by grasping forceps, but this is likely to be an underestimate because this review reported that the cause could not be specified in

Fig. 1 Dundee prehensile grasper

84 injuries (30 %). Ideally laparoscopic tissue graspers should be able to safely secure tissue without causing damage or tissue slippage from the instrument. In a reported study on the forces [5], it was found that a laparoscopic instrument is required to transmit forces ranging from of 2.5–5 N, which fortuitously approximated to the average forces trained surgeons applied to manipulate the colon for effective dissection.

The grip of gaspers on tissues is influenced by (i) the occlusion mechanism of the grasper and (ii) surface features of the opposing jaws of the gaspers, e.g., fenestrations and surface profiling. Fenestrations often are included in laparoscopic graspers, because they are thought to minimize tissue slippage due to the tissue bulging within the fenestration(s). However, this perceived effect of fenestrations has not been confirmed in the only published study [6], which concluded that fenestrations have a negative effect on tissue grasping as they lead to more frequent tissue damage at lower applied loads. This study also reported that fenestrations by reducing the surface contact area between instrument and tissue produce higher local pressures and hence increased risk of damage. Surface profiling of the grasper jaws is commonly used to increase the grip and reduce slippage. Marucci et al. [7] reported that a 2 mm wave profile significantly eliminates tissue trauma compared with toothed profile, but it produces a less secure grip. Heinsdijk et al. [8] concluded that a large contact area and a slight profile produced the safest grip as this configuration lowered the pressure on tissue. The occlusion mechanism of the graspers is very important, because it influences the distribution of the forces on the tissues between the opposing jaws. For the usual and predominant scissors or pivot mechanism used in laparoscopic graspers, one study has documented high pinch forces at the proximal opening of the jaws and high pressures the distal tip [2], ranging from 210 to 650 kPa and increasing as the angle of incidence increases. In contrast, parallel occlusion results in even pressure distribution on the tissues being grasped and is therefore less traumatic, but despite this, it is very rarely used in for the design of laparoscopic graspers probably because of reduced grasping efficiency and increased difficulty in the design and manufacture of efficient parallel occlusion. A novel prehensile-type atraumatic grasping forceps was developed by Frank and Cuschieri [9]. This instrument is held in the hollow of the hand and the segmented jaws automatically reflect the position of the fingers, varying from the "ring grasping" to flat parallel occlusion grasping. Despite its functionality, the instrument has remained unpopular with the majority of laparoscopic surgeons (Fig. 1) and is currently available as a 10-mm device.

The purpose of the present study was to investigate the effect of fenestrations and surface profiling of jaws on grasping efficiency as the basis for the design an improved laparoscopic tissue grasping instrument.

Methods and materials

Three aspects of jaw geometry were investigated in three separate experiments: (i) fenestrations, (ii) ratio of contact surface to fenestration area, and (iii) surface profiling.

Fenestration design

The first experiment investigated whether the fenestration should be confined to one large area or consists of a number of smaller openings. Three designs were studied: one large rectangular opening, two smaller rectangles, and three circles (both equalling the area of the single large fenestration). The width of the single and twin fenestrations was 7 mm, and the diameter of the circular fenestrations was 6 mm. A pair of featureless nonfenestrated jaws were machined and used as benchmark controls. To ensure that a constant pressure was exerted on the tissue, all jaw designs had the same surface contact area: 208 mm^2, i.e., for each 1 N applied force, the pressure exerted on the tissue is 4.81 kPa (Fig. 2). The same surface contact area was used for one of the control jaws.

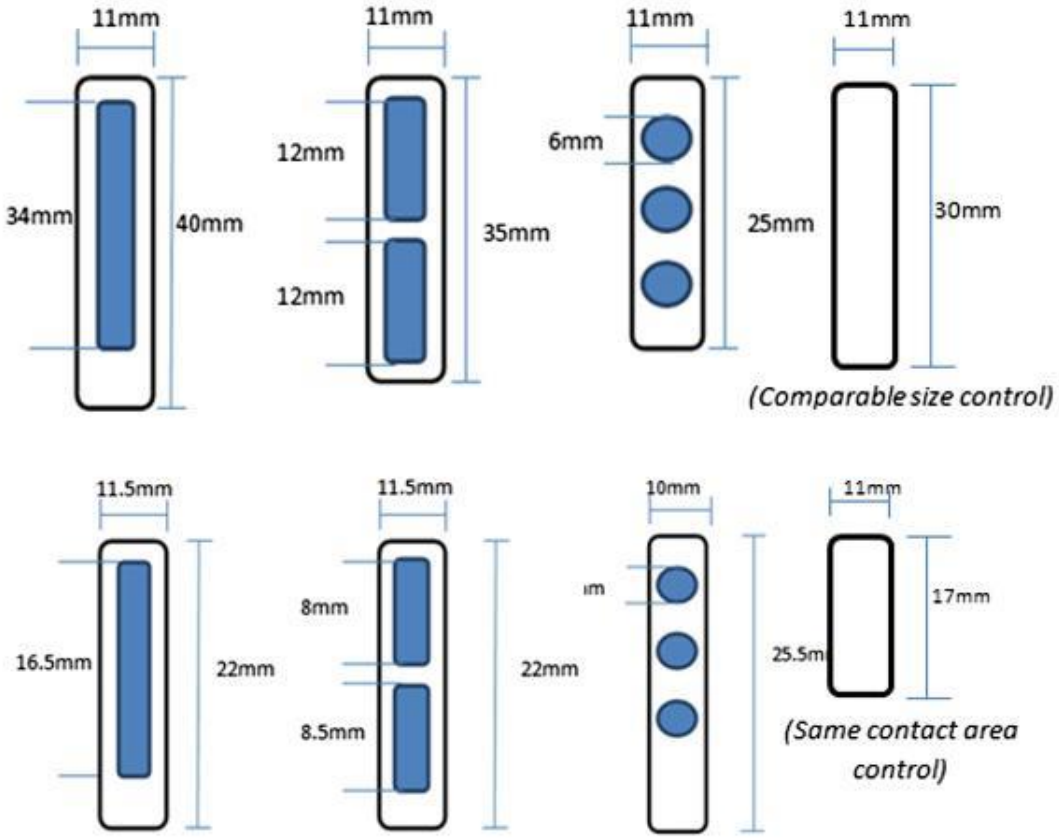

Fig. 2 *Top row* Dimensions of constant surface contact area jaws. *Bottom row* Dimensions of the 1:0.8 ratio fenestrated jaws

Ratio of surface contact area to fenestration area

The second experiment investigated the optimum ratio of surface contact to fenestration area, testing the following ratios: 1:0.4, 1:0.8, 1:1, 1:1.2, 1:1.6. The same three designs (single rectangle, two smaller rectangles, and three circles) were used and the surface contact area was kept constant. All the variants were benchmarked against a pair of plain jaws of identical dimensions. All jaws used in the first and second experiments did not have any surface profiling and were designed for inclusion in a novel parallel occluding slip sensing graspers (reported elsewhere).

Surface profiling

The surface profiles investigated are shown in Fig. 3 and were compared with smooth jaws of the same size, which served as controls. The profiles investigated had been studied and reported previously [7], but the current goal was to determine the effect of fenestration on the performance of these surface profiles. All profiles studied had an opposing jaw with a profile, which interdigitated with the opposite jaw to secure the tissue.

Experimental test rig and procedure for measurement of forces

Ex vivo porcine large bowel was placed between the jaws and various loads (1, 2, 4, 6 N) commonly encountered during laparoscopic surgery were then applied to the upper jaw [5]. The tissue was then pulled until free from the jaws through a pulley system at an angle of 90° by an Instron tensiometer (MA, USA) (Fig. 4) using traction at a rate of 3 mm/s and with recording of data on a personal computer.

Statistical analysis

All results were analysed using ANOVA and consequently the Tukey alpha post hoc test where significance had been found. Since the means of multiple pairs are being compared and all group sizes are equal this data set lends itself to the often more powerful Tukey alpha post hoc test. To provide a single "figure of merit" to aid comparisons, results are expressed as a ratio of retraction force to applied force (R_f/A_f): a high value of this ratio indicates a good grasp of the tissue with minimal pressure.

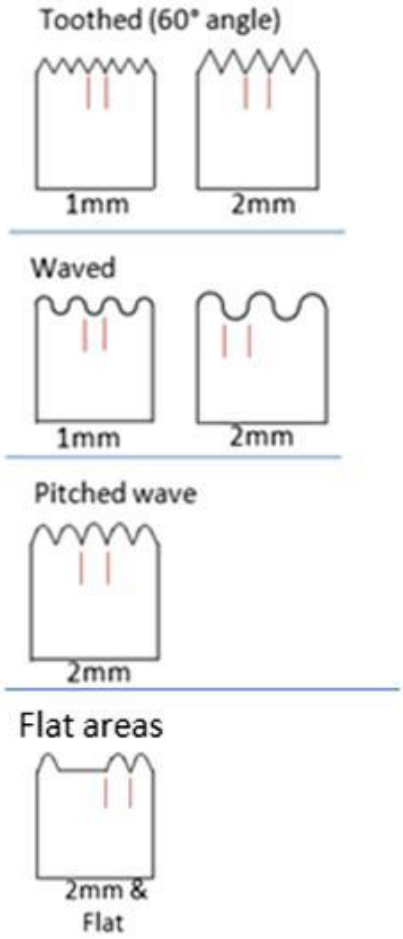

Fig. 3 Designs of the surface profiles which were investigated

Results

Effect of fenestrations design

At all applied forces the retraction force needed to pull tissue from any fenestration design is significantly more than the force necessary to pull tissue from non-fenestrated jaws ($p < 0.05$; Graph 1). It also was observed that at no point was there a significant difference in retraction forces needed to pull tissue from the two plain jaw designs (one of the same surface contact area and one of comparable size to the fenestrated jaws). No consistent significant difference could be found between the three fenestration designs studied.

Ratio of surface contact to fenestration area

The results of the second experiment for the three fenestration designs are shown in Graphs 2, 3, and 4. The ratio

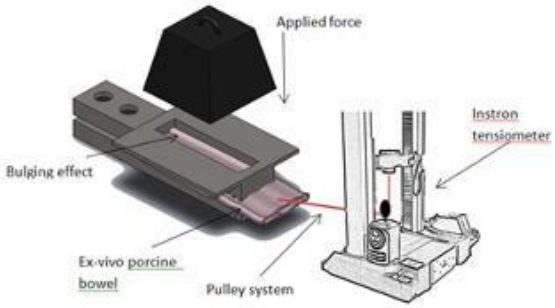

Fig. 4 Experimental test rig

of 1:0.4 (obtained with very small fenestrations) performed significantly worse than the others ($p < 0.05$, indicating that the ratio should exceed this, with the best tissue retention being encountered with ratios ranging from 1:0.8 to 1.1.

Surface profiling

All the profiles studied were made in jaws with a single fenestration and with a surface contact to fenestration area ratio of 1:0.8. The results of this experiment show that all of the profile designs performed significantly better than the control ($p < 0.005$) with no consistent significant differences between the profile designs with the exception that the 1 mm waved profile performed significantly worse than the other designs ($p < 0.004$), although still better than the smooth nonprofiled jaws, as shown in Graph 5. The mean and standard deviation of the retention to applied force ratio across all applied load conditions obtained by this experiment were 1.23:1.0 for the 1 mm waved profile, and 1.7:1.0 for the 1 mm toothed profile with standard deviations for the corresponding retention force of ±0.45 and ±0.38 respectively. In other words with the 1-mm toothed profile, only 1 N of clamping force is needed to retain tissue despite this being pulled by a force of 1.7 N.

Discussion

Contrary to the findings of a previous report [6], the present study has been shown that fenestrations in the jaws of laparoscopic graspers significantly increase the retention of tissue. The present study failed to document the optimal ratios of contact to fenestration area as this is influenced by many variables requiring more extensive studies and replicates than the present investigation. The only conclusion possible at this stage is that the different fenestration designs studied in the present study gave comparable results without any consistently significant differences.

Graph 1 Ratio of retention force to applied force (±σ) for various fenestrated and plain jaws, all of which had the same contact area

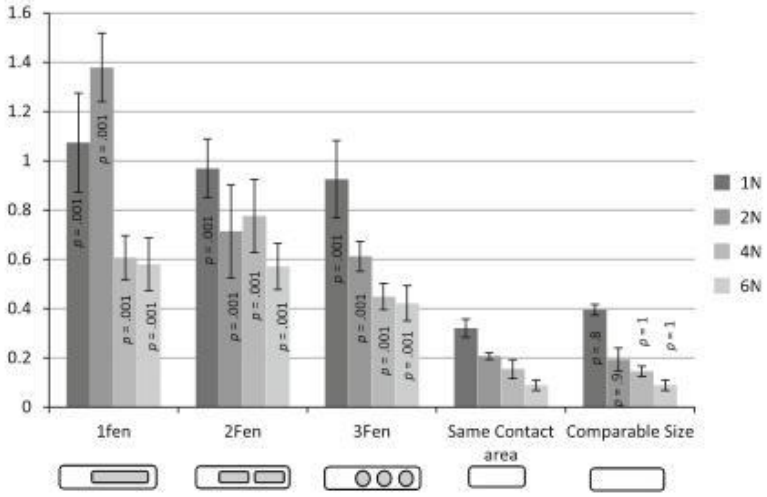

Graph 2 One fenestration; ratio of retention force to applied force (±σ). *p* values shown are with respect to the jaws of ratio 1:0.4

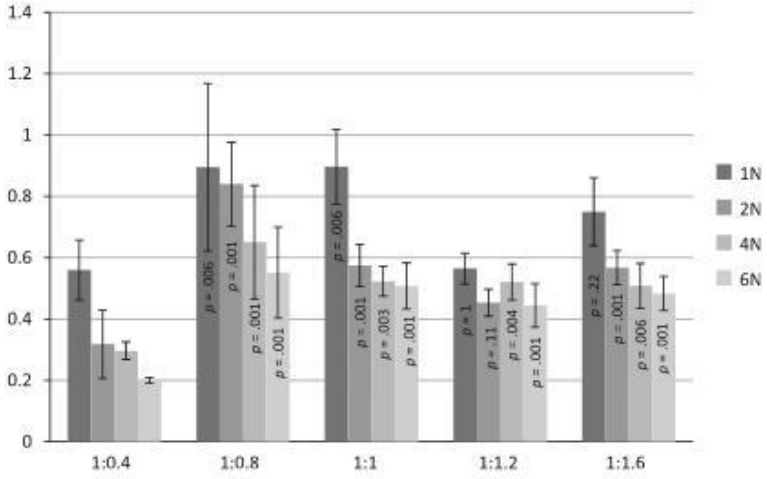

Graph 3 Two fenestrations; ratio of retention force to applied force (±σ). *p* values shown are with respect to the jaws of ratio 1:0.4

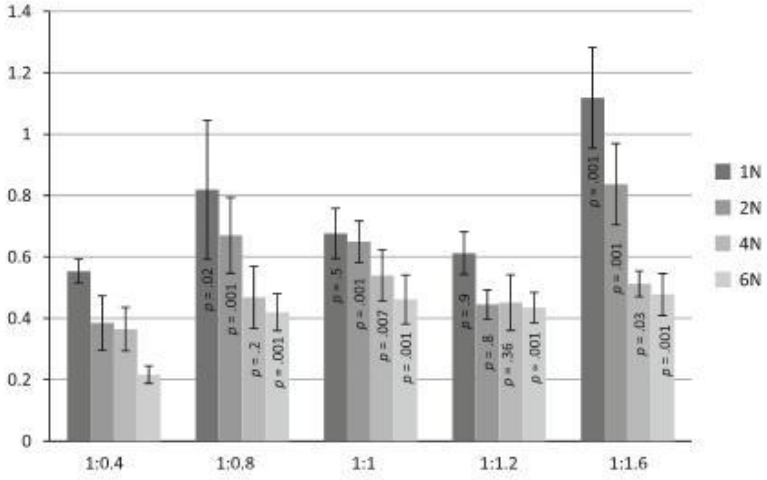

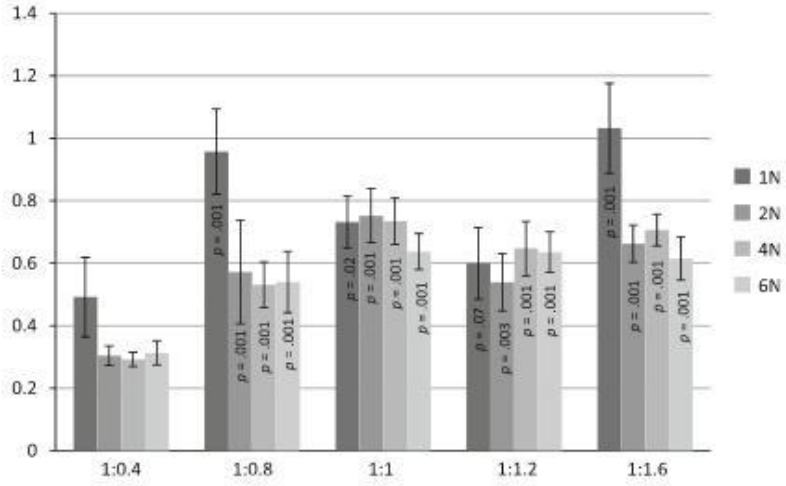

Graph 4 Three fenestrations; ratio of retention force to applied force ($\pm\sigma$). p values shown are with respect to the jaws of ratio 1:0.4

Both the toothed and wave profiles significantly increase the retraction force needed to pull tissue from the jaws when compared to a nonprofiled fenestrated jaw. The retention ability of the 1.0 mm toothed profile was significantly better than the 1.0 mm waved profile, which in is agreement with findings reported by Marucci et al. study [3]. Although less clamping force is required to retain tissue in the jaws with toothed instrument compared with one with a wave profile, it is likely that the toothed instrument carries a greater risk of damage to the grasped tissue [7].

On the basis of the results of the present study for parallel occlusion graspers, the selected jaw design will employ a single fenestration with a ratio of 1:0.8 and a profile design that will have rounded off teeth and intervening flat areas. This configuration including the ratio will maximise the surface contact area with the tissue (thus minimising the pressure) while retaining the benefits which the fenestration provides. The waved profile design has less potential to damage tissue compared with a toothed profile [7] but has a lower grasping hold compared with the toothed profile. Thus by combining these two profiles, we hope to minimise the potential to cause damage by reducing high stress areas whilst retaining the high grasping force associated with a toothed profile. A 5.0-mm instrument of this design would provide a 5 N retention force for an applied force of 2.8 N. This would give a pressure on the tissue of 70 kPa if the surface contact area is 25 mm^2, i.e., well below the force known to cause bowel perforation [10].

We acknowledge that the lack of histological data is a shortcoming of the present study but this would have necessitated the use of live animals requiring a UK Home Office Project license. The assumption that the reduced

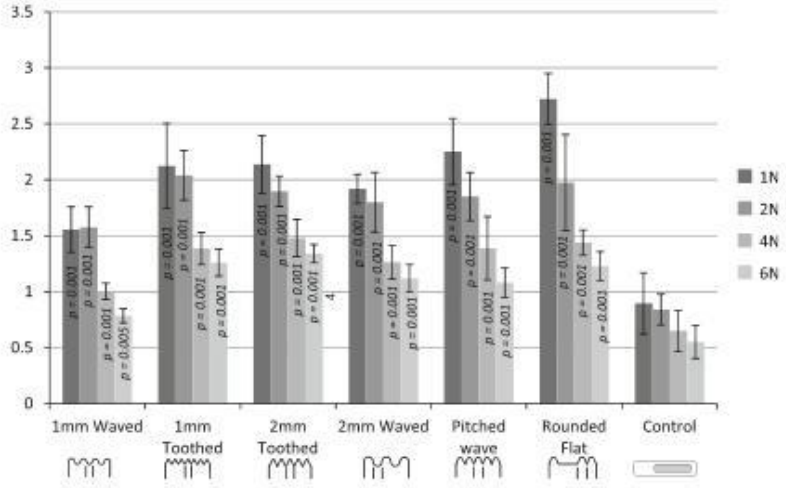

Graph 5 Ratio of retention force to applied force ($\pm\sigma$). p values shown are with respect to the control

pressure exerted on the tissue by an improved grasper design demonstrated by the present study will translate to decreased tissue damage requires confirmation by in vivo animal studies and detailed histology of the grasped tissue, which is planned subject to animal licensing approval.

The results of the present study are being used in the design and construction of a smart powered parallel-occlusion instrument, which will autonomously apply the necessary grasping forces to secure the tissue [11]. These graspers will incorporate sensors and a closed loop control system to retract tissue avoiding excessive forces being applied to the tissue and capable of detecting and preventing slip by close loop force adjustments in real time.

Acknowledgments The authors gratefully acknowledge the grant support from the Engineering and Physics Research Council of the UK, under Grant EP/HO 10033/1.

Disclosures Andrew W. Brown, Stuart I. Brown, Donald Mclean, Zhigang Wang, Alfred Cuschieri have no conflicts of interest or financial ties to disclose.

References

1. Shakeshaft AJ et al (2001) A curved edge moderates high pressure generated by a laparoscopic grasper. Surg Endosc 15(10):1232–1234
2. Cartmill JA et al (1999) High pressures are generated at the tip of laparoscopic graspers. Aust N Z J Surg 69(2):127–130
3. Heijnsdijk EAM, Dankelman J, Gouma DJ (2002) Effectiveness of grasping and duration of clamping using laparoscopic graspers. Surg Endosc 16(9):1329–1331
4. van der Voort M, Heijnsdijk EAM, Gouma DJ (2004) Bowel injury as a complication of laparoscopy. Br J Surg 91(10):1253–1258
5. Visser H et al (2002) Forces and displacements in colon surgery. Surg Endosc 16(10):1430–14263
6. Heijnsdijk EAM et al (2005) Fenestrations in the jaws of laparoscopic graspers. Minim Invasive Ther Allied Technol 14(1):45–48
7. Marucci DD et al (2000) Patterns of failure at the instrument–tissue interface. J Surg Res 93(1):16–20
8. Heijnsdijk EAM et al (2004) Slip and damage properties of jaws of laparoscopic graspers. Surg Endosc 18(6):974–979
9. Frank TG, Cuschieri A (1997) Prehensile atraumatic grasper with intuitive ergonomics. Surg Endosc 11(10):1036–1039
10. Heijnsdijk EAM et al (2003) Inter- and intraindividual variabilities of perforation forces of human and pig bowel tissue. Surg Endosc 17(12):1923–1926
11. Brown A et al (2012) PVDF to detect and autonomously prevent slip during retraction in laparoscopic surgery. Society for American Gastrointestinal and Endoscopic Surgeons, San Diego, CA, 3–7 March 2012

Appendix 1

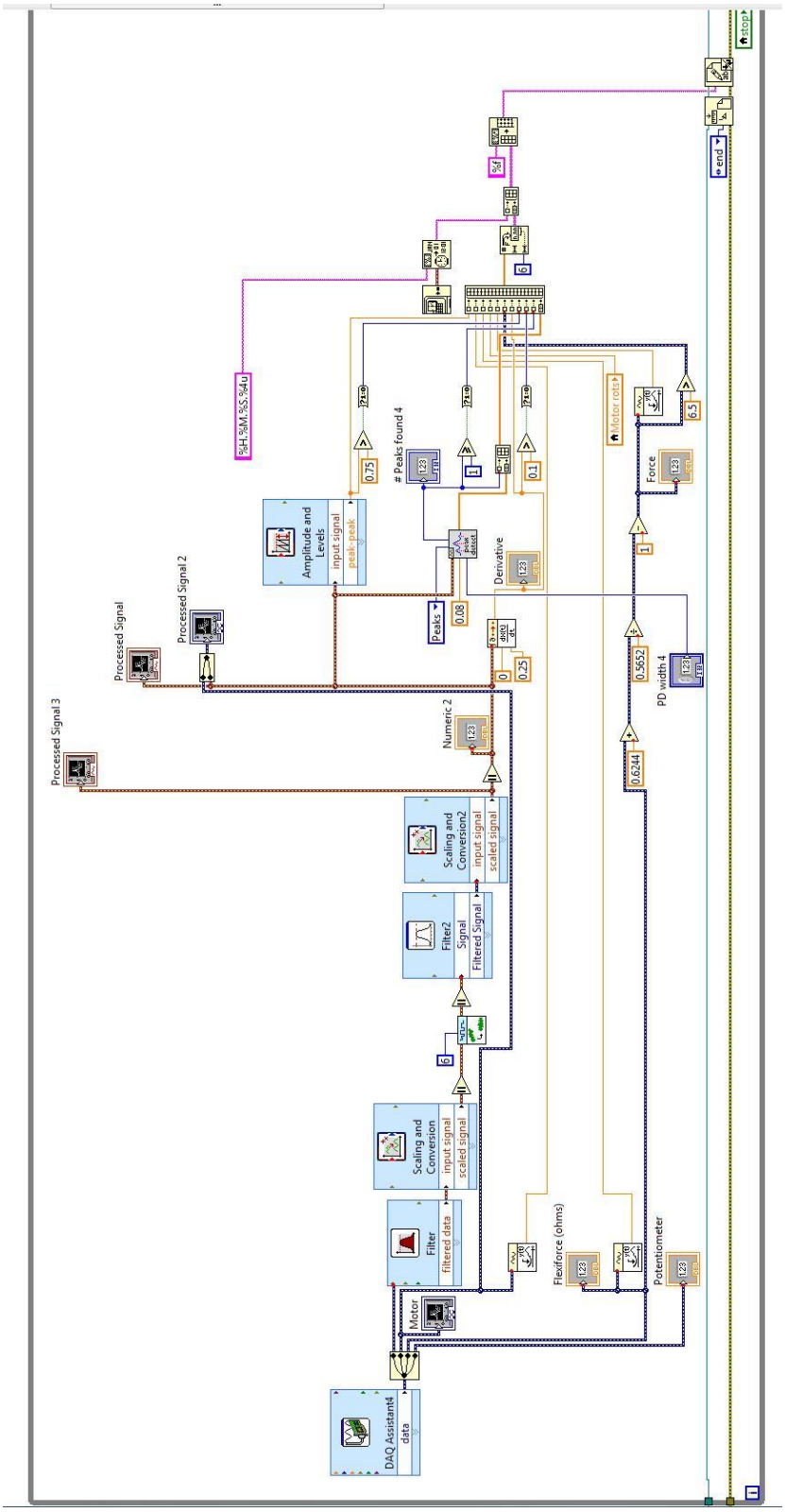

Fig AP1; Data Acquisition of all signal and initial filtering. A local variable is used to parse data to the state selector.

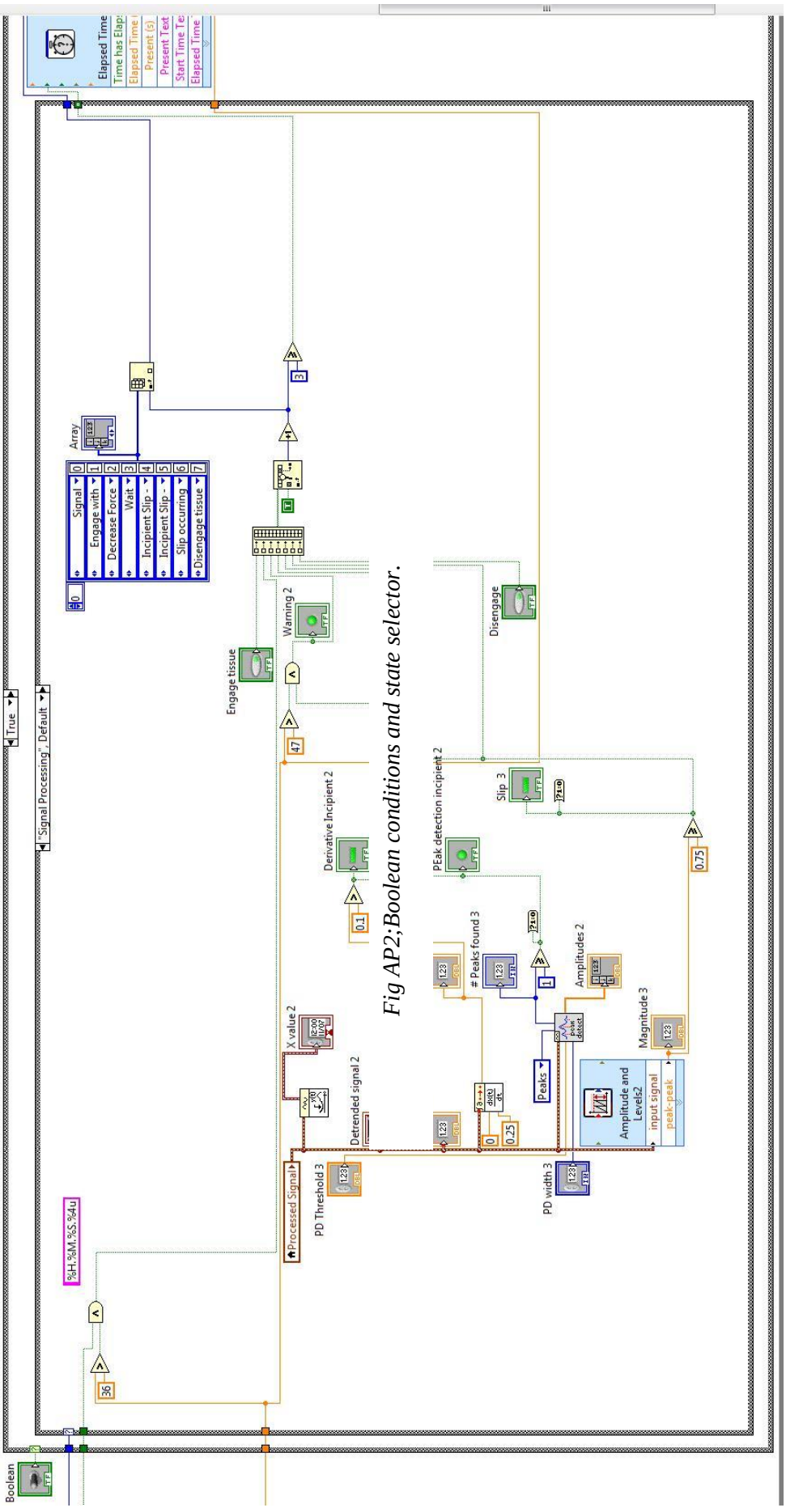

Fig AP2;Boolean conditions and state selector.

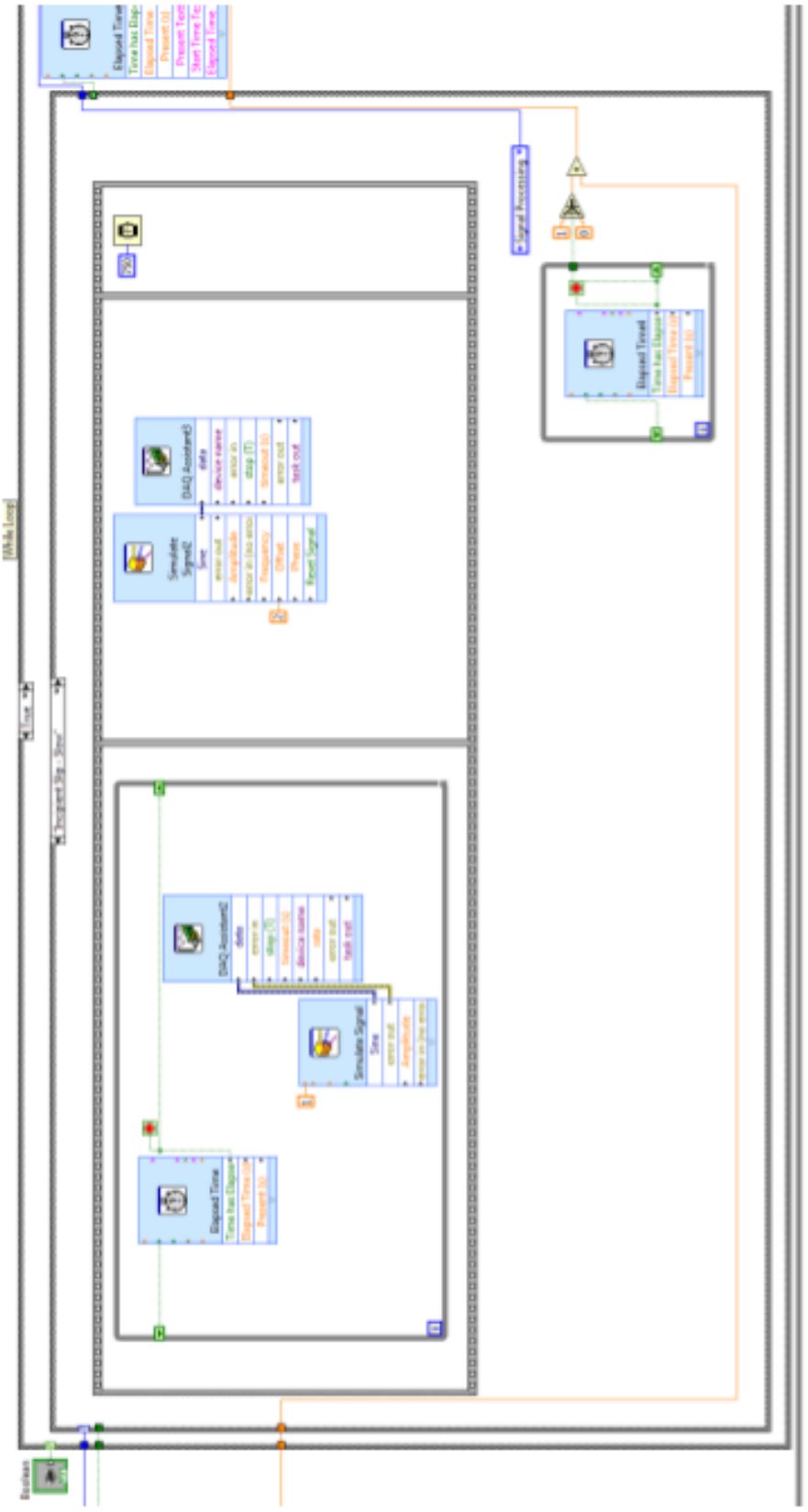

Fig AP3; An example of one of the motor control states. All other states are variations of this which contain differing motor outputs but are not visible from these screen grabs.